

University of Nevada, Reno

Metal-Mold Reactions in CMSX-4 Single Crystal Superalloy Castings

A thesis submitted in partial fulfillment of the
requirements for the degree of Master of Science in
Metallurgical Engineering

By

Enhai Wang

Dr. Jeffery C. Lacombe/Thesis Advisor

May, 2009



THE GRADUATE SCHOOL

We recommend that the thesis
prepared under our supervision by

ENHAI WANG

entitled

Metal-Mold Reactions In CMSX-4 Single Crystal Superalloy Castings

be accepted in partial fulfillment of the
requirements for the degree of

MASTER OF SCIENCE

Jeffrey C. Lacombe, Ph.D., Advisor

Qizhen Li, Ph.D., Committee Member

Eric L. Wang, Ph.D., Graduate School Representative

Marsha H. Read, Ph. D., Associate Dean, Graduate School

May, 2009

Abstract

Metal-mold reaction (MMR) layers are often found on the surface of as-cast CMSX-4 single-crystal alloy parts. These layers cannot be removed prior to solution heat treatment of cast parts because of the sensitivity of the single-crystal castings to recrystallization (RX) defect formation. Removal of the reaction layer after solution heat treatments is very costly, as the layer is very hard, and requires abrasive water jet and pressure (grit) blasting processes. To address this manufacturing concern, it was desirable to understand the mechanisms of reaction layer formation and hardening after solution heat treatment. With this understanding, we developed methods for minimizing the reaction layer formation, which will potentially bring a big cost saving for the CMSX-4 casting processes.

In this work, we confirmed experimentally that silica (SiO_2) reacts with Al, Hf, and Ti, facilitating surface oxidation and formation of a tenacious surface eutectic phase. To avoid this, elimination of the Si is desired. However, Si is present in many of the refractory and pattern materials used in the casting system, which can transfer into the alloy during the solidification process in both liquid and solid state.

A two-path solution was investigated: 1) eliminate all Si sources, and 2) create surface diffusion barriers to prevent reaction of the SiO_2 with the metal. Potential sources of silica/silicon in the casting system include: the CMSX-4 charge material (nominal Si content less than 400 ppm), thermocouple protection quartz tube (100% silica), crucible (4% silica), bushing (80% silica), funnel (if used-60% silica), ash in pattern waxes, mold

release (silicone-based), binder for facecoating (includes nanoscale silica-4% in facecoat), and cores (when used-80% silica).

For a diffusion barrier, an yttria slurry (short lifetime and high cost of fine yttria flour), was replaced with an yttria aerosol spray coating, applied directly to the wax pattern before normal zircon primary facecoating. This was followed by an yttria binder washing and soaking, applied on top of the spray coating shell after dewaxing for strengthening. This process showed good bonding in casting trials in an argon atmosphere Bridgman casting furnace.

Optical microscopy, SEM/EDS, AES and XPS techniques were employed for characterization of MMR interfaces of both the CMSX-4 casting and the shell mold. These characterization methods revealed MMR layers with oxidation, Si and Hf rich features.

In this study, the yttria spray (alone) slightly reduces the amount of MMR of CMSX-4, but when the yttria spray was combined with the binder wash, the reaction was further reduced.

Acknowledgments

My sincere thanks go to:

My thesis advisor, Dr. Jeffery C. Lacombe, who provided invaluable guidance, inspiration, and support for the duration of my graduate studies.

My MS committee members Dr. Eric L. Wang and Dr. Qizhen Li for their guidance.

Chemical and metallurgical department chair Dr. Maurice C. Fuerstenau for his guidance.

Chromalloy Nevada, Mr. Frank Goodwater, Mr. Kevin Updegrove, Dr. Anil Monga, Mr. Kelly Thomas, Mr. Cy Massar and all my coworkers for their support and help.

DAF Associates, Dr. David A. Ford for his invaluable consultancy.

Remet corporation, Mr. Manuel Guerra for his invaluable consultancy.

Rocky Mountain Laboratory, Mr. Tom massopust, Mr. Colin W. Davis and Mr. Patrick R. Stevens for performing surface analysis for this project.

My wife, Chengxue Yu, without her patience, understanding, and support, I never could have succeeded.

Table of Contents

	<u>Page</u>
List of Tables	viii
List of Figures	ix
1 Motivation & Objectives	1
2 Background	5
2.1 Overview of the Process	5
2.2 Materials Used	6
2.3 CMSX-4 Superalloys	6
2.4 The Wax Pattern	11
2.5 Investment Casting Wax	14
2.6 Wax Composition	17
2.7 The Shell System	18
2.8 Shell Materials	19
2.9 Other Materials in the Casting System	21
2.10 Shelling Process & Equipment	23
2.11 Shell Mold Dewaxing and Burnout Process & Equipment	25
2.12 Dewaxing	27
2.13 Casting Process & Equipment	29
2.14 Heat Treatment Process & Equipment	31
2.15 Surface Finishing Process & Equipment	36
2.16 Inspection, Analysis and Test Methods & Apparatus	37
2.17 Contributions of this Work	40

3. Literature Review	41
3.1 Definition of Metal-Mold Reactions	41
3.2 Test Procedure of Metal/Ceramic Reactions	61
3.3 Chemical Properties of CMSX-4 Superalloy	61
3.4 Physical Properties of CMSX-4 Superalloy	65
3.5 Creep-Rupture/Phase Stability of CMSX-4 Superalloy	66
3.6 Processing Properties of CMSX-4 Superalloy	69
3.7 Key Parameters for the Successful Casting of Reactive Alloys	72
3.8 Summary	79
4. Methodology & Materials	80
4.1 Experimental Procedure	82
4.2 Materials used in the Experiment	85
4.3 Characterization Techniques	89
4.4 Characterization of Metal-Mold Reaction Interfaces	109
5. Results & Discussion	113
5.1 Results of Mold Making and CMSX-4 Casting Trial	113
5.2 Results of Examination by Optical Microscopy	121
5.3 Results of Analytical Examinations	130
5.4 Discussion	163
6. Conclusions	172
7. Future Work	173
References	175
Appendices	186

List of Tables

No.	Description	Page
1	A comparison of compositions, densities, and melting ranges of nickel base single crystal superalloys	10
2	Typical properties of four investment casting waxes used in CMSX-4 castings	15
3	Average compositions of as-cast CMSX-4 dendritic pattern and partition	35
4	International classification of common casting defects about MMR	43
5	TCP phase stability of CMSX-4 alloy proven by long term creep-rupture testing	67
6	Comparison of Oxide Properties Listed in order of most negative, i.e., most stable, to least negative Free Energy of Formation.	74
7	Reactive Alloys and Generally Compatible Refractories	76
8	Comparison of Oxide Properties Listed in order of decreasing melting points.	77
9	Comparison of Oxide Properties Listed in order of decreasing density.	77
10	Relative elemental surface composition of samples as determined by EDS analysis (atom %).	131
11	Relative elemental surface composition of samples as determined by AES analysis (atom %).	152
12	Relative elemental surface composition of samples as determined by XPS analysis (atom %).	161
13	Silicon contamination in a plutonium rod cast in a quartz tube	166
14	Diffusion distances of some relevant alloying elements in pure Ni	166

List of Figures

No.	Description	Page
1	The visual appearances of metal-mold reactions of CMSX-4 castings	3
2	A photo tour of investment casting process	7
3	A historic development of the materials capability	9
4	Charge (Ingot) for melting operation of CMSX-4 castings	11
5	A typical wax pattern assembly of CMSX-4 single crystal castings	13
6	A pattern wax injection machine for CMSX-4 castings	13
7	The use of silicone release agents within a process can significantly contribute to the Ash levels	15
8	Thermocouple protection quartz tubes used in CMSX-4 castings	22
9	Materials for melting operation of CMSX-4 castings	24
10	A robotic dipping and rainfall stuccoing system for shelling of CMSX-4 casting	26
11	A typical autoclave dewax system for CMSX-4 castings Figure	30
12	A typical shell mold burnout/firing furnace for CMSX-4 castings	30
13	Methods of casting turbine blades	32
14	Main features of Rolls Royce production unit for manufacture of directionally solidified gas turbine blades	32
15	A typical argon atmosphere Bridgman single crystal casting furnace	34
16	Photomicrographs of as-cast CMSX-4.	35
17	Scanning-electron micrographs of CMSX-4 following the standard solution heat treatment.	35
18	A typical vacuum solution heat treatment furnace for CMSX-4 castings	36
19	A typical abrasive water jet machine for MMR layer removing	38
20	Metal core reaction of CMSX-4 casting	42
21	Metal-Mold Reaction, Orange Peel and Alligator Skin	44
22	A typical metal mold reaction layer on the CMSX-4 airfoil casting	47
23	Surface eutectic layer of CMSX-10N	49
24	Standard free energy of formation of oxides (at room temperature) vs oxide melting point.	53
25	CMSX-4 SX casting with metal mold reaction and gas hole defect	57
26	CMSX-4 SX casting with metal mold reaction and secondary grain defect	58
27	CMSX-4 SX casting with metal mold reaction and hot tears defect	59
28	Visual appearance of CMSX-4 casting (Sample 2) and shell mold surface using zirconia slurry facecoat	81
29	Visual appearance of CMSX-4 casting (Sample 3) and shell mold surface (Sample 9) using yttria slurry facecoat	81
30	NYACOL Yttria binder used as strengthening binder in this project	83

No.	Description	Page
31	Y ₂ O ₃ Y Aerosol spray coating on zircon facecoat MOR test bars	83
32 a)	Samples (1-5) sectioning for surface characterization	86
32 b)	Samples for surface characterization	87
32 c)	Shell molds of CMSX-4 SX castings for sample 8 and sample7	88
33	Leica Optical Microscope with Digital Camera	90
34	JSM-6400 SEM with iXRF Model 510D EDS	93
35	Hummer VI-A Sputtering System (Gold coating)	94
36	Perkin Elmer PHI 610 Scanning Auger Microprobe	101
37 a)	AES kinetic energy spectrum and AES mapping capability	102
37 b)	AES depth-profiling capability	102
38	KRATOS Analytical XPS Instrument, Model: Kratos Axis His	107
39	Philips Analytical (PANalytical) X' Pert X-ray Diffractometer	109
40	Wax pattern assembly after Y aerosol spray coating	114
41	Wax pattern assembly after Y aerosol spray coating, normal zircon facecoating and stuccoing	114
42	Four side view of R & D test shell after dewaxing	115
43 a)	Bottom filtration for casting trial	115
43 b)	Shell mold after burnout/firing for casting trial	115
43 c)	Washing shell mold after dye penetration inspection	115
44	Four side view of shell mold after casting	116
45	Visual appearance of CMSX-4 casting trial using shell mold with yttria aerosol spray coating and yttria binder washing and soaking.	117
46	Visual appearance of CMSX-4 casting trial using shell mold with yttria aerosol spray coating but without yttria binder washing and soaking	118
47 a)	Visual appearance of top surface of pouring basin of CMSX-4 casting trial showed some dross.	119
47 b)	More dross on the surface of pouring basin of CMSX-4 casting with secondary grain defect	119
47 c)	No dross on the surface of pouring basin of CMSX-4 casting with hot tear defect.	120
48	Visual appearance of gating system of CMSX-4 casting trial	120
49	20X optical image of Sample 1	121
50	80X optical image of Sample 1	121
51	13.4X optical image of Sample 2	122
52	50X optical image of Sample 2	122
53	13.4X optical image of Sample 3	123
54	50X optical image of Sample 3	123
55	13.4X optical image of Sample 4 Backup	124
56	50X optical image of Sample 4 Backup	124
57	13.4X optical image of Sample 5	125
58	80X optical image of Sample 5	125
59	24X optical image of Sample 6	126
60	80X optical image of Sample 6	126

No.	Description	Page
61	13.4X optical image of Sample 7	127
62	80X optical image of Sample 7	127
63	24X optical image of Sample 8	128
64	80X optical image of Sample 8	128
65	24X optical image of Sample 9	129
66	80X optical image of Sample 9	129
67	Y ₂ O ₃ identification on the Y ₂ O ₃ Y Aerosol spray coating MOR test bar after dewaxing by XRD	130
68	1500X SEM image of shiny spot on Sample 1	132
69	1500X BSE image of shiny spot on Sample 1	132
70	EDS spectrum of Area 1 in Figure 69.	133
71	EDS spectrum of Area 2 in Figure 69.	133
72	EDS spectrum of Area 3 in Figure 69.	134
73	1000X BSE image of shiny spots on Sample 1	134
74	EDS spectrum of Area 1 in Figure 73.	135
75	EDS spectrum of Area 2 in Figure 73.	135
76	EDS map of Area in Figure 73.	136
77	150X BSE image of dark and golden area on Sample 1	136
78	EDS spectrum of Area 1 in Figure 77.	137
79	EDS map of Area in Figure 77.	137
80	100X BSE image of Sample 2	138
81	EDS spectrum of Area 1 in Figure 80. (Optically light colored area)	138
82	EDS spectrum of Area 2 in Figure 80. (Optically dark colored area)	139
83	EDS spectrum of Area 3 in Figure 80. (Optically gold colored area)	139
84	100X BSE image of Sample 2	140
85	EDS spectrum of Area 1 in Figure 84. (Optically light colored area)	140
86	EDS spectrum of Area 2 in Figure 84. (Optically dark colored area)	141
87	100X BSE image of Sample 3	141
88	EDS spectrum of Area 1 in Figure 87. (Optically dark colored area)	142
89	EDS spectrum of Area 2 in Figure 87. (Optically gold colored area)	142
90	EDS spectrum of Point 3 in Figure 87.	143
91	200X BSE image of gold colored area on Sample 3	143
92	EDS spectrum of Area 1 in Figure 90.	144
93	50X BSE image of Sample 5	144
94	EDS spectrum, Area 1 in Figure 93.	145
95	EDS spectrum, Point 2 in Figure 93.	145
96	EDS spectrum, Area 3 in Figure 91.	146

No.	Description	Page
97	100X BSE image of Sample 5	146
98	EDS spectrum of Area 1 in Figure 97.	147
99	500X BSE image of Sample 5	147
100	EDS spectrum of Point 1 in Figure 99.	148
101	EDS spectrum of Area 2 in Figure 99.	148
102	50X BSE image of Sample 8 Back up	149
103	300X BSE image of Sample 8 Back up	149
104	EDS spectrum of Point 1 in Figure 103.	150
105	EDS spectrum of Point 2 in Figure 103.	150
106	800X BSE image of Sample 8	151
107	EDS map of area in Figure 106.	151
108	AES surface survey of shiny spot on Sample 1	152
109	AES sputter depth profile of shiny spot on Sample 1	153
110	AES sputter depth profile of shiny spot on Sample 1, 0-40% plot	153
111	AES sub-surface survey of shiny spot on Sample 1	154
112	AES surface survey of gold colored area on Sample 3	154
113	AES sputter depth profile of gold colored area on Sample 3	155
114	AES sputter depth profile of gold colored area on Sample 3, 0-20% plot	155
115	AES surface survey of gold colored area on Sample 4	156
116	AES sputter depth profile of gold colored area on Sample 4	156
117	AES sputter depth profile of gold colored area on Sample 4, 0-20% plot	157
118	AES surface survey of grey colored area on Sample 4	157
119	AES sputter depth profile of grey colored area on Sample 4	158
120	AES sputter depth profile of grey colored area on Sample 4, 0-20% plot	158
121	AES surface survey of shiny spot on Sample 4	159
122	AES sputter depth profile of shiny spot on Sample 4	159
123	AES sputter depth profile of shiny spot on Sample 4, 0-20% plot	160
124	AES sub-surface survey of shiny spot on Sample 4	160
125	XPS surface survey of Sample 6	161
126	XPS surface survey of Sample 7	162
127	XPS surface survey of Sample 8	162
128	XPS surface survey of Sample 9	163
129	Microanalysis of phases in CMSX4 superalloy – μ -EDS vs Si-EDS spectra	165
130	Microanalysis of Trace Elements by μ -EDS	165
131	Using quartz tubes as immersion thermocouple protection tubes, and alumina crucibles, CMSX-4 melt slag showed oxidation features.	169
132	Alumina crucibles were wetted by CMSX-4 melt	169
133	Grain defects in single crystal turbine blades	170

1. Motivation & Objectives

CMSX-4®¹ is an ultra high strength, single crystal alloy, developed by the Cannon Muskegon Corporation (CMC). The introduction of CMSX-4 from CMC [1] shows “Gas turbine engine designers seek improved fuel efficiency, power to weight performance, improved hot section durability, and lower life-cycle costs. To achieve the desired improved performance and efficiencies, designers tend to utilize increasingly capable single crystal alloys. In particular, many employ CMSX-4. This second generation rhenium-containing, nickel-base single crystal alloy is capable of high peak temperature/stress operation of at least 2125°F (1163 °C). CMSX-4 is readily produced in large tonnages, and its use is established in various applications. For example, Solar® Turbines report blade lives (to overhaul) of 25,000 - 30,000 hours in their 15,000 hp Mars 100 industrial gas turbine. Gas turbine airfoils are a principal application for the CMSX-4 alloy.”

Stephen J. Balsone pointed out the importance of cost factor in gas turbine industry [2]:

“Gas turbine engines, both aircraft and industrial power generation, represent one of the most aggressive environments for structural materials. With ever growing demands for increasing performance and efficiencies, all classes of materials are being pushed to higher temperature capabilities. These materials must also satisfy stringent durability and

¹ The alloy CMSX-4 is copyrighted © 1999, 2004 The C-M Group. Specialty Material and Alloys Group. All rights reserved. Information in this document is subject to change without notice. Other products and companies referred to herein are trademarks or registered trademarks of their respective companies or mark holders. CMSX-4® alloy is a registered trademark of Cannon-Muskegon Corporation.

reliability criteria. As materials are developed to meet these demanding requirements, the processing of these materials often becomes very complicated and expensive. As a result, the cost of materials and processes has become a much larger consideration in the design and application of high performance materials. Both the aircraft engine and power generation industries are highly cost competitive, and market advantage today relies on reducing cost as well as increasing performance and efficiency .”

Metal-mold reaction layers were found on the surface of CMSX-4 single crystal superalloy as-cast parts [3-13], These layers (**Figure 1**) can not be removed before solution heat treatment of casting parts because of the sensitivity to recrystallization (RX) defects formation [13-16]. For example, exposure of grit-blasted single crystal nickel-based Superalloy as-cast specimens to 1300 °C for 4 h results in surface recrystallization to a depth of 0.17 mm [17]. Alternatively, removing the reaction layers after the solution heat treatments is very costly, as it requires abrasive water jet and pressure (grit) blasting processes. Clearly it is more desirable to discover the mechanisms of reaction layer formation and reaction layer hardening after solution heat treatment. It is hoped that with this understanding, appropriate processing methods for minimizing the reaction layers can be developed, which will potentially bring a big cost saving for the CMSX-4 casting processes.

The key objective of this project is to develop a cost-effective method for avoiding the formation of metal-mold reactions in CMSX-4 single crystal castings. In reaching this end, this project will involve the following tasks.

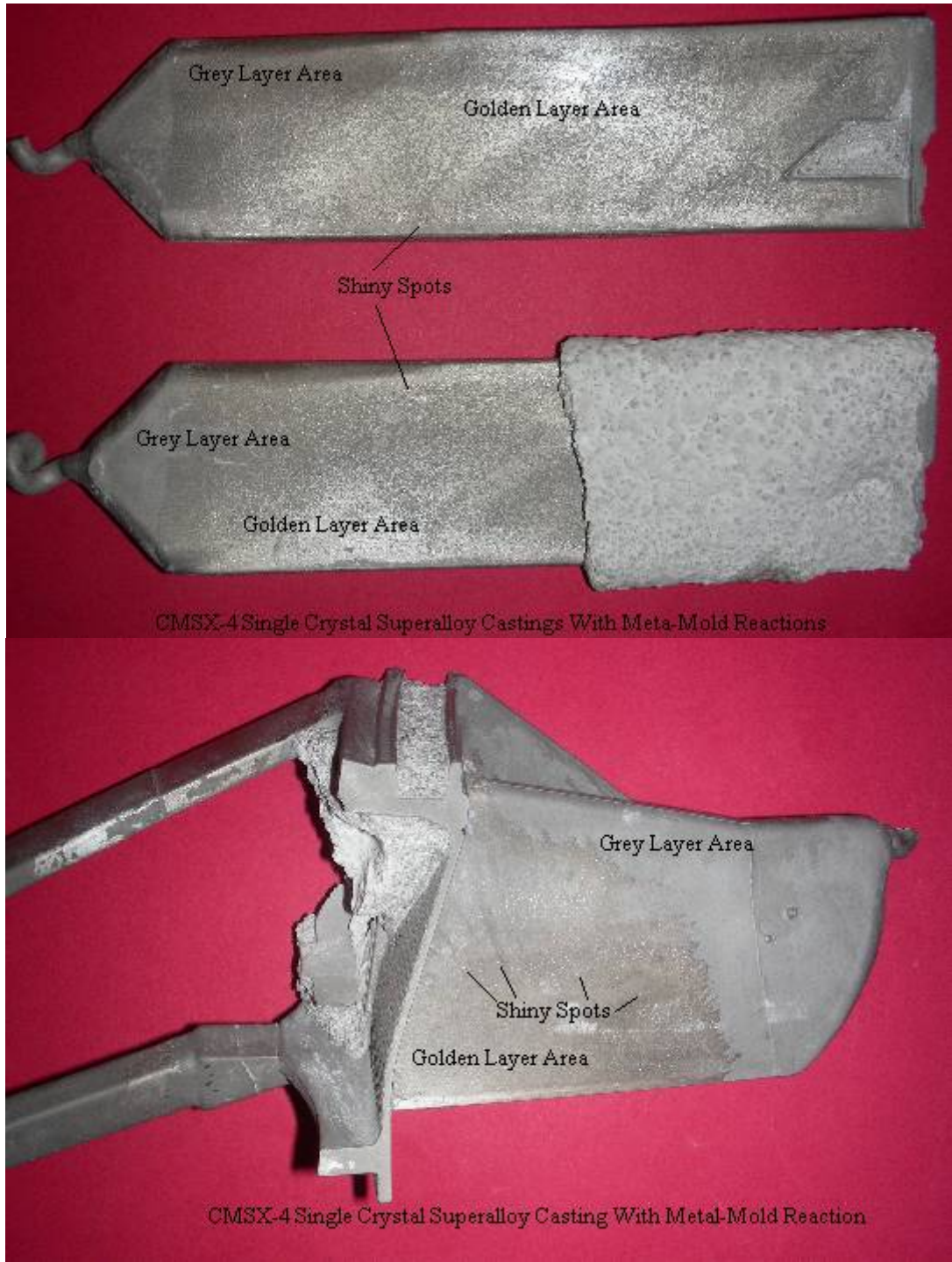


Figure 1. The visual appearances of metal-mold reactions of CMSX-4 castings

The main tasks of this thesis project are:

- ✧ Review the literature of metal-mold reactions in CMSX-4, René N5® and PWA1484® single crystal superalloy castings, and gain an understanding of the relevant issues that may contribute to developing a remedy.
- ✧ Identify the meta-mold reaction layers by some surface analysis techniques.
- ✧ Analyze the mechanisms of reaction layer formation and reaction layer hardening after solution heat treatment.
- ✧ Implement solution methods in test castings.
- ✧ Recommend a method for minimizing the metal-mold reaction layers in CMSX-4 castings.

2. Background

2.1. Overview of the Investment Casting Process

Also known as the LOST WAX PROCESS. Wax is injection molded in a die to form a dimensionally accurate pattern of the desired geometry with the added features or gating required manufacturing the casting. Individual patterns are assembled onto a wax cluster. The cluster is dipped into ceramic slurry, coated with ceramic sand, and dried. This process is repeated several times until a mold shell of the necessary thickness has formed around the wax. The wax is removed from the ceramic mold in a steam autoclave or gas fired furnace. Metal is then poured into the mold in a specially designed furnace to control the way the metal solidifies. Solidification control yields Equiax, Directionally Solidified, and Single Crystal castings with enhanced properties for high temperature, high stress applications like turbine airfoils. The shell is removed from the cast mold and the individual castings are cut off of the mold. Most castings are heat treated to further enhance casting properties. The gating is removed with a variety of techniques and machinery including: belt grinders, wheel grinders, CNC saws, and CNC mills. Castings are finished with a variety of belts and stones to remove any remaining gating evidence and ensure visual quality. Castings are dimensionally verified using an assortment of dedicated gages, CMM, and ultrasonic wall inspection. Before shipment, further NDT Inspection includes: Internal Airflow, Fluorescent Penetrant Inspection (FPI), and X-ray, a photo tour of investment casting process is shown in **Figure 2** [18].

2.2. Materials Used in the Casting Process

We will discuss the materials used throughout the casting system because it is believed that the problem at hand (the metal-mold reaction) is possibly related to the composition of some component in the overall system.

2.3. CMSX-4 Superalloys

Aero engine test experience of CMSX-4 alloy [19]:

CMSX-4 alloy is a second-generation nickel-base single crystal superalloy containing 3% (wt) rhenium (Re) and 70% volume fraction of the coherent γ' precipitate strengthening phase. It's finely balanced composition offers an attractive range of properties for turbine airfoil applications. In particular, the alloy's combination of high strength in relation to creep-rupture, mechanical and thermal fatigue, good phase stability following extensive high temperature, stressed exposure and oxidation, hot corrosion and coating performance, are attractive for turbine engine applications where engine performance and turbine airfoil durability are of prime importance.









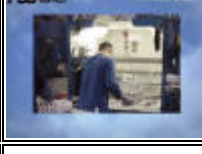










<i>Investment Casting Process - Photo Tour</i>					
	Wax Injection		Wax Pattern		Wax Assembly
	Ceramic Dip		Ceramic Dip		Steam Autoclave
	Mold Fire		Cast		Knockout & Cutoff
	Grain Inspection		Gating Removal - Belt Grinder		Finishing - Belt
	Finishing Stone		Gaging		CMM
	Ultrasonic Wall		Airflow		FPI
	X-ray				

Figure 2. A photo tour of investment casting process

Economically-competitive single crystal casting yields are being achieved in the Rolls-Royce production facilities and extensive vacuum heat treatment experience confirms the CMSX-4 alloy to have a practical production solution heat treat/homogenization "window" that permits it to meet the desired performance characteristics.

The use of hot-isostatic-pressing (HIP) has been shown to eliminate single crystal casting micropores, which along with the essential absence of γ/γ' eutectic phase, carbides, stable oxide, nitride or sulfide inclusions, results in remarkably high mechanical fatigue properties in smooth and notched specimens. The Re addition to the alloy has been shown to not only benefit creep and mechanical fatigue strength (with and without HIP), but also bare oxidation, hot corrosion (sulfidation) and coating performance. The high level of balanced properties (determined by extensive laboratory evaluation) has been confirmed during engine testing of the Rolls-Royce Pegasus turbofan.

Cleanliness of the alloy appears to be key to casting success. Extremely clean superalloys can be produced in optimized and well-maintained the vacuum induction melting (VIM) processes. Non-filtered and non-electron beam cold hearth refining (EBCHR) processed VIM alloy product originating at "committed" (quality - guaranteed) producers are successfully used in some of the most demanding turbine blade and vane component casting applications in existence [20].

CMSX-4 single crystal superalloy Features [1]:

- ✧ Density 0.314 lb./in³ (8.70 kg/ dm³).
- ✧ Good single crystal castability with moderate to high thermal gradient, industrial casting processes - similar to CMSX-2® and CMSX-3® production experience.
- ✧ Solution heat treatment "window of approximately 19°C (35°F) - capable of full γ' and γ eutectic and γ/γ' solutionizing without incipient melting.

- ✧ Specific (density corrected) stress-rupture advantage of 35°C (63°F) over CMSX-2/3 alloys.
- ✧ Stress - 1% creep advantage of 62°C (111°F) over DS CM 247LC®.
- ✧ Oxidation resistance (both bare & coated) at least as good as CMSX-2 and CMSX-3 alloys. Improved hot corrosion resistance.
- ✧ Excellent phase stability and tolerant of rare earth elemental ppm residual additions of lanthanum and yttrium for enhanced bare oxidation resistance and thermal barrier coating adherence.

A historic development of superalloy materials capabilities for gas turbine applications is shown in **Figure 3** [21]. A comparison of compositions, densities, and melting ranges of selected nickel base single crystal superalloys is shown in **Table 1**[22]. A typical CMSX-4 charge (ingot) is shown in **Figure 4**.

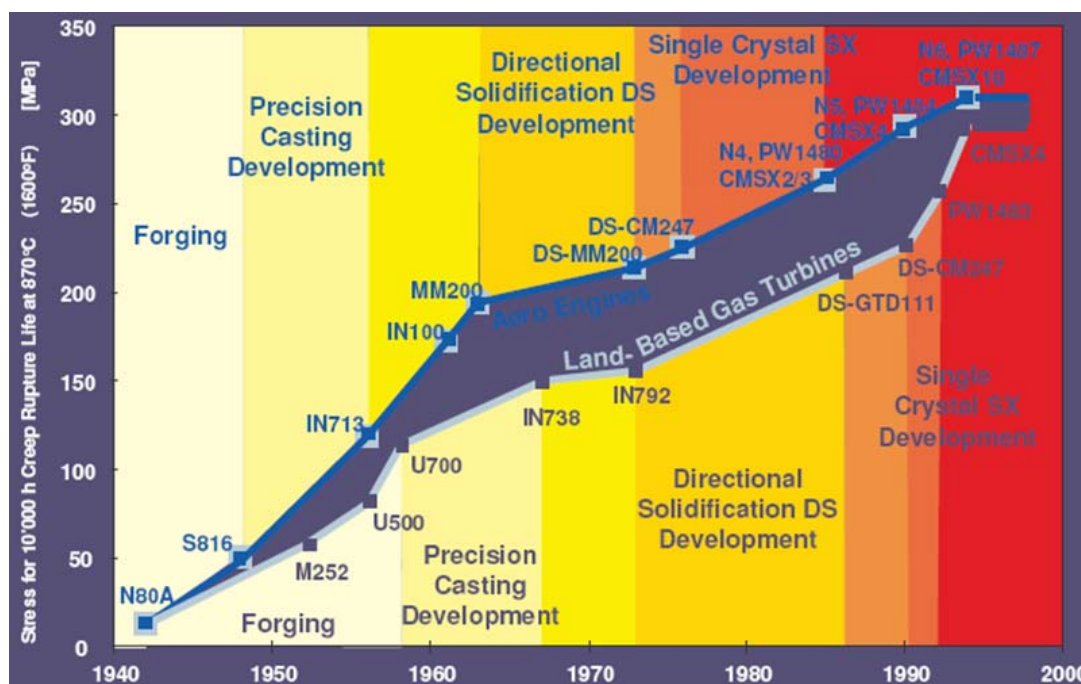


Figure 3. A historic development of the materials capability

Nickel Base Single Crystal	C	Cr	Ni	Co	Mo	W	Nb/Cb	Ta	Ti	Al	B	Zr	Hf	Fe	Re	Other	Density g/cm ³	Density lb/in ³	Approximate Melting Range °F	Approximate Melting Range °C
PWA 1480	-	10	53	5	-	4	-	12	1.5	5	0.003	-	-	-	-	-	8.70	0.314	2350-2450	1290-1340
PWA 1484	-	5	53	10	1.9	5.9	-	8.7	-	5.65	-	-	0.1	3	3	-	8.95	0.323	-	-
PWA 1487	-	5	53	10	1.9	5.9	8.4	5.65	-	5.65	-	0.25	3	Y 0.013	3	-	8.95	0.323	-	-
René' N4	-	10	53	8	2	6	0.5	5	3.5	4.2	-	-	0.2	-	-	-	8.56	0.309	-	-
René' N5	-	7	53	8	2	5	-	6	-	6.2	-	-	0.2	3	-	-	8.63	0.312	-	-
René' N6	-	4	53	12	1	6	-	7	-	5.8	-	-	0.2	5	-	-	8.97	0.324	-	-
CMSX-2	-	8	53	5	0.6	8	-	6	1	5.6	-	-	-	-	-	-	8.56	0.309	2415-2500	1320-1370
CMSX-3	-	8	53	5	0.6	8	-	6	1	5.6	-	-	0.1	-	-	-	8.56	0.309	2420-2510	1325-1375
CMSX-4	-	6.5	53	9	0.6	6	-	6.5	1	5.6	-	-	0.1	3	-	-	8.70	0.314	2415-2515	1320-1380
CMSX-4 [LUS][La+Y]	-	6.5	53	9	0.6	6	-	6.5	1	5.6	-	-	0.1	3	La+Y 0.002	-	8.70	0.314	-	-
CMSX-4 [B/C][MK4]	0.04	6.5	53	9	0.6	6	-	6.5	1	5.6	0.006	-	0.2	3	-	-	8.70	0.314	-	-
CMSX-6	-	10	53	5	3	-	-	2	4.7	4.8	-	-	0.1	-	-	-	7.98	0.288	-	-
CMSX-10K	-	2	53	3	0.4	5	0.1	8	0.2	5.7	-	-	0.03	6	-	-	9.05	0.327	2480-2575	1360-1410
CMSX-10N	-	1.5	53	3	0.4	5	0.05	8	0.1	5.8	-	-	0.03	7	-	-	-	-	2480-2575	1360-1410
CMSX 486	0.07	5	53	9	0.7	9	-	4.5	0.7	5.7	0.015	0.005	1	3	-	-	8.85	0.319	-	-
SRR 99	-	8	53	5	-	10	-	3	2.2	5.5	-	-	-	-	-	-	8.56	0.309	-	-
RR 2000	-	10	53	15	3	-	-	-	4	5.5	-	-	-	-	1V	-	7.87	0.284	-	-
AM 1	-	8	53	6	2	6	-	9	1.2	5.2	-	-	-	-	-	-	8.59	0.310	-	-
AM 3	-	8	53	6	2	5	-	4	2	6	-	-	-	-	-	-	8.25	0.298	-	-
SC 180	-	5	53	10	2	5	-	8.5	1	5.2	-	-	0.1	3	-	-	8.84	0.319	-	-

Table 1. A comparison of compositions, densities, and melting ranges of nickel base single crystal superalloys



Figure 4. Charge (Ingot) for melting operation of CMSX-4 castings

2.4. The Wax Pattern

Success in producing high quality investment castings in the metal of choice depends on the production of high quality patterns and runner assemblies. In an investment casting process, a (positive) replica of the part is fabricated in wax, and then invested in a shell.

The wax is then melted out, leaving a negative mold into which the molten metal is poured and cast. The wax pattern assembly consists not only of the part replica(s), but the mold's filling system is typically also built at this stage out of the same wax.

Wax is the most widely used pattern material, due to its ability to be shaped in either liquid, semi-plastic, or plastic states, wax is the key component. If the wax pattern is wrong, the casting will be wrong - it follows that the correct choice of wax type and

product is critical [23].

Wax selection is determined by the particular application and the process criteria are [24]:

- ✧ Injection- state/setting rate/rheology/geometry/equipment/surface finish
- ✧ Removal, handling, assembly- strength/hardness/setting rate/stability/ability to make joins
- ✧ Dimensional control- thermal expansion/contraction/cavitation/distortion
- ✧ Shelling/mould making- strength/wetability/resistance to binders and solvents
- ✧ Dewax and burnout- melting point/viscosity/thermal expansion/thermal diffusivity/ash content
- ✧ Other : cost/availability/recycling/toxicity/environmental

Typical concerns in wax choice include how readily it can be used to form the replica, its properties as a function of temperature, its strength. Its dimensional stability, surface quality and adhesion characteristics are also important.

Definition of Wax Assemblies: The building of one or more wax patterns, involves the integration of ingates and runner bars into a wax pattern assembly prior to the shell building/block moulding process [25].

A typical wax pattern assembly, made using four kinds of waxes (dark red dip seal wax, blue runner wax, light green pattern wax and red pattern wax) for CMSX-4 single crystal castings, is shown in **Figure 5**. A pattern wax injection machine for CMSX-4 single crystal castings is shown in **Figure 6**.

and ultimately the quality of castings produced. Correct wax product choice, coupled with strict process & quality control procedures is essential [24].

Investment casting waxes tend to be complex, consisting of many different components



Figure 5. A typical wax pattern assembly of CMSX-4 single crystal castings



Figure 6. A pattern wax injection machine for CMSX-4 castings

and exhibiting a range of properties designed to influence pattern behavior in the foundry. The level of ash in the selected wax material and wax pattern injection lubricant has been reported to be one of the critical factors for reducing metal-mold reactions of reactive alloy castings. The use of silicone release agents within a process can significantly contribute to the Ash levels (**Figure 7**). Certain alloys will react with this Ash since, it will leach into the shell at fire off. Filler can be a problem with reactive alloys [25]. The typical **ash contents** of the four kinds of waxes currently used in Chromalloy Nevada (CNV) are shown in **Table 2**. A silicone based aerosol spray lubricant (S202 Dry Mist Silicone Mold Release) is applied in the pattern wax injection process in CNV (Spraying S202 mold release on the top and bottom die before wax injection operation to avoid wax patterns difficult to remove from the die after injection). Both silicone and non-silicone sprays are available for pattern wax injection, but silicone spray will increase ash levels. [26].

The ash content is described as the percentage of non-combustible compounds left after complete combustion in air. It is determined by burning a known weight of wax with a Bunsen burner, and then firing the leftover carbon deposits in a furnace at 1000°C.

Finally, the remainder in the crucible is weighed and the ash percentage is calculated.

A wax with high ash content will cause visual defects on the finished parts. [27].

2.5. Categories of Investment Casting Wax [28]

Filled Pattern Wax

Filled pattern wax has the largest use of wax compounds currently produced. The addition of specialized filler materials gives excellent injection characteristics to the wax.

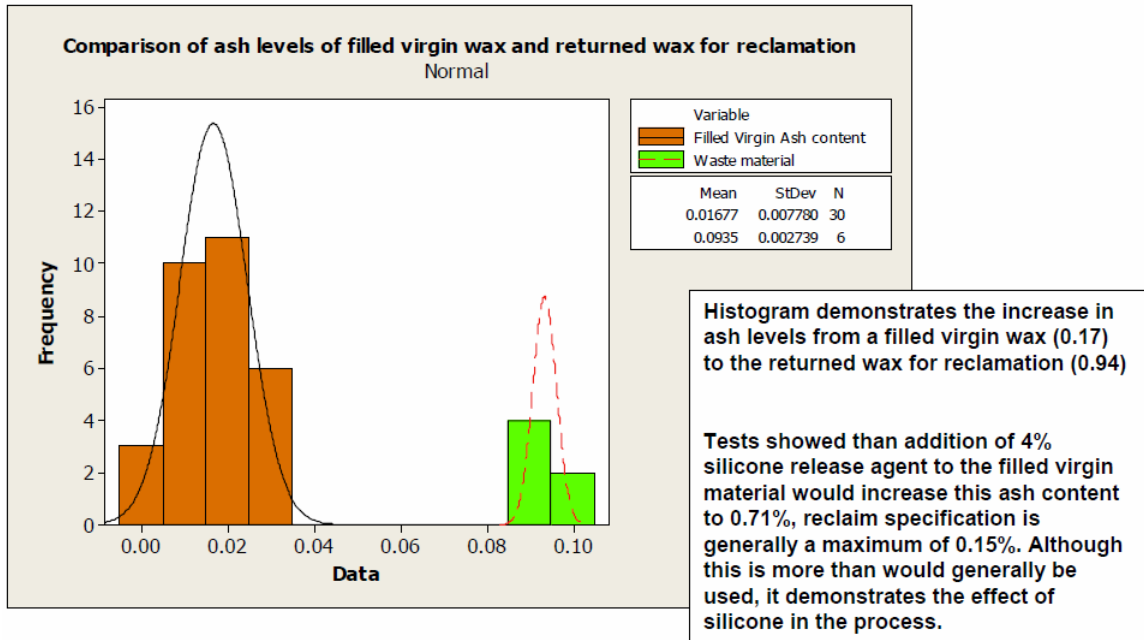


Figure 7. The use of silicone release agents within a process can significantly contribute to the Ash levels

	KC 4640F Ceramic Binder Wax Dark Red	983 Cerita SpruWax Blue	Remet Castylene® 2224 Pattern Wax Light Green	KC 3898 N RR Pattern Wax Red
Ash content %	0.005	0.001	0.001	0.007
Ring & Ball Softening Point °F	135	149	154	167

Table 2. Typical properties of four investment casting waxes used in CMSX-4 castings

The contraction range for filled pattern wax sets the standard for the investment casting industry with a wide variety of properties. Filled pattern waxes are available in a range of low to high viscosities, can be injected in liquid or paste form, are useable with screw

and automatic injection technologies, and have a relatively low expansion.

Emulsified Pattern Wax

These waxes have a low to medium range of viscosity, with excellent surface finish properties. Emulsified wax has a low adhesive factor and therefore can easily be removed from a die cavity. These compounds are environmentally friendly due to the recycling process they offer. There are a variety of contraction rates to suit all types of investment casting applications. The properties of emulsified pattern wax are that they are available in a range of low to medium viscosities, provide good surface finish, have low die adhesion, and are useable in both liquid and paste injection processes.

Straight Pattern Wax

This wax is used where specific, specialized requirements exist. The wax range has a full spectrum of available compounds, from low viscosity to high and fast setting production materials. The main properties of straight pattern wax are that they provide good surface finish, are flexible and tough, and can be made high-strength. Their customizability is their key feature.

Specialist Wax

These compounds are used to help in the production of finished wax patterns ready for assembly. As shown below they include wax for repairing, adhesive wax, wax for forming shapes and a range of water-soluble waxes. This category includes soft and hard repair wax, adhesive wax, dip seal wax, rod wax, spiral forming wax, water soluble wax, and strong and tough waxes.

Runner Wax

Runner waxes are usually formulated with a slightly lower melting point than the pattern was in use, and with a low viscosity for easy dewaxing. Whereas virgin products are available, more often, reclaimed wax is used from the autoclave. The formulation may be straight (unfilled) or with a percentage of filler retained for improved injection, higher strength, faster setting, or with additives to adjust toughness, flexibility, melting point, rheology. These properties are typically adjusted to suit individual foundry requirements.

2.6. Composition of Investment Casting Wax [29]

Wax is the oldest thermoplastic material known to man and originally beeswax was used, but today the name 'wax' applies to any substance having wax-like properties. Modern blends of investment casting wax are complex compounds containing numerous components:

- ✧ Hydrocarbon wax
- ✧ Natural ester wax
- ✧ Synthetic wax
- ✧ Natural resins
- ✧ Synthetic resins
- ✧ Organic filler materials
- ✧ Water

Hydrocarbon wax, natural ester wax, many types of synthetic wax, and some of the resins used are compounds of straight-chained carbon atoms (aliphatic compounds).

Additionally some of the other resins and filler materials used are compounds of ring structured carbon atoms (aromatic compounds). Fundamentally, the length and the complexity of the carbon chains of the various components influence the properties of the final wax. Accordingly, many variations are formulated to suit differing foundry requirements and key properties such as melting point, hardness, viscosity, expansion and contraction, setting rate, etc are all influenced by the structure and composition of the wax compound. The complex composition of modern wax products manifests itself in a physical behavior different to that of other substances. Unlike other homogeneous chemical compounds, wax does not melt immediately on heating but passes through several intermediate states:

SOLID ↔ PLASTIC ↔ SEMI-PLASTIC ↔ SEMI-LIQUID ↔ LIQUID

Similarly, the structure and components used in an investment casting wax will influence the expansion and contraction characteristics. Like other materials, wax expands on heating and contracts on cooling, and In comparison with a metal, the expansion is relatively high. Wax expansion and contraction rates are not uniform but vary with phase and structure changes during heating/cooling. This can complicate the process of wax selection and pattern assembly design.

2.7. Materials used in shell system

With the wax pattern prepared, it is next encased in a shell that is capable of withstanding the temperatures of the molten metal. Typically, the wax is invested in a shell of a ceramic slurry, which is dried and fired to give it the necessary strength to withstand the

casting process. Important characteristics of the shell are that it must faithfully replicate the shape and surface qualities of the part, and must obviously be able to survive the casting process before it is then broken off of the solidified and cooled part.

2.8. Materials Used in Shell System

Ceramic Shell Basic Technology [30]

Definition of slurry - A ceramic bath comprised of a liquid binder and solid refractory flour(s) used to create a ceramic shell mold by applying coats, followed by stucco, to a wax pattern or previously applied shell coat.

Types of Slurry:

Primary slurry (First one or two shell coats)

- ✧ Capture the detail of the pattern
- ✧ Provide the refractory surface to cast metal against

Backup slurry (All coats after the primaries)

- ✧ Build shell strength and bulk
- ✧ Determines shell properties
- ✧ Determines shell dimensions

Primary slurry :

- ✧ Remet Ramesol® LP-BV as a water based colloidal silica binder
- ✧ Remet Adbond® Advantage Concentrate as a polymer
- ✧ Aerosol OT-75 as a wetting agent
- ✧ Burst® RSD10 as a antifoam agent (Defoamer)

Backup slurry:

- ✧ Remasol® LP-BV as a water based colloidal silica binder
- ✧ Adbond® BV Concentrate as a polymer
- ✧ Victawet® 12 as a wetting agent
- ✧ Burst® RSD10 as a antifoam agent (Defoamer)

Materials used in refractory system

Refractory selection [31]

Zircon: Naturally occurring material obtained from beach sand, zircon should be calcined to remove impurities.

Advantages of Zircon:

- ✧ Very low reactivity - Good for primary coats
- ✧ Fine particle size for good surface quality
- ✧ High strength
- ✧ Excellent rheology
- ✧ High solids loading

Alumina:

Bauxite is reduced in an electrical arc furnace whereby fused alumina is produced and impurities are removed. Typically used in two grades – Tabular (or alpha) Alumina and Fused White Alumina (FWA)

Advantages of Alumina:

Excellent refractoriness

Good strength

Limited variety of stucco sizes

Relatively high thermal expansion

Moderately expensive

Primary coat (Facecoat)

- ✧ Slurry flour: Remet® Zircon (Zirconium Silicate) flour 325-mesh blended with 200-mesh zircon flour
- ✧ Stucco: Treibacher Schleifmittel Alodur® White Fused Aluminum Oxide 70-Grit (made in germany)

Backup coat:

- ✧ Slurry flour: C-E Minerals® Fused White Alumina 325-mesh flour
- ✧ Stucco: C-E Minerals® Fused White Alumina Grit, Grain Size 14 x 28

2.9. Other Materials used in casting system

Thermocouple Protection Tubes: Quartz tubes are shown in **Figure 8 a)** and **Figure 8 b)**.

Melting crucibles: Fireline, Inc. Alumicon 4. (A4L High Alumina Surface).

Nominal Alumina content: surface 95% Alumina and body 63%Alumina-36% SiO₂.

Typical test results

- ✧ Apparent Porosity: 16-18%.
- ✧ Lead<25ppm,
- ✧ Bismuth<1ppm.

CMSX-4 Penny: CMSX-4 penny casting for pouring temperature control.

Ceramic bush: Fused silica (80 wt. %) -zircon based bush for melt flow rate control.

Typical materials used in casting system are shown in **Figure 9 a)** and **Figure 9 b)**.

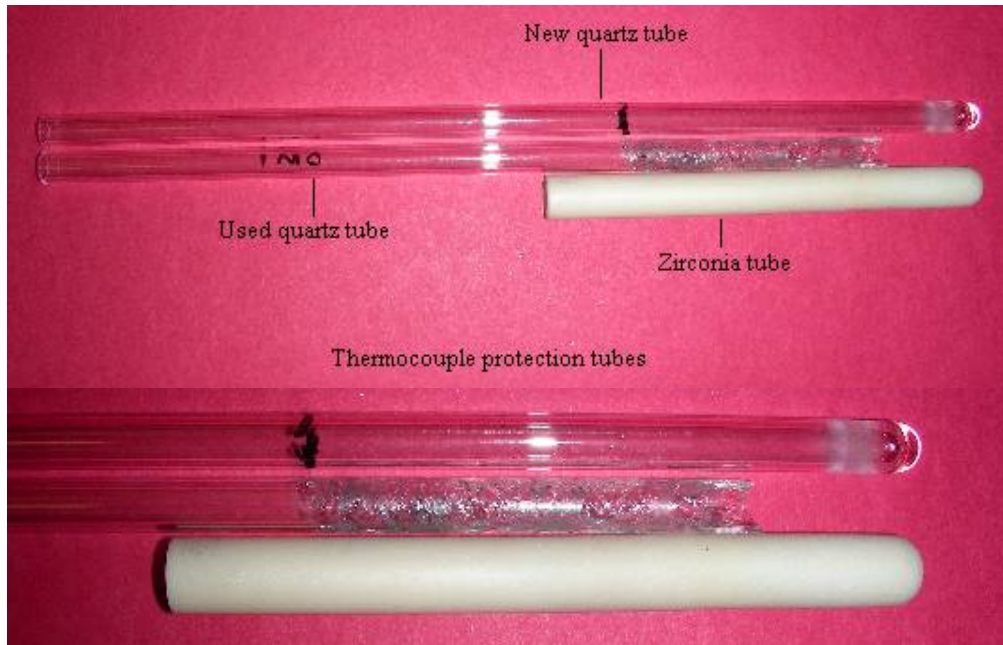


Figure 8. a) thermocouple protection Quartz tubes used in CMSX-4 castings



Figure 8. b) One thermocouple protection quartz tubes used in CMSX-4 castings

2.10. Shelling Process and Equipment

Manufacture of Ceramic Shell Molds [32]

Investment shell molds are made by applying a series of ceramic coatings to the pattern clusters. Each coating consists of a fine ceramic layer with coarse ceramic particles embedded in its outer surface. A cluster is first dipped into a ceramic slurry bath. The cluster is then withdrawn from the slurry and manipulated to drain off excess slurry and to produce a uniform layer. The wet layer is immediately stuccoed with relatively coarse ceramic particles either by immersing it into a fluidized bed of the particles or by sprinkling the particles on it from above.

The fine ceramic layer forms the inner face of the mold and reproduces every detail of the pattern, including its smooth surface. It also contains the bonding agent, which provides strength to the structure. The coarse stucco particles serve to arrest further runoff of the slurry, help to prevent it from cracking or pulling away, provide keying (bonding) between individual coating layers, and build up thickness faster.

Each coating is allowed to harden or set before the next one is applied. This is accomplished by drying, chemical gelling, or a combination of these. The operations of coating, stuccoing, and hardening are repeated a number of times until the required mold thickness is achieved. The final coat is usually left unstuccoed in order to avoid the occurrence of loose particles on the mold surface. This final, unstuccoed layer is sometimes referred to as a seal coat.

Shelling process

Wax pattern cleaning using Citriwash solution



Figure 9. a) Materials for melting operation of CMSX-4 castings



Figure 9. b) Crucible for melting operation of CMSX-4 castings

Pre-wetting using Aerosol OT-75 solution

Robotic dipping and stuccoing: one or two time for primary coating followed by rainfall stuccoing and six or seven times back-up coating followed by rainfall stuccoing. Two hours dry box drying between each layer building up. Final seal dipping with slurry only and no stuccoing followed.

Shelling equipment

A typical robotic dipping and rainfall stuccoing system for shelling of CMSX-4 castings is shown in **Figure 10**.

2.11. Shell mold dewaxing and burnout/firing process and equipment

Pattern removal and firing [33]

“Following the initial setting and air drying stages, the next operation is pattern elimination and consolidation of the bond by evaporation of the remaining volatile constituents. The importance of the early drying stages in avoiding shrinkage cracking in the primary coating has already been stressed (Shrinkage of the gelled binders during drying tends to produce cracking of the coating, a problem minimized by close control of temperature and humidity as well as by maintaining consistency in the composition and grading of both slurry and stucco materials); a further factor in cracking is expansion of the pattern on heating, which can generate significant stresses in the ceramic shells with their much lower coefficients of expansion. This problem can be overcome by rapid heating to develop a steep temperature gradient through the thickness of the ceramic shell and into the wax. Superficial melting of the pattern surface is then achieved before the

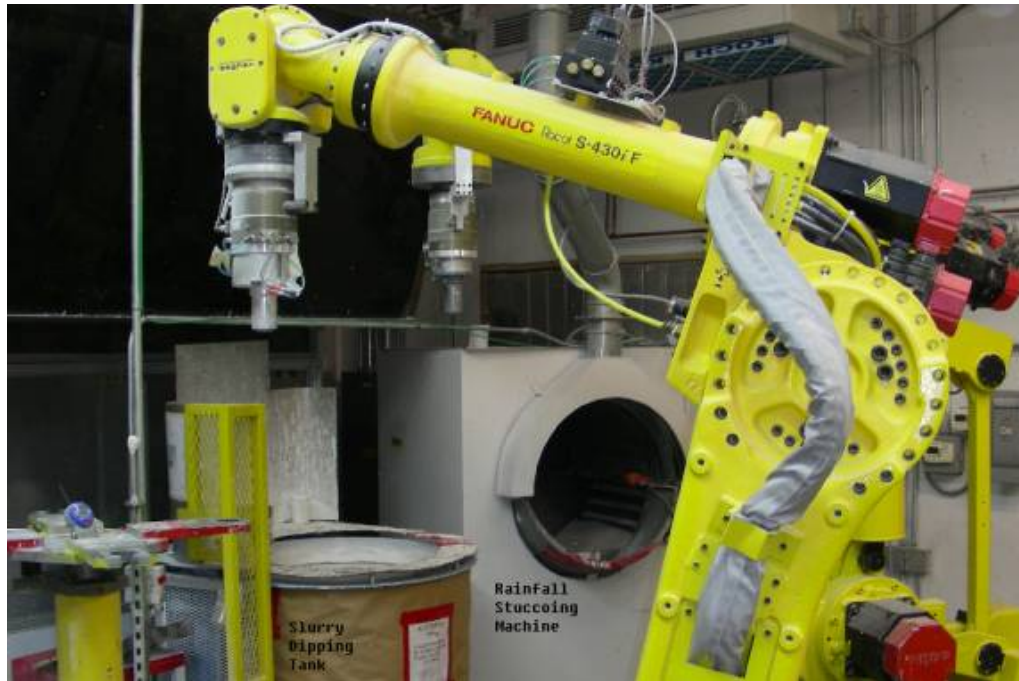


Figure 10. A robotic dipping and rainfall stuccoing system for shelling of CMSX-4 casting

main bulk of the wax undergoes applicable expansion. The molten wax film is partly absorbed by the adjacent shell (the degree of this absorption depends on its capillary attraction of the molten wax), enabling the remainder of the pattern to expand freely. Two principal techniques employed to achieve this condition are steam autoclave treatment and flash dewaxing. The autoclave system is most widely adopted: a steam pressure of several atmospheres is almost instantaneously developed in the loaded chamber and dewaxing is completed in a few minutes at temperatures below 200°C, with high wax recovery. In flash dewaxing, the temperature is raised rapidly to approximately 1000°C by placing the mould directly into the firing furnace. Wax is drained through the furnace base but recovery is lower owing to volatilization and partial combustion. Mold firing is commonly carried out at temperatures around 1000°C in either batch or continuous furnaces. The process completes the volatilization and combustion of pattern

residues and organic mould constituents and the dehydration of the binder, including elimination of combined water. Sintering contributes to the full development of strength and stability in the ceramic. The firing process thus ensures fully inert conditions for contact with the molten alloy. A further purpose in many cases, is preheating before casting to facilitate metal flow and the reproduction of intricate features, although this may be carried out as a separate operation. In general, higher firing and preheat temperatures are commonly required for molds to be subjected to directional solidification.”

Directional solidification casting process for DS and SX superalloys generally uses higher pouring temperature and mold temperature than equiax superalloys so as to gain the higher thermal gradient cooling for smaller dendrite arm spacing, better compositional and microstructural homogeneity [34, 35].

The following widely accepted relationship for primary and secondary dendrite arm spacings (PDAS- λ_1 and SDAS- λ_2 , respectively) and as a function of G and V [35]:

$$\lambda_1 \propto G^{-1/2} * V^{-1/4}, \quad \lambda_2 \propto (G * V)^{-1/3}$$

Where, **G** is Thermal gradient, **V** is growth rate or solidification front velocity.

2.12. Shell mold dewaxing and burnout/firing process

Steam autoclave dewaxing process

Steam autoclave dewaxing refers to the method of utilizing steam under pressure for removal of the wax pattern assembly from the completed ceramic shell mold. The key point is the significant difference between the low thermal expansion of the ceramic

materials and the high thermal expansion of the waxes. Successful dewaxing by steam autoclave depends on applying sufficient heat to the exterior of the ceramic shell so that a thin skin of wax is adjacent to the primary shell coat melts before the underlying bulk of the wax is heated. The molten layer will then soak into the ceramic shell progressively, allowing the wax to expand freely without distorting or cracking the shell.

Summary of the best practice of steam autoclave dewaxing [36]

- ✧ Speed - fast pressurisation
- ✧ Record autoclave performance
- ✧ Don't overload
- ✧ Handle with care
- ✧ Control depressurisation
- ✧ Train and maintain

The following is a typical process of steam autoclave dewaxing:

- ✧ Open steam cycle valve within 6 seconds
- ✧ Apply 100 psi pressure to the vessel within 10 seconds
- ✧ Maintain the steam pressure for 15 minutes
- ✧ Depressurisation shall be slowly done taking more than 5 minutes
- ✧ Drain the water and wax
- ✧ Remove the shell mold to a cooling rack

Burnout and firing process

The burnout operation follows dewaxing and is performed for removal of residual wax

and other pattern materials by combustion. Secondly, firing the ceramic shell sinters the ceramic, forming the completed shell, ready for casting in a predetermined and consistent form. Burnout and firing are performed together, in a continuous thermal cycle. The following is a typical burnout and firing process:

- ✧ Load molds with pourcup in the upright position at ambient onto clean furnace hearth.
- ✧ Heat up to 400 deg. F
- ✧ Ramp to 1200 deg. F in 1 hour and Soak at 1200 deg. F for 1 hour
- ✧ Ramp to 1800 deg. F in 2 hours and Soak at 1800 deg. F for 2 hours
- ✧ Furnace cooling down to 600 deg. F and open furnace door at or below 600 deg. F
- ✧ Remove molds at or below 400 deg. F

Shell mold dewaxing and burnout/firing equipment

A typical steam autoclave dewaxing system is shown in **Figure 11**.

A typical electric box furnace for burnout/firing is shown in **Figure 12**.

2.13. Casting process and equipment

Casting process

In the present application with CMSX-4 single crystal castings, bottom gating and tilt gating systems are used. Single crystal castings eliminate grain boundaries altogether, as parts are produced that consist of a single crystal. The current method employed to produce these castings requires stringent control of the solidification cycle and the entire investment casting process [37]. The Bridgman method, used here for single crystal blade casting, is shown in **Figure 13** [38].



Figure 11. A typical autoclave dewax system for CMSX-4 castings



Figure 12. A typical shell mold burnout/firing furnace for CMSX-4 castings

Casting parameters

The follow are the typical parameters of CMSX-4 castings

Immersion temperature: 2720-2780 deg. F

Alloy weight: 7.9-8.1lbs

Top mold temperature: 2710-2750 deg. F

Bottom mold temperature: 2710-2750 deg. F

Mold pre-heating Ramp time: 30 min.

Mold pre-heating Soak time: 30 min.

Withdrawal velocity (rate): 10 inches per hour

Chill plate base size: 6.0 inches

Casting equipment

An illustration of Bridgman directionally solidified furnace is shown in **Figure 14** [39].

This combines a self tapping induction melting unit with the facility for controlled mould withdrawal from the hot zone, the whole being maintained under vacuum or protective inert gas atmosphere throughout melting and solidification. A typical argon atmosphere Bridgman single crystal casting furnace for CMSX-4 casting is shown in **Figure 15**.

2.14. Heat treatment process and equipment [40]

Single-crystal nickel-based superalloys are known for their high strength and creep resistance at high temperatures. These alloys are used extensively in the aerospace industry for turbine blades and vanes in the “hot section” of today’s gas turbine engines. While these properties depend largely on the alloy composition, they also rely on proper heat treatments to bring out these exceptional properties. Traditionally, two heat

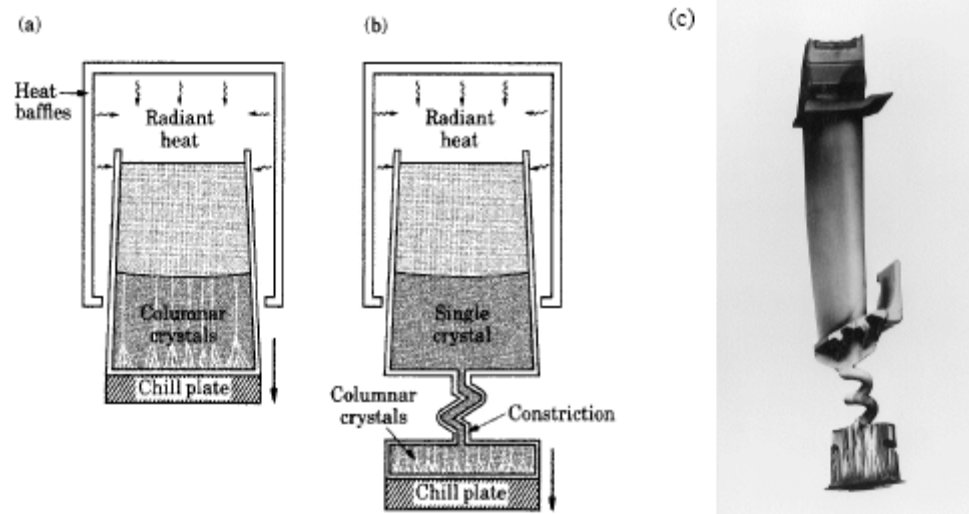


Figure 13. Methods of casting turbine blades:
 (a) directional solidification;
 (b) method to produce a single-crystal blade; and
 (c) a single-crystal blade with the constriction portion still attached.

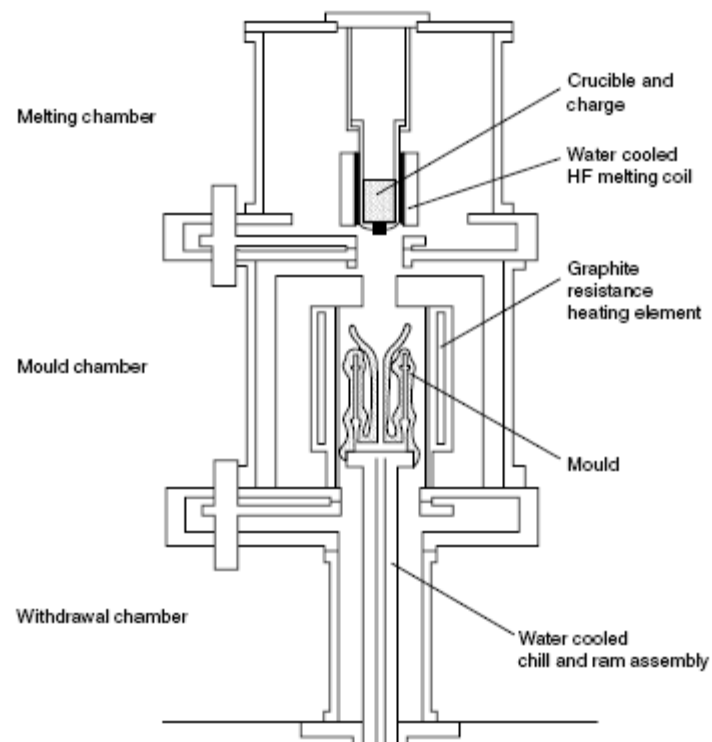


Figure 14. Main features of Rolls Royce production unit for manufacture of directionally solidified gas turbine blades (courtesy of Rolls Royce plc)

treatments are used for nickel-based superalloys. First is the solution heat treatment, designed to homogenize the microstructure and reduce the effects of elemental segregation. The second is one or more aging heat treatments, designed to develop a cuboidal γ/γ' microstructure.

As-cast CMSX-4 is highly segregated, which is a large contributor to the need for a solution heat treatment. Average compositions of as-cast CMSX-4 Dendritic Pattern and Partitioning Coefficients (in wt. %) are shown in **Table 3** Photomicrographs of as-cast CMSX-4 are shown in **Figure 16**.

Solution heat treatments, though long and expensive, are required to achieve the desired microstructure (and attending properties). Following the standard solution heat treatment, the microstructure becomes very uniform. The γ/γ' eutectics have been dissolved and a fine γ' (Approx. 0.3 – 0.5 microns) phase is apparent throughout the microstructure. Once the solution heat treatment is completed, the aging heat treatment is performed. Aging serves to slightly coarsen the γ' to 0.5 micron in size and to form the very uniform, cuboidal structure often associated with γ' . Photomicrographs of heat-treated CMSX-4 are shown in **Figure 17**.

Heat treatment process

The following is the typical heat treatment process:

Vacuum level: 5×10^{-4} mm Hg

Inert gas (argon) atmosphere: Inert gas (argon) partial pressure: during heat up and hold cycles shall be 750 microns Hg.

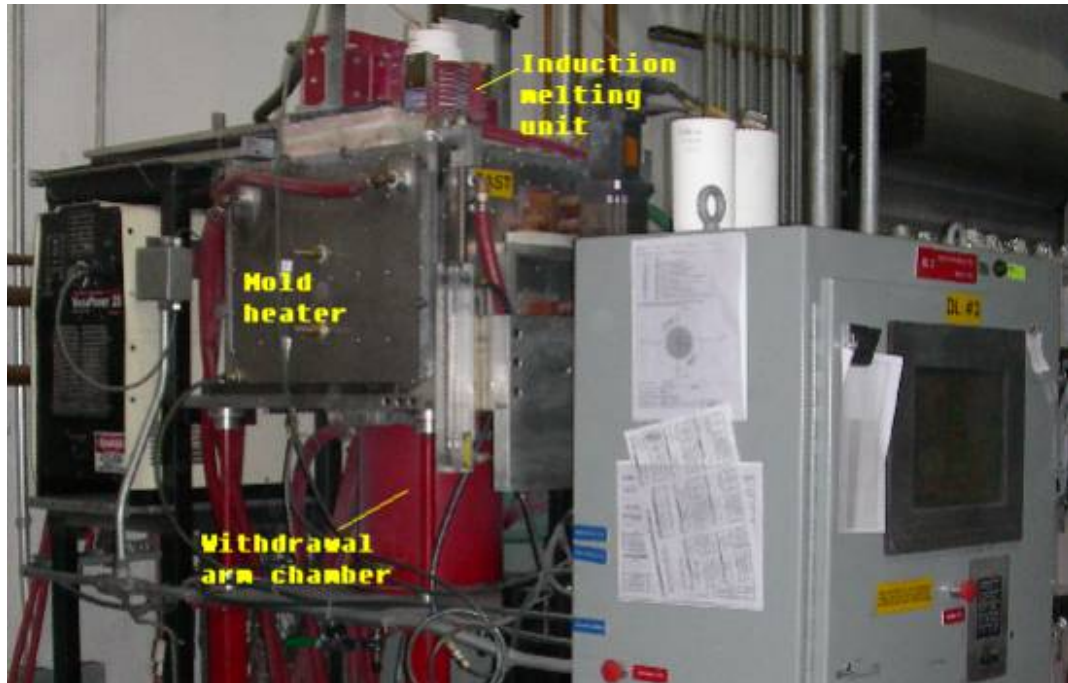


Figure 15. A typical argon atmosphere Bridgman single crystal casting furnace

Inert gas (argon) Dew Point: Inert gas dew point shall be -60 deg. F (-51 deg. C).

Solution heat treatment: From 60 deg. F ramp to 2250 deg. F using about 84 minutes, from 2250 deg. F ramp to 2300 deg. F using 25 minutes, 2 hours soak at 2300 deg. F, from 2300 deg. F ramp to 2320 deg. F using 20 minutes, 2 hours soak at 2320 deg. F, from 2320 deg. F ramp to 2350 deg. F using 5 hours, 10 hours soak at 2350 deg. F and gas fan quench at cooling rate 100 deg. F/minute, γ' size should be $0.3-0.5$ microns and γ/γ' eutectic shall be less than 5%. Parts shall exhibit no more than one percent incipient melting in airfoils. If pore size is greater than 0.0016 inch (40 microns), Hot Isostatic Pressing (HIP) process may be necessary.

Aging heat treatment: 2 hours soak at 2085 deg. F and gas fan quench for primary age, 20 hours soak at 1600 deg. F and gas fan quench for second age.

	Ni	W	Re	Al	Ti	Ta	Co	Cr
Average Composition	61.42	6.40	2.90	5.64	1.03	6.60	9.60	6.40
Dendrite Core	60.06	7.91	5.82	4.94	0.59	4.23	10.34	6.10
Interdendritic Area	61.94	5.86	3.63	5.71	0.92	6.23	9.79	5.94
Eutectic Area	61.64	4.67	2.87	5.61	1.18	6.93	10.07	7.03
Partitioning Coefficient	0.97	1.69	2.03	0.88	0.50	0.61	1.03	0.87

Table 3. Average compositions of as-cast CMSX-4 dendritic pattern and partitioning coefficients (in wt. %)

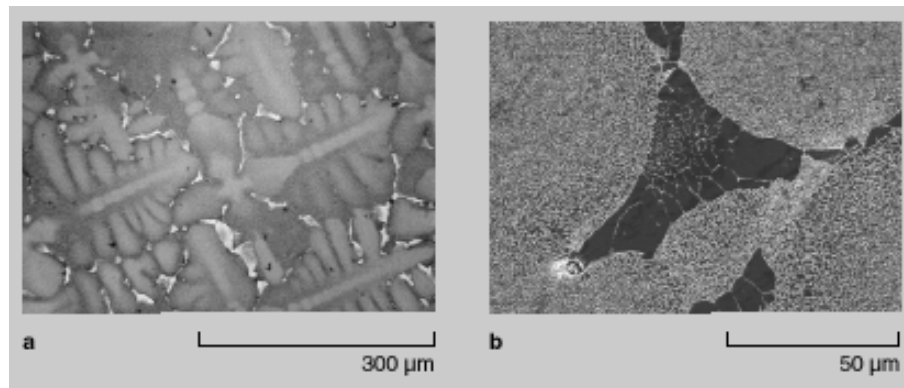


Figure 16. Photomicrographs of as-cast CMSX-4. (a) Optical micrograph of dendrites with secondary and tertiary arms extending from the primary dendrite, as well as γ/γ' eutectic areas in between. (b) Scanning-electron micrograph of coarsening γ/γ' morphology approaching the eutectic region in the center. A dendrite core can be seen to the left of the image.

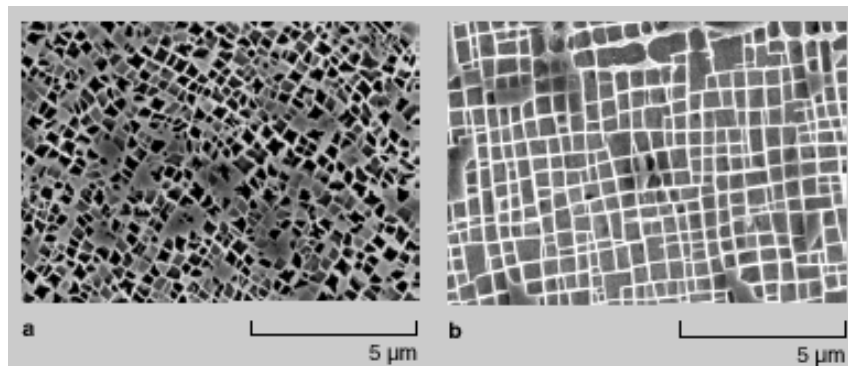


Figure 17. Scanning-electron micrographs of CMSX-4 following the standard solution heat treatment. (a) Prior to aging, γ' irregular in size and shape. (b) Following aging, γ' has coarsened and become more regular.

Heat treatment equipment

A typical vacuum solution heat treatment furnace is shown in **Figure 18**.



Figure 18. A typical vacuum solution heat treatment furnace for CMSX-4 castings

2.15. Surface finishing process and equipment

The surface finishing process is needed for removal of the metal-mold reaction layers after heat treatment operation. Abrasive water jet (Hydrogrit) is used firstly on the whole surface of the casting; pressure (grit) blasting is needed when the abrasive water jet (Hydrogrit) result is failed.

Surface finishing process

Abrasive water jet (Hydrogrit)

Water pressure: 20000 psi.

Abrasive grit: 220 grit of garnet abrasive grains [(Fe, Mg)₃ Al₂(SiO₄)₃] from Barton Mines Company, L.L.C.

Processing time: 7-28 minutes.

Thickness removed: 0.003-0.006 inches per operation

Rework: No rework of abrasive water jet is allowed due to the risk of over removing surface materials.

Pressure (grit) blasting

Pressure (grit) blasting: Cold etches to verify all surfaces are clear of metal-mold reaction layers, if not, grit blasting will be used to clear the rest ones.

Pressure of grit blasting: 60-80 psi

Abrasive material for pressure blasting: Aloblast® 220grit, brown aluminum oxide abrasive in grain.

Surface finishing equipment

A typical abrasive water jet (Hydrogrit) machine is shown in **Figure 19**.

2.16. Inspection, analysis and test methods and equipments

The following are the some of inspection, analysis and test methods and equipment for CMSX-4 castings:

Raw materials inspection

A full chemical analysis both on ingots and casting bars of the as-received CMSX-4 is

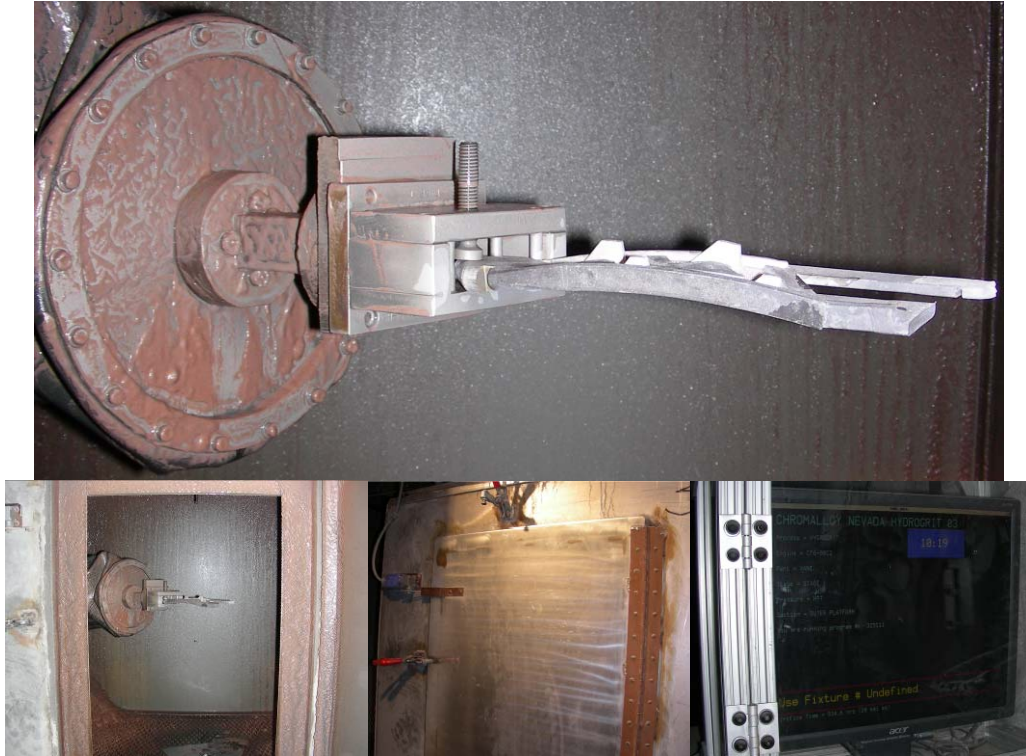


Figure 19. A typical abrasive water jet machine for metal-mold reaction layer removing

performed using the following techniques:

- ✧ XRF for **Ni, Cr, Co, and Mo** elements;
- ✧ GDMS (Glow Discharge Mass Spectrometry) for **trace elements**;
- ✧ DCP (Direct Current Plasma) for **Al, Ti, Re, W, and Ta** elements;
- ✧ IG (Inert Gas Fusion) for **O and N** elements;
- ✧ CO (Combustion-Leco) for **C** element.

CMSX-4 master heat qualification through a stress rupture test:

Temperature: 2000 deg. F (1093 deg.C)

Stress: 23000 psi (159 MPa)

Minimum life: 19 hours

Production monitoring and casting qualification

- ✧ Innov-X portable handheld XRF (X-ray Fluorescence Spectroscopy) analyzer for alloy identification;
- ✧ Leco TC500 for Oxygen and nitrogen analysis;
- ✧ Leco CS600 for Carbon and Sulfur analysis;
- ✧ PerkinElmer AA (Atomic Absorption) -Analyst800 for Bismuth analysis;
- ✧ Laue X-ray radiography test for grain structure inspection;

Metallographic inspection:

✧ **Metal -mold reaction**

Surface attack: None allowed on gas path surface. Internal and non-gas path surfaces may exhibit local areas of metal-mold reaction up to 0.001 inch maximum depth provided that they have met all the nondestructive test requirements of the drawing. All such areas shall be required.

Carbide oxidation: For cobalt base alloys carbide oxidation up to 0.005 inch is permitted, for nickel base alloys up to 0.0005 in depth is permitted [41].

- ✧ **Dendrite arm spacing** shall be determined using the Buehler Omninet imaging software or Scanning electron microscope (SEM): average distance between dendrites shall not exceed 450 microns.
- ✧ **Incipient melting and unsolutioned primary γ/γ' eutectic** examination (50-100 X)

Fluorescent Penetrant Inspection (FPI): Micro shrinkage up to 0.125 inch diameter allowed.

X-ray Radiographic inspection:

- ✧ **Sponge and dendritic shrinkage** shall not exceed that of ASTM E192 plate number 1 for 1/8 inch wall thickness for all section of the casting.
- ✧ **Linear shrink indication** shall not exceed that of ASTM E192 plate number 1 for 1/8 inch on or directly adjacent to the airfoil/platform fillet radius and shank.

2.17. Contributions of this Work

The main contributions of this thesis are:

- ✧ First time systematically review the literatures about metal-mold reaction issues.
- ✧ First time applied yttria aerosol spray coating before normal primary coating to identify the root cause of CMSX-4 metal-mold reaction problem.
- ✧ First time perform surface analysis on both CMSX-4 castings and ceramic shells to identify the nature of metal-mold reaction of CMSX-4 castings.
- ✧ First time systematically discuss the mechanisms of CMSX-4 metal-mold reaction layer formation and the reaction layer hardening after solution heat treatment.
- ✧ First time point out the potential problems induced by CMSX-4 metal-mold reactions.

3. Literature review

3.1. Definition of metal-mold reactions

The term of metal-mold reaction [16, 42-50] also was called as metal-mold/core reaction [51, 52] mold-metal reaction [53-57], or metal/ceramic reaction [58].

Surface reaction layer or oxide layer sometime was called as scale [57, 58, 59, 60, 61].

Metal-mold reaction phenomena commonly exist in magnesium alloy, aluminum alloy, titanium alloy, cast iron, steel and superalloy castings.

Many researches about metal-mold reaction were performed and reported, trademarked and patented, but some of them such as **CMSX-4**, **René N5**, and **PWA 1484** single crystal superalloy castings were still regarded as proprietary.

Due to the high temperatures and long times in the liquid state, **metal-mold reaction** is a big area of concern in the single crystal casting process. This is especially important in Lamilloy® cooled airfoils where fine casting details is mandatory. Surface mold reaction has not been observed with **CMSX-4** parts with SCO (Allison production facilities) facecoats. A small amount of reaction with conventional single crystal core material is typically seen. However this reaction is less than 0.0025mm (0.001 inches) in depth and within specification (**Figure 20**). SCO 's CastCool® method of casting lamilloy cooled airfoils uses a core that does not react with **CMSX-4** during the casting process [16].

Single crystal (SC) blades were initially put into commercial service in 1982 in Pratt & Whitney's engine for the Boeing 767 aircraft and the Airbus A 310 (alloy **PWA 1480**).

Lamilloy® and CastCool® are registered trademarks of Allison Engine Company

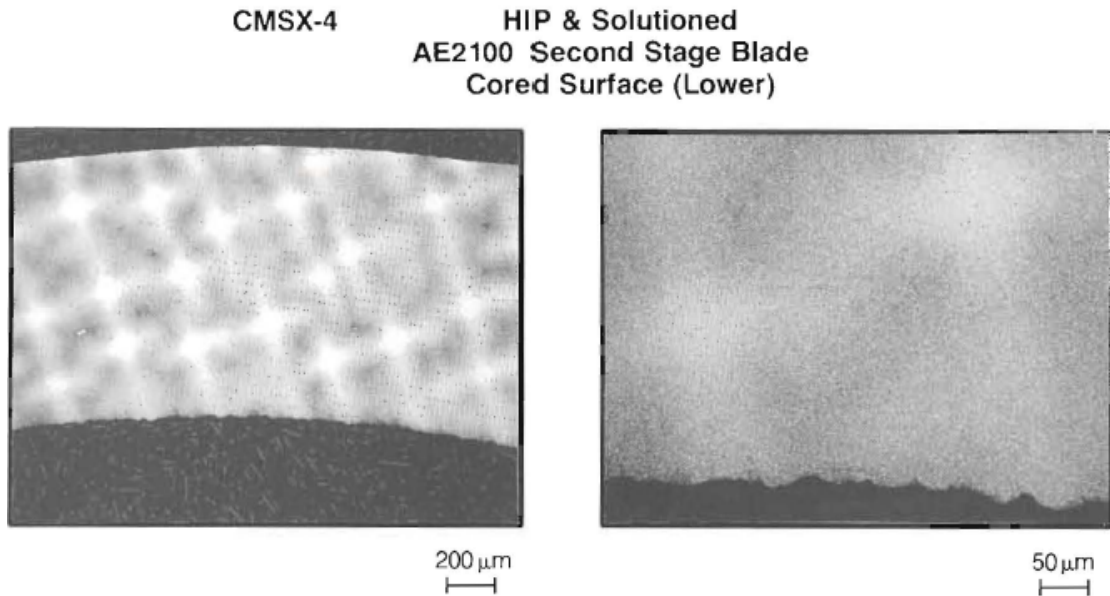


Figure 20. Metal core reaction of CMSX-4 casting

Howmet, a leading producer of SC casting for aircraft components has shipped more than 10,000 single crystal castings. All major aircraft engine manufacturers have developed and applied new SC alloys in recent years. The only use of SC alloys in land-based turbines until recently has been the use of **CMSX-4** alloy in Solar industrial turbine Mars T-14000 engine in 1990. Single crystal alloy blades made of **PWA1483** are currently in use in Siemens V84/94.3a GTs. Alloy **René N5** has found a place in GE 7H turbines as first row blading. Pallotta has reported on a Westinghouse development of a SC alloys and has shown properties but without the composition. At the time the Westinghouse DS alloy was reported to have a temperature capability of more than 50% greater than Inco 738LC and the SC alloy has a capability 100% greater.

Some of the key improvements needed in SC technology are as follows.

- ✧ Current SC alloys are too low in Cr and not hot corrosion resistant enough.
- ✧ Large thermal gradients (7EC/mm) are needed in the casting process because of the

large size. Insufficient gradients lead to

- Casting defects such as equiaxed grains, freckles, low angle boundaries;
 - Porosity and reduced fatigue strength;
 - Large dendrite spacings which are difficult to solutionize. Lower growth rates can counter these effects, but decrease output and increase cost.
- ✧ Need to cast single blades gives low throughput.
- ✧ To accommodate large gradients, high superheat temperature ($> 1500\text{EC}$) and **metal-mold reactions**-casting parameters need to be optimized.
- ✧ Need defect acceptance criteria.

In summary, cost effective, high quality SC manufacturing technology is needed [62].

3.1.1. General definition of metal-mold reactions

Metal-Mold Reaction, Orange Peel and Alligator Skin:

Metal-mold reaction is under the defect surface category in the International classification of common casting defects (**Table 4**)


No.	Description	Common name	Sketch
Defective Surface			
D 130:	Grooves on the casting surface		
D 134	Casting surface entirely pitted or pock-marked	Orange peel, metal mold reaction, alligator skin	

Table 4. International classification of common casting defects about metal-mold reaction [48]

This is a defect where areas of the casting are covered with hollow blemishes resembling

an orange peel (**Figure 21**) Dimensions of the blemishes may vary according to the severity of the condition. They are larger on thick heavy sections.

Possible Causes: Improper casting parameters (everything too hot and too fast). This can also be caused by substandard investment at the casting surface [63].

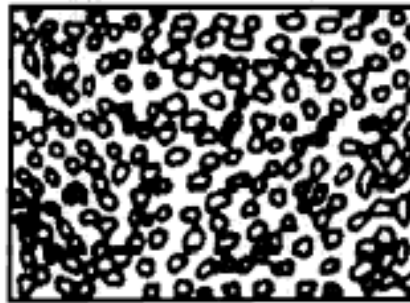


Figure 21. Metal-Mold Reaction, Orange Peel and Alligator Skin

3.1.2. Specific definition of metal-mold reactions

Definition of metal-mold reactions for investment cast turbine blades and vanes

Metal-mold /metal-core reaction: An oxidation reaction of the alloy and the mold or core materials characterized by a metallic oxide layer or by intra-carbide oxidation of the carbide rich phase as the mold/core interface [51, 64].

Definition of metal-mold reactions for René 220 castings

Metal –mold reaction: An affected layer at the cast surface of intra or intergranular attack [65].

Definition of metal-mold reactions for René N4 and René N5 castings

Metal –mold-reaction: A condition wherein, at metal solidification temperatures, the mold or core materials react with the surface of part through an oxidation process. It may be characterized by an affected layer, usually consisting of discrete oxide particles, at the

surface. It may also be characterized, as is frequently the case in cobalt base alloys, by intracarbide oxidation. Intracarbide-carbide oxidation is preferential attack of carbide phases at or near surface [66, 67, 68].

3.1.3. Definition of metal-mold reactions of CMSX-4 castings

Metal-mold reaction/metal core reaction: A result of aluminum reaction with the SiO₂ binder in the mold. This generates the Al₂O₃ + Si which can form a eutectic phase beneath the Al₂O₃ layer. This phase is observed after heat treatment [52].

Metal-mold reaction: The metal-mold reactions occur between the active elements in the alloy and reactive elements in the shell. The alloy element which usually reacts with the shell is **aluminum** and can form an **aluminum silicate** with the **silica** in the shell. Silica is the binder compound in the slurry. The higher the **mold temperature** and the **silica binder content** in the shell, the higher metal-mold reaction tendency. In extreme cases this reaction can cause a **hard layer** at the surface of the casting which is difficult to remove [69].

3.1.3.1. Is eutectic layers caused by metal-mold reaction?

The typical metal-mold reaction layers were shown in **Figure22 a)** and **Figure22 b)** [10]

The external surface eutectic layers were measured as the metal mold reaction layers in this report.

G. BREWSTER, H.B. DONG, N.R. GREEN, and N. D'SOUZA have studied some aspects pertaining to the formation of surface eutectic at the external casting surface during directional solidification of a typical Ni-base superalloy, CMSX10N. From a systematic characterization of the extent of coverage of the surface eutectic layer as well

as the morphology we have examined some of the possible mechanisms that could account for the experimental investigations. Mechanisms relating to mold/metal interaction and the primary dendrite inclination with the mold wall can be discounted. A most likely mechanism relates to the latter stages of solidification when the interdendritic liquid is in contact with the mold wall. Lateral solid contraction accompanied by local interdendritic liquid flow to compensate for this contraction can lead to increased microsegregation ahead of the advancing secondary dendrite arms leading to the formation of surface eutectic at the external casting surface [70]. **Figure 23** showed surface eutectic layer of CMSX-10N [70].

3.1.3.2. Possible chemical reactions in the metal-mold reactions

Classification of Mold-Metal Reactions in Investment Castings

1. $M_xO_y = xM(\text{dissolved}) + yO(\text{dissolved})$
2. $M_xO_y + zMA(\text{dissolved}) = MA_zO_y(g) + xM(\text{dissolved})$
3. $M_xO_y + zMA(\text{dissolved}) = MA_zO_y + xM(\text{dissolved})$
4. $M_xO_y + zMA(\text{dissolved}) = MA_zM_{x-w}O_y + wM(\text{dissolved})$
5. $M_xO_y = xM(g) + yO(\text{dissolved})$
6. $M_xO_y = M_xO_y$ where

M_xO_y = an oxide; MA= an element in the alloy

Reaction 1 describes the dissolution of shell material into the liquid metal. For instance

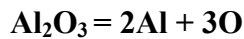




Figure 22.a) A typical metal mold reaction layer on the CMSX-4 airfoil casting



Figure 22.b) A typical metal mold reaction layer on the CMSX-4 platform casting

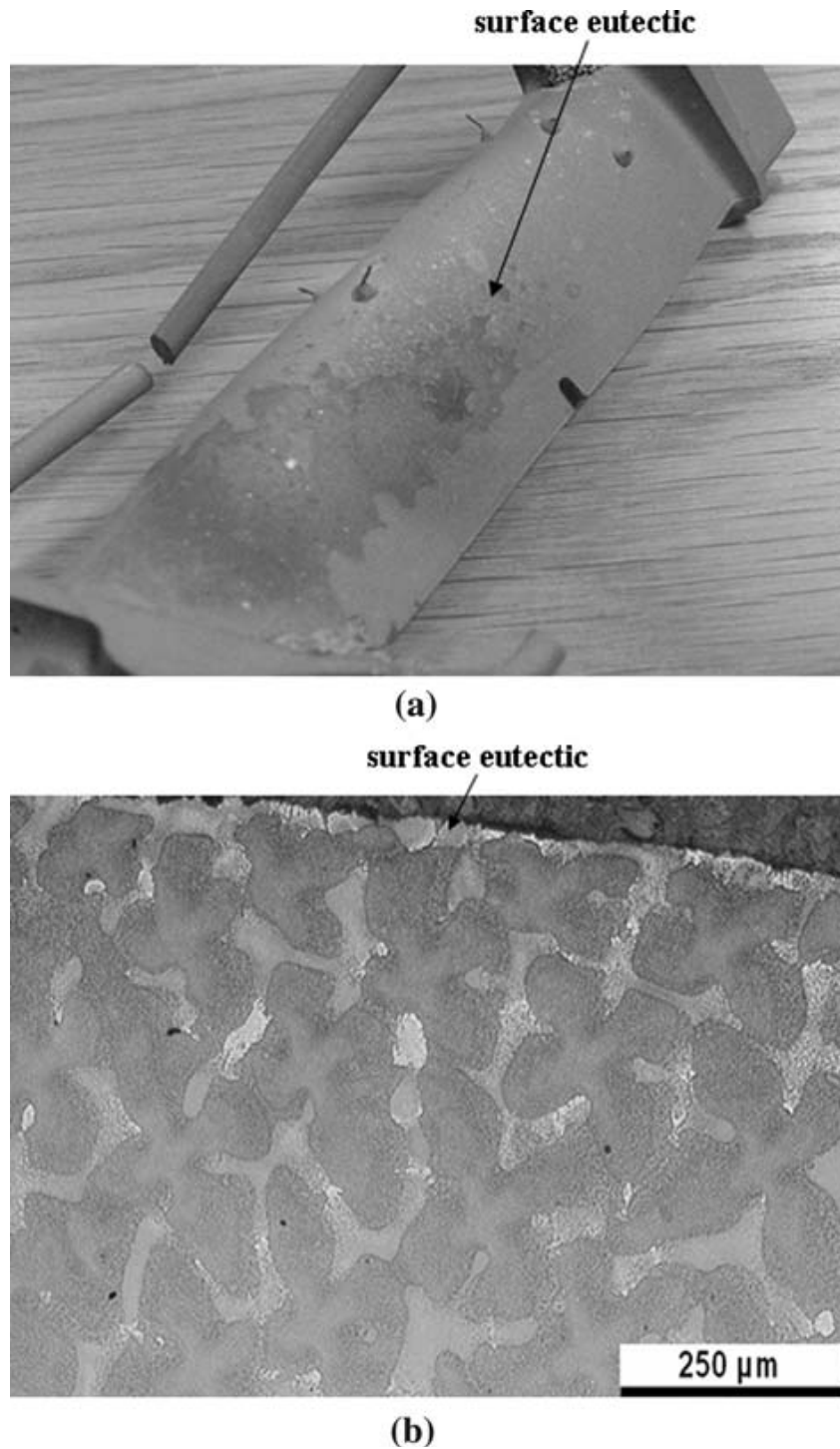


Figure 23. Surface eutectic layer of CMSX-10N

If titanium is melted in an **alumina crucible**, substantial amounts of oxygen and aluminum metal dissolves into molten titanium regardless of the fact that the ΔG of

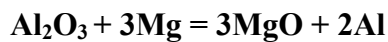
alumina is more negative than that of TiO_2 . The reason for this is the formation of sub-oxides. The ΔG for the formation of sub-oxides of titanium (i.e. TiO) is more negative than the ΔG of alumina.

Reactions 2, 3, and 4 characterize the reaction of the molten metal with the mold.

An example of reaction 2 is the rapid decarburization of NiTaC alloy based on the following reaction



Reaction 3 involves reduction of the mold by the metal to form another metal oxide. For example:



Another good example is the reaction between **Ti, Al, or Hf in superalloys** with the **mold oxides**. The above reactions normally produce thin layers of molten metal oxide at the metal-mold interface. Such interfacial reactions are commonly stable and may be beneficial for the cast part by hindering further reactions between mold and the molten metal. Another example of reaction 3 is the reaction between the titanium and the mold oxides in molten titanium alloys to form TiO or TiO_2 . The above oxides are frequently not seen because these oxides dissolve rapidly in the molten metal.

The primary parameters, which influence the formation of the alpha case on the exterior surface of cast titanium are related to the strong affinity of titanium to oxygen. The sources of oxygen include:

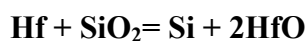
- a. Initial oxygen content of the melt.
- b. The oxygen picked up by the metal as it travels through the gating system.

c. Oxygen picked up from the furnace atmosphere. This is negligible in vacuum melting.

d. The oxygen dissolved from the mold when the metal comes to rest in the casting.

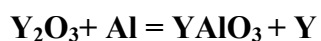
According to Piwonka, only the last is of significance. When the molten metal comes to rest there is no oxygen gradient in the metal. However, as the metal lies against the mold surface, the mold dissolves in the molten titanium alloy, and oxygen begins to diffuse into the casting. Even if titanium reacts with some mold elements, such as silica, to form TiO_2 , as the free energy of formation of TiO_2 is more negative than that of SiO_2 , TiO_2 is also soluble in the molten titanium (13), little TiO_2 is found on the surface of the casting.

Molten metal reacts with the mold: The actual reaction of molten metal with the mold material may also occur but it is rare. What is usually considered to be a mold/metal reaction is actually often a reaction with the atmosphere in the mold. However the **titanium** and **aluminum** in **superalloys** can react with the **silica** in the mold to form a thin reaction layer at the interface. Also Hf in superalloys may react with molds and cores.



Hf reacts also with zirconia to form hafnium oxide. The formation of hafnia is good for the quality of the castings; as it is stable it can stop further reactions between metal, mold and core.

Molten metal may form double oxides with the mold material as shown in reaction 4. An example is the reaction between Al and rare earth oxides:



The ΔG of rare earth oxides is normally more negative than the ΔG of alumina. Therefore the ΔG of double oxides comprised of alumina and a rare earth oxide are more negative than those for pure Al_2O_3 . This explains why the molten Al is more reactive with rare earth shell molds than it appears to be on the basis of the single oxide ΔG data [53].

Figure24 showed standard free energy of formation of oxides (at room temperature) vs oxide melting point. MgO and Y_2O_3 are among the most stable oxides (very large negative values for $\Delta G_{f,298}^\circ$) [53].

3.1.3.3. The wettability of ceramic materials by liquid metals

The efficiency of coatings or washes can be addressed to decreased wettability and to the higher bulk density of the mold surface. Wettability is enhanced by the addition of impurities in the liquid in several systems. For instance, oxides of transition metals such as Ta_2O_5 can be added to glass to increase the wettability when coating stainless steels with glass.

Some refractories are known to be “non-wettable” by definite metal alloys. This is a useful property when the refractory is used as a melting crucible. For instance, (contrary to alumina crucibles), zirconia crucibles are not wetted by nickel-base superalloys. This increases crucible life [53].

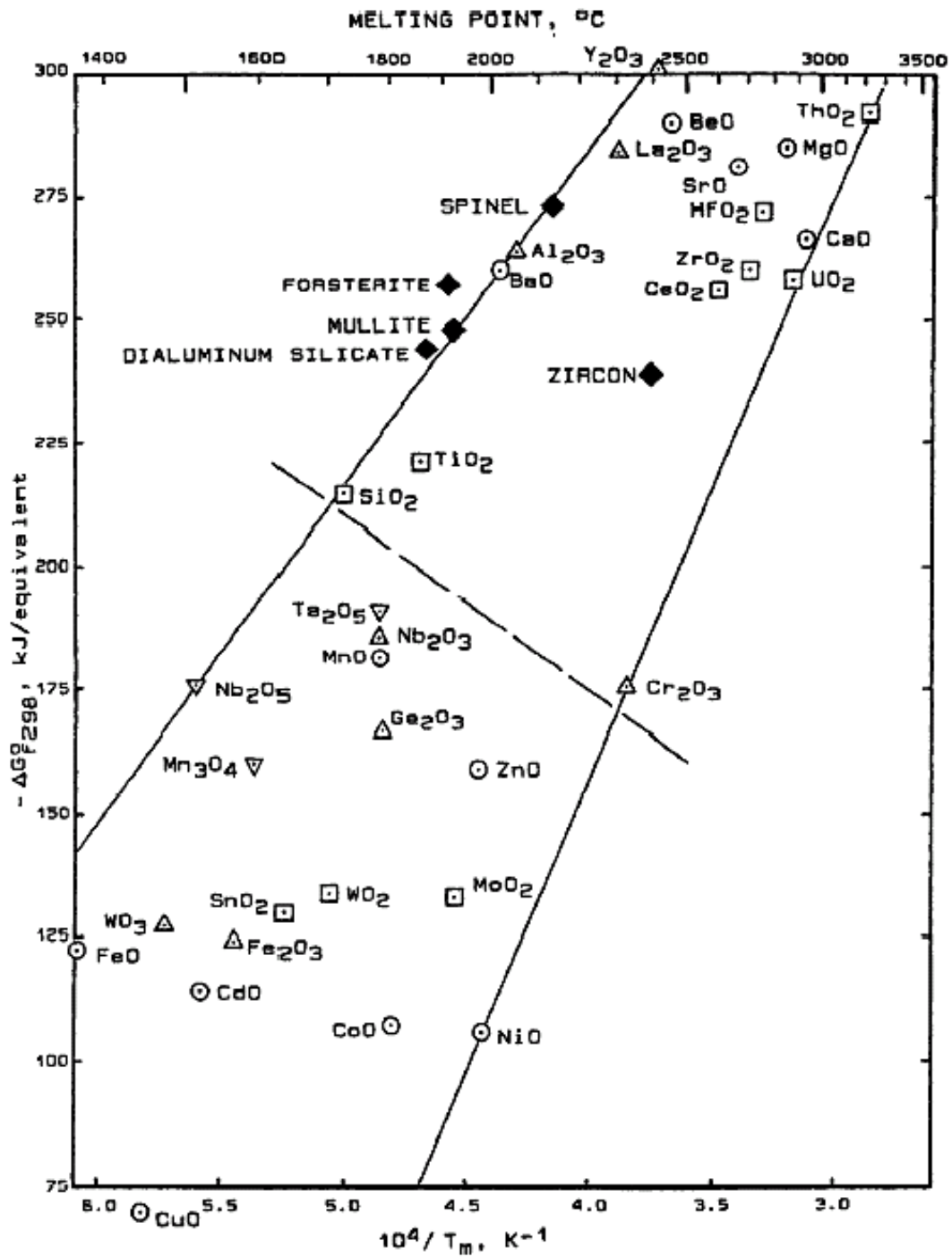


Figure 24. Standard free energy of formation of oxides (at room temperature) vs oxide melting point. MgO and Y₂O₃ are among the most stable oxides (very large negative values for $\Delta G_{f,298}^{\circ}$) [53]

3.1.3.4. Possible defects induced by metal-mold reaction

One or more of the following defects might be caused by metal mold reactions:

- ✧ **Defective surface** [48]
- ✧ **Alloy depletion** [58]
- ✧ **Gases defects**

Gases may be present in castings in solution, as chemical compounds or as included cavities: the latter are the true gas defects. The gas may result from entrapment of air during pouring, from evolution on contact between liquid metal and molding material, or may be precipitated during solidification as a result either of **chemical reaction** or of a change in solubility with temperature.

Defects take the form of internal blowholes, surface blows, airlocks, surface or subcutaneous pinholes or intergranular cavities, depending upon the immediate cause.

The gaseous origin is frequently evident from rounded contours but in some cases the shape of the cavity is governed by other factors: in the case of intergranular porosity, for example, concave walled cavities can result from constraint by solid–liquid interfaces existing at the time of precipitation.

Other defective conditions include **embrittlement** and **cracking** following retention of gases in solution in the solid state; the occurrence of gas–metal compounds as solid **inclusions** has been referred to in an earlier section.

Gases also affect the distribution of **shrinkage cavities** and **segregates** in castings. The present discussion will, however, be concerned mainly with specific defects rather than with more general influences of gas content.

Although the causes of the defects vary widely they may be conveniently considered in two main groups roughly analogous to those already used for non-metallic inclusions: those caused by physical entrapment on pouring and those resulting from precipitation by the metal on cooling [71].

Figure 25 showed a CMSX-4 casting with metal mold reaction and gas hole defect.

✧ **Inclusion defects**

Higher temperatures and longer holding times at temperature increase the possibility for reaction and the production of inclusions associated with refractory wear and erosion.

Therefore, melt overheating, especially for long periods of time, is to be avoided.

The scale on scrap surfaces can also lead to refractory erosion and exogenous inclusions.

Rust or ferrous scrap can be considered a hydrated iron oxide that, when heated and dehydrated, can form low-melting complex oxides with the refractories.

Inclusion difficulties have also been known to increase when adhering mold materials remain on charged revert scrap.

The severity depends on the nature of the mold-bonding agent; bentonite and organically bonded mold materials would display different tendencies toward refractory attack.

The above observations can be applied to reaction between the mold materials and the molten metal. This is not to be confused with metal penetration, in which molten metal merely fills the void spaces between grains of the mold material.

However, the solution to the problem--for example, a **mold wash**--may be the same. In this case, the wash fills the voids between sand grains and isolates the mold material from contact with a potentially aggressive molten metal or oxide.

Longer solidification times merely increase the possibility for **mold-metal reaction** and

the accompanying inclusion-forming tendency [57].

E.g. the addition of Hf to high strength cast superalloys is used to combat DS grain boundary cracking problems, with levels of 2% and greater being common. Increasing levels of Hf, unfortunately, increase component rejection rate and quality assurance problems due to the occurrence of **HfO inclusions** in the DS components usually resulting from **Hf/ceramic core/shell reactions** [72].

✧ **Grain defects**

Grain defects will increase with the increasing of inclusions level.

Figure 26. Showed a CMSX-4 casting with metal-mold reaction and secondary grain defects.

✧ **Hot tears**

The occurrence of hot tears is influenced by three factors, namely alloy composition, the design of the individual casting and foundry technique [73].

Metal-mold reaction may increase Si level in the superalloy. High Si content in nickel base superalloys may cause hot tear defect [72, 73].

CNV Specification of CMSX-4 requires low-level Si content: 0.04 Wt % Max. [52].

Figure 27 Showed a CMSX-4 casting with metal-mold reaction and hot tears defects.



Figure 25. CMSX-4 SX casting with metal mold reaction and gas hole defect.

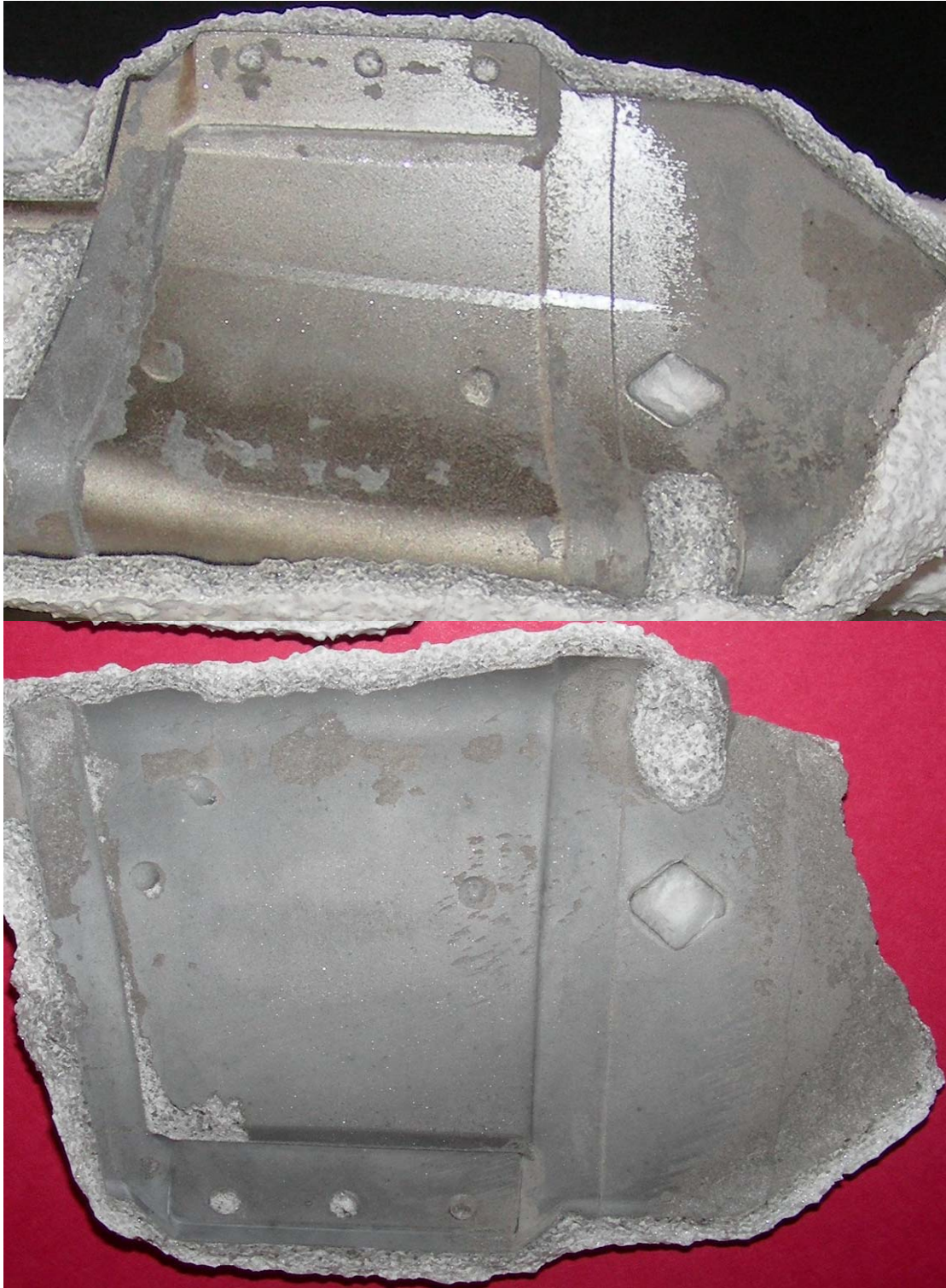


Figure 26. CMSX-4 SX casting with metal mold reaction and secondary grain defect



Figure27. CMSX-4 SX casting with metal mold reaction and hot tears defect

✧ $\text{Mo}(\text{Ni}, \text{Si})_2$ Laves phase formation in the Mo containing alloys [75]

CMSX-4 superalloy contain nominal 0.60 Wt % Mo, so Si contamination is still a risk of forming $\text{Mo}(\text{Ni}, \text{Si})_2$ Laves phase.

✧ **Metal losses and lack of filling defects**

Molten metal react with crucible and gating system will increase the metal losses and it may cause the lack of filling defects.

3.1.4. Some important definitions related metal mold reaction

For investment cast turbine blades and vanes

Alloy depletion: A change in microstructure of the alloy resulting from a depletion of one or more elements [51].

Intergranular attack (IGA): Corrosion or oxidation attack concentrated at the grain boundaries.

For René N4 and René N5 castings

Alloy depletion: A condition at or adjacent to the surface of a part wherein the material is deficient in one or more elements of its normal composition.

Alloy layer: Surface contamination of parts, visible as a resolidified layer.

Carbide layer: Carburization of surface during heat treating.

Freckles: A chain of small surface grains generally aligned parallel to the growth direction.

Interdendritic attack (IDA): A form of corrosion or oxidation attack in which preferential reactions are concentrated at interdendritic regions of the part. The condition can be aggravated by the subsequent attack of the oxidized material by chemical enchants.

Slivers: narrow grains of high reflectivity which often parallel the growth direction [63].

3.2. Test procedure of metal/ceramic reaction

Investment Casting Institute establishes a test procedure of metal/ceramic reaction:

Some information of this procedure is shown below:

Scope: This procedure applies to any ceramic that comes in contact with molten alloy including ceramic cores and shell mold.

Purpose:

The purpose of this test is to determine the degree of reaction between a ceramic material and metal under casting conditions.

A casting trial pour where the test ceramic is subjected to the actual production metal pouring environment, is the best practice for reaction product testing. There are a variety of reaction conditions to look for including **alloy depletion**, **inter carbide oxidation**, and reaction layers thickness [59].

3.3. Chemical properties of CMSX-4 superalloy

3.3.1. Oxidation behavior of CMSX-4 superalloy

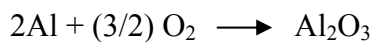
Superalloys are naturally protected to a certain extent by the formation of impermeable stable oxides, such as Cr_2O_3 or Al_2O_3 . In general, the higher the γ' volume fraction, the lower the chromium content of the alloy and the higher that of aluminium. Where necessary, the oxidation resistance can be improved by the use of coatings. The kinetics of alumina formation is considerably slower than those for chromia, so that higher temperature is necessary to obtain a layer of significant thickness.

The highest oxidation resistance is apparently obtained in CMSX-4 alloy and the lowest

in MC2. (in 1st to 3rd generation SX superalloys) In general, a high W/Ta ratio and high contents of both these elements have an unfavorable effect on oxidation resistance. Similarly, concentrations of molybdenum great than about 5 wt. % can also have a harmful effect [76].

Mechanisms of Metal Oxidation

In 1923, N.B. Pilling and R.E. Bedworth classified oxidizable metals into two groups: those that formed protective oxide scales and those that did not. They suggested that unprotective scales formed if the volume of the oxide layer was less than the volume of metal reacted. For example, in the oxidation of aluminum:



the Pilling-Bedworth Ratio is:

$$\text{PBR} = (\text{Volume of 1 mol of Al}_2\text{O}_3) / (\text{Volume of 2 mol of Al})$$

where the volumes can be calculated from molecular and atomic weights and the densities of the phases. If the ratio is less than 1, as is the case for alkali and alkaline earth metals, the oxide scales are usually unprotective, with the scales being porous or cracked due to tensile stresses and providing no efficient barrier to penetration of gas to the metal surface. If the ratio is more than 1, the protective scale shields the metal from the gas so that oxidation can proceed only by solid-state diffusion, which is slow even at high temperatures. If the ratio is much over 2 and the scale is growing at the metal/oxide interface, the large compressive stresses that develop in the oxide as it grows thicker may eventually cause the scale to spall off, leaving the metal unprotected.

Exceptions to the Pilling-Bedworth theory are numerous, and it has been roundly criticized and rejected by many. Its main flaw is the assumption that metal oxides grow

by diffusion of oxygen inward through the oxide layer to the metal. In fact, it is much more common for metal ions to diffuse outward through the oxide to the gas. Also, the possibility of plastic flow by the oxide or metal was not considered. Nevertheless, historically, Pilling and Bedworth made the first step in achieving understanding of the processes by which metals react with gases. And although there may be exceptions, the volume ratio, as a rough rule-of-thumb, is usually correct. The Pilling-Bedworth volume ratios for many common oxides are listed in **Appendix I**[77].

Summary of Pilling-Bedworth Ratio

- ✧ For good oxidation resistance the oxide should be adherent to the surface
- ✧ Adherence of the oxide
 = f(the volume of the oxide formed /the volume of metal consumed in the oxidation)
 = f(Pilling-Bedworth Ratio)
- ✧ $PBR < 1$: tensile stresses in oxide film-brittle oxide cracks
- ✧ $PBR > 1$: compressive stresses in oxide film-uniformly cover metal surface and is protective
- ✧ $PBR \gg 1$: too much compressive stresses in oxide film-oxide cracks [78]

3.3.2. Importance of trace element control of CMSX-4 superalloy

Holt, R. T. pointed out the importance of impurities and trace elements in nickel base superalloys as early as April 1984 [79].

Nickel base superalloys, by virtue of their excellent high temperature properties coupled with corrosion resistance, have been widely used as gas turbine engine components.

The physical metallurgy of superalloys demands the highest degree of process consistency and reproducibility, requiring melters of these alloys to exercise strict control

and discipline during manufacture. The need for improved gas turbine operating efficiency and reliability has resulted in extremely stringent acceptance criteria. Gases, particularly oxygen and nitrogen, are required to be controlled to < 10 ppm, while several tramp elements which are considered deleterious, needs to be controlled to < 1 ppm.

These restrictions are a big challenge to metallurgists and suitable strategies should be evolved from basic thermodynamic considerations in order to get desired results.

Elements which are present in superalloys in parts per million (ppm) level are generally known as trace elements. While most of them are undesirable, some elements, especially Mg, B, Zr, Y, Ce etc are sometimes deliberately added in controlled amounts to enhance the hot workability or high temperature performance[80].

Investment foundries manufacturing aerospace turbine components employ close control of trace elements, in both the raw materials and the finished castings (AMS2280). The properties principally affected by trace element in Ni-based alloys are creep life and ductility. Results of experimental research have shown that the most detrimental element is Bi, which can reduce creep life by 20% at a contamination level of 0.2 ppm. This element is followed in the severity of its effect on these properties by Te, Se, Pb, and Ag, in that order. Gases in alloys affect the degree of microporosity formation in vacuum-cast Ni-based alloys. Rolls-Royce practice is to monitor all non-metallics used for **mold** making, e.g. **cores**, **investment shell**, and **pattern materials**. [81].

CNV specification of CMSX-4 castings requires very low-level trace elements control, e.g. O less than 10 ppm. Bi Less than 0.5 ppm.(less than 0.3 ppm in ingots) [52].

3.3.3. Compositional modification of CMSX-4 superalloy

There are two compositional modified CMSX-4 alloys. CMSX-4 [SLS][LA+Y] alloy is commercially available and CMSX-4 (B/C) [MK4] is proprietary.

CMSX-4 [SLS][LA+Y] alloy incorporates melt desulfurisation techniques to bring the S level down to <1 ppm combined with excellent alloy cleanliness represented by 2 to 3 ppm [O]. This SX alloy melting and desulfurisation technology provides lower levels of The required La+Y ppm in the SX castings to give the resultant dramatic increases in bare oxidation resistance, coating and TBC performance In turn this SX casting process flexibility for required **ceramics (shell and core)** and improves SX casting process yield. Extensive SX varied component casting trails have shown the alloy can be cast with conventional SX ceramics and achieve high SX grain yield, with the require control of La+Y ppm microchemistry top to bottom of cores SX airfoil castings. The La + Y ppm additions are normally made on the SX casting furnace, although heats can be pre-alloyed. These highly reactive elements tie up the <1 ppm S in the alloy as high stable La + Y sulfides, which prevent the migration the migration/ diffusion of S to the free surface, which destroys the strong Van der Waal's bond between the a **alumina scale layer** and the base alloy/ coating/ bond coat [82].

CMSX-4 (B/C) [MK4] alloy is proprietary by Allison Engine Company.

CMSX-4 (B/C) [MK4] alloy nominally contains 0.04 wt. % carbon and 0.006 wt. % Boron

3.4. Physical properties of CMSX-4 superalloy

Table 1 showed density and approximate melting range of some Ni base superalloys.

Density (gm/cm^3) of CMSX-4, PWA 1484 and René N5 is 8.70, 8.95 and 8.65 respectively.

Approximate melting range of CMSX-4 alloy showed in **Table 1** is 2415-2515 °F

Differential Thermal Analysis (DTA) results of melting ranges of CMSX-4, CMSX-4 [SLS][LA+Y], PWA 1484 and René N5 from the **heating curve** is shown below.

- ✧ CMSX-4– 2473.3 °F (solidus) and 2543.0 °F (liquidus)
- ✧ CMSX-4 [SLS][LA+Y]– 2484.7 °F (solidus) and 2556.7 °F (liquidus)
- ✧ PWA 1484– 2506.7 °F (solidus) and 2552.7 °F (liquidus)
- ✧ René N5– 2457 °F (solidus) and 2559 °F (liquidus) [83].

3.5. Creep-rupture/Phase stability of CMSX-4 superalloy

The long-time phase stability of CMSX-4 in terms of its resistance to topologically-close-packed (TCP) phase formation was a major aspect in all stages of the development of the alloy. Specifically the Cr content was fixed at 6.5 % and the overall chemistry balanced to give phase stability with the presence of 3% Re and 6.4% W and also to give acceptable hot corrosion (sulphidation) resistance. TCP phase stability of CMSX-4 alloy has been proven by long term creep-rupture testing as shown in **Table 5**. where there are no fall-offs in the log-stress to log-life linear property relationships at the longer lives due to undesirable microstructural changes, such as the significant occurrence of TCP phases. Also, following stress-rupture testing between 1100°C (2012°F) and 1150°C (2102°F) no TCP phases were detected following 700 Hrs. at 1100 °C (2012°F) and just a small amount of TCP needle phase was observed within the dendrite cores after 1750 Hrs. at

1121 °C (2050°F). The TCP phase has been analyzed on the SEM and TEM to be **W + Re + Cr** rich. TCP phases are potentially damaging for two reasons; they tie up γ and γ' strengthening elements in non-useful form, thus reducing creep strength. They also can act as crack initiators because of their brittle nature and reduce impact and fatigue strength. CMSX-4 has excellent long-term creep-rupture strength at 1121°C (2050°F) [18].

CMSX-4 LONG TERM CREEP-RUPTURE DATA

Test Conditions	Stress-Rupture Life Hrs.	Elongation %4D	RA %
95 MPa/982°C (13.8 ksi/1800°F)	17016.2 17009.2	28.5 35.0	36.1 42.1
90 MPa/1038°C (13.0 ksi/1900°F)	9340.7	16.2	25.4
76 MPa/1093°C (11.0 ksi/2000°F)	7391.1	11.3	21.7
69 MPa/1121°C (10.0 ksi/2050°F)	5603.0	6.4	20.4
41 MPa/1149°C (6.0 ksi/2100°F)	9049.6	NA	15.8

Table 5. TCP phase stability of CMSX-4 alloy proven by long term creep-rupture testing

Phasial stability number of nickel base superalloys

Pratt & Whitney Aircraft (PWA) and GE Aircraft Engine (GEAE) require not only the composition but also the phasial stability to the nickel base superalloys.

Phasial stability number N_{V3B} is defined by the **PWA N-35** method of nickel-based alloy electron vacancy TCP phase control factor calculation. **CMSX-10** has a **phasial stability number** N_{V3B} less than about 2.10. Advantageously, the phasial stability number N_{V3B} is less than 1.85 and, preferably, the phasial stability number N_{V3B} is less than 1.65. [84].

The typical phasial stability number N_{v3B} of CMSX-4 VIM ingot is 2.19 which the specification (**CM KH 8/22/99**) required 2.24 Max [85].

Phasial stability number N_{v3} is defined by the GEAE specification **E50TF47** PhaComp Electron Vacancy-Number Calculations (N_{v3}) Method [67, 68].

Phasial stability number N_{v3} of **René N4** was required less than 2.32 [67].

Phasial stability number N_{v3} of **René N5** was required 2.07-2.15 [68].

The **PWA N-35** method of nickel-based alloy electron vacancy TCP phase control factor calculation is as follows:

EQUATION 1- Conversion for weight percent to atomic percent:

$$\text{Atomic percent of element } i = P_i = \frac{W_i/A_i}{\sum_i(W_i/A_i)} \times 100$$

where: W_i = weight percent of element i , A_i = atomic weight of element i

EQUATION 2-Calculation for the amount of each element present in the continuous matrix phase:

Element	Atomic amount R_{ii} remaining
Cr	$R_{Cr} = 0.97P_{Cr} - 0.375P_B - 1.75P_C$
Ni	$R_{Ni} = P_{Ni} + 0.525P_B - 3(P_{Al} + 0.03P_{Cr} + P_{Ti} - 0.5P_C + 0.5P_V + P_{Ta} + P_{Cb} + P_{Hf})$
Ti, Al, B, C, Ta, Cb, Hf	$R_i = 0$
V	$R_V = 0.5P_V$
W	$*R_{(W)} = P_W - 0.167P_C \frac{P_W}{P_{Mo} + P_W}$
Mo	$R_{(Mo)} = P_{(Mo)} - 0.75P_B - 0.167P_C \frac{P_{Mo}}{(P_{Mo} + P_W)}$

***Note:** weight percentage Re is added to weight percentage W for the calculation above.

EQUATION 3-Calculation of N_{v3B} using atomic factors from Equations 1 and 2 above:

$$N_i^j = \frac{R_i}{\sum_i R_i} \text{ then } N_{v3B} = \sum_i N_i (N_v)_i$$

Where:

i = each individual element in turn.

N_i = the atomic factor of each element in matrix.

$(N_v)_i$ = the electron vacancy No. of each respective element.

This calculation is exemplified in detail in a technical paper entitled "PHACOMP Revisited", by H. J. Murphy, C. T. Sims and A. M. Beltran, published in Volume 1 of International Symposium on Structural Stability in Superalloys (1968), the disclosure which is incorporated by reference herein [84].

3.6. Processing properties of CMSX-4 superalloy

3.6.1. Castability of CMSX-4 superalloy

Single crystal materials must not only show improved mechanical properties, but must also possess good processability in order that components can be produced economically and with guaranteed consistent properties. As described in Goulette's paper "Cost Effective Single crystals: The Rolls-Royce Approach", the Rolls-Royce DS furnace design features a high temperature gradient mould heater, which minimizes thermal convection. As a consequence, a wide range of compositions can be considered without the risk of unacceptable chemical segregation. The criteria for good castability are freedom from stray grain and sliver formation, chemical segregation and porosity. The alloy must also be able to develop its single crystal structure at economical mould withdrawal rates [86].

Single crystal castability of CMSX-4

One of the premier concerns of a single crystal foundry is the castability, (casting quality and yield performance), of an alloy. Casting or grain defects that often plague single crystal airfoils are high angle boundaries (HABs), freckles, and slivers. All these can be attributed to or aggravated by an alloy with a characteristically unstable solidification front. In particular, freckles (trails of equiaxed grains) are associated with alloys exhibiting a large mushy zone (freezing range) and high tungsten, low tantalum content. As a result of the initial alloy design to enhance the castability of CMSX-4 through tantalum content and refractory element balance, the alloy offers low propensity to the formation of crystal structure defects. Slivers are grains forming streaks in the microstructure. They are usually close to the primary direction but misoriented in the transverse direction. The formation of slivers is believed to be related to the metal inclusion content during solidification, the higher the inclusion content, the greater the tendency to form slivers.

It has been shown that targeting 50 -150 ppm residual yttrium in CMSX-4 single crystal castings significantly lowers the incipient melting point, resulting in incipient melting micropores in the eutectic phase in fully g' solutioned microstructures, which reduce HCF and LCF properties in specimens without **HIP**. Interference film optical metallographic techniques used during this research have shown that the incipient melting occurs at a low melting point nickel-yttrium phase which occurs interdendritically and is closely associated with the normal γ/γ' eutectic pools. Also the restricted peak solution temperature in these castings result in increased propensity to TCP phase formation following stressed-high temperature exposure, due to enhanced refractory element

residual microsegregation. Single crystal castability studies show that these relatively high levels of residual yttrium nucleate grain defects particularly slivers in the castings due to yttrium-ceramic oxidation reactions and subsequent complex stable oxide product formation [16].

The castability of CMSX-4 is somewhat improved at a **higher solidification rate** [87].

3.6.2. Heat-treatability of CMSX-4 superalloy

The heat treatment of single crystals is a critical operation. The process is essential to develop the full property potential of material, and design data is based on correctly heat treated material. Commercial heat treatment practice incorporates allowances for temperature excursions either side of a heat treatment band. The design of single crystal alloy compositions must allow for the inaccuracy of temperature measurement and achievable consistency of temperature control. The Rolls-Royce alloys are designed with a minimum heat treatment window of 25 °C. This is defined as the temperature difference between the gamma prime solvus and incipient melting point obtained following commercial heat treatment practice. Heat treatment windows = gamma prime solvus - incipient melting temperature [86].

CMSX-4 Solution heat treatment “window” of approximately is 19°C (35°F) - capable of full γ' and eutectic g and γ/γ' solutioning without incipient melting [1].

Comparing the Rolls-Royce alloys are designed with a minimum heat treatment window of 25 °C, CMSX-4 Solution heat treatment “window” is relatively smaller.

René N6 has rather high γ' solvus and incipient-melting temperatures, 1299 °C (2370 °F) and 1340 °C (2444 °F), respectively, the difference giving it an adequately wide heat-

treating window, 41 °C (74°F) [88]. The optimum solution heat treatment cycle for René N6 was determined to be 1315-1335 °C for approximately six hours [89].

3.7. Key successful factors for the casting of reactive alloys

3.7.1. Wax pattern

3.7.1.1. Low ash and special filler pattern wax

REMET TIWAX 288P28 was developed primarily to meet the stringent requirements of Titanium alloy casters. The patented “P” filler is a water soluble, clean burning material which minimizes **metal-mold reaction**.

Key product features:

- ✧ Good surface finish.
- ✧ Water soluble filler: very clean shell, which minimizes metal mold reaction.
- ✧ Very low ash: minimizes metal mold reaction.
- ✧ Low Thermal expansion minimizes shell cracking during dewaxing.
- ✧ Low cavitation.
- ✧ Patterns retain flexibility long enough to allow easy removal from the die.
- ✧ Made in ISO 9000 registered facility: product consistency that results in performance consistency.
- ✧ Excellent primary coat adhesion [38]

3.7.1.2. Contamination free wax pattern making operation

- ✧ Use non-silicon mold release for wax pattern injection
- ✧ Make sure no contamination during wax pattern injection and assembly operations

✧ Perform good wax pattern cleaning and etching before facecoating

3.7.2. Shell mold

3.7.2.1. Non-reactive facecoat [16]

Binder

Face coat binders used in investment casting have traditionally been Silica based. This creates a problem for many foundries because Silica is readily attacked by the reactive components of the alloys. **Table 6** shows some light on why this may be the case: SiO_2 has the lowest stability as measured by Free Energy of Formation of the Oxide for any of the commonly used binders. Non-Silica based binders would then seem to be the logical choice for many reactive alloys.

However, they require special processing conditions for both coat application and pattern removal. Traditional methods do not work well, for example, with Alumina and Zirconia Sol binders since the bond which forms can be re-dissolved. Newer generation binders such as REMET's TICOAT™ N offer a different chemistry approach to a Zirconia bond. This binder is a solution of Ammonium Zirconium Carbonate versus the discrete particles in the Zirconia Sols. The resulting bond is, after, firing, all ZrO_2 . Combining the refractory with the proper binder presents certain slurry stability problems. While these problems are formidable, they are not impossible to overcome on a practical basis. Zirconia bonded systems do require high temperature firing to minimize reaction tendencies. The higher the firing temperature the lower the subsequent reaction tendency.

Yttria is one of the least reactive refractory materials that can be used to cast reactive alloys. It is a highly basic and reactive compound. Slurry stability is minimal.

Oxide	Free Energy of Formation (k cal/mole)	Melting Point (°C)	Density (g/cc)
Y ₂ O ₃	-455	2415	4.8 – 5.0
Dy ₂ O ₃	-445	2340	7.8
Pr ₆ O ₁₁	-432	2200	6.51
La ₂ O ₃	-428	2250	3.97
Al ₂ O ₃	-400	2054	3.97
ThO ₂	-292	3050	9.86
HfO ₂	-274	2910	9.68
ZrO ₂	-262	2715	5.85
CeO ₂	-260	1950	7.3
SiO ₂	-217	1423	2.65
CaO	-152	2950	3.25
MgO	-143	2800	3.58

Table 6. COMPARISON OF OXIDE PROPERTIES **

** Listed in order of most negative, i.e., most stable, to least negative Free Energy of Formation.

Work done by Feagin showed alpha case depths ranging from less than 0.0001 inches (0.003mm) to isolated areas of alpha case depths of 0.009 inches (0.229 mm). These results were for Ytria bonded Ytria on “fingers” that were approximately four inches (101.6 mm) long and approximately 1 inch (25.4 mm) in diameter. The significant reduction in alpha case levels creates a strong impetus to develop commercially viable Ytria based systems. REMET CORPORATION is continuing to work on this technology. [83].

NYACOL Nano Technologies, Inc. also provides NYACOL® colloidal zirconias for investment casting with slurry formulation guide [84].

U. S. patent 4947927 owned by PCC Airfoils, Inc. reported that the improved slurry contains yttria to form an inert surface which is exposed to the molten reactive metal such

as titanium or nickel-chrome superalloys containing rare earths. The invention showed good results on GE René N5 castings which contained at least 20 ppm yttrium [85].

Refractory

Depending upon the degree of reactivity of the alloy, the foundryman has had a wide range of refractories from which to make a selection. (See **Table 7**) The commonly available ones include Tabular and Fused White Alumina, Zircon, Zirconia and Yttria. The Tables on the following pages show the properties of these as well as of other, less commonly used refractories. **Table 6** lists these oxides in order of decreasing stability as measured by Free Energy of Formation. **Table 8** lists them in order of decreasing melting points. Finally, **Table 9** lists these oxides in the order of decreasing density. All three properties are important in making a refractory selection. While stability is a primary concern, the melting point of the material must be above that of the metal being poured. Product density is also a concern as the foundry must be able to keep the refractory suspended in the slurry. If the density is too high, the refractory will tend to settle out; the slurry will be inconsistent and so will the foundry's casting results [83].

Secondary coating

While most of the reaction between the primary coat and the alloy occurs at this interface, there are still good reasons to use non-reactive binders and/or flours on the second coat and, perhaps even on the third coat. With casting of large cross-section, any additional protection from the alloy will usually lower the overall level of reaction. In addition, because of the liquid nature of the binder, there can be some "break through" of the binder components and **the smallest flour particles of the succeeding coats into the face coat**. This can result in some reaction occurring, even though a relatively inert

facecoat has been used. After the facecoat and any subsequent non-reactive dip coats have been applied, a typical backup slurry or Zircon, Alumino-Silicate or Alumina is used. **Fused Silica** can be used for **some reactive superalloys**, but its use should be **avoided** with **highly reactive alloys** such as Titanium [83].

SUPER ALLOYS (E.g., CM-247LC, CMSX-4, Inconel 718, Mar-M-509, etc.)
Zircon (ZrSiO₄)
Alumina (Al₂O₃)
TITANIUM AND ITS ALLOYS (E.g., Ti-6-4, etc.)
Zirconia (ZrO₂)
Yttria (Y₂O₃)
Graphite (C)
Thoria (ThO₂)

Table7. REACTIVE ALLOYS AND GENERALLY COMPATIBLE REFRACTORIES

Wash coating

NYACOL® colloidal yttria for investment casting

NYACOL® yttria sols are finding increasing use in investment casting shells as an yttria wash coat. Such a surface coating on the shell provides for a very low reactivity surface for the casting of titanium and the nickel and cobalt superalloys [86].

3.7.3. Ceramic core

Cores represent another challenge for the foundryman. The cores must not react with the alloy despite being exposed to molten metal and high temperatures for longer time periods than the shell. Core removal is another important issue: the foundryman must also be able to remove the core from the casting without destroying the casting.

Core washes have usually been the most practical alternative for reactive alloy casting.

Oxide	Melting Point (°C)	Free Energy of Formation (k cal/mole)	Density (g/cc)
ThO ₂	3050	-292	9.86
CaO	2950	-152	3.25
HfO ₂	2910	-274	9.68
MgO	2800	-143	3.58
ZrO ₂	2715	-262	5.85
Y ₂ O ₃	2415	-455	4.8 – 5.0
Dy ₂ O ₃	2340	-445	7.8
La ₂ O ₃	2250	-428	3.97
Pr ₆ O ₁₁	2200	-432	6.51
Al ₂ O ₃	2054	-400	3.97
CeO ₂	1950	-260	7.3
SiO ₂	1423	-217	2.65

Table 8. COMPARISON OF OXIDE PROPERTIES **

** Listed in order of decreasing melting points.

Oxide	Density (g/cc)	Melting Point (°C)	Free Energy of Formation (k cal/mole)
ThO ₂	9.86	3050	-292
Y ₂ O ₃	4.8 – 5.0	2415	-455
HfO ₂	9.68	2910	-274
Dy ₂ O ₃	7.8	2340	-445
CeO ₂	7.3	1950	-260
Pr ₆ O ₁₁	6.51	2200	-432
ZrO ₂	5.85	2715	-262
La ₂ O ₃	3.97	2250	-428
Al ₂ O ₃	3.97	2054	-400
MgO	3.58	2800	-143
CaO	3.25	2950	-152
SiO ₂	2.65	1423	-217

Table 9. COMPARISON OF OXIDE PROPERTIES **

** Listed in order of decreasing density.

These allow the foundry or the core maker to put on a **non-reactive coating** based upon Alumina, Yttria or Zirconia on the surface of the typical silica-based core. Consistency of coating thickness is necessary in order to achieve proper core dimensions. Usually, this technique works best for **smaller cores**. Large core bodies will stay hot for a relatively longer time and the coating may break down because of this.

Cores are a technology requiring special expertise. The foundryman would be well served to discuss his specific needs with his core supplier. This will provide the greatest opportunity for appropriate expertise to be brought to bear on the foundry's needs [83].

3.7.4. Crucible

David Alan Ford showed results of the invention of crucible for melting superalloys in U.S. patent 4006891, Feb. 8, 1977.

A crucible for melting a nickel-based superalloy containing one or more of the elements aluminum, titanium, and hafnium is made of magnesia grains boned by tinaia, hafnia or yttria. The purity of the magnesia is not less than 97% [87].

From wettability consideration, zirconia crucible has best performance [46], but it is difficult to be detected by X-ray for inclusion inspection in nickel base superalloy. So special care needed in X-ray inspection when use zirconia crucible.

3.7.5. Casting parameters

Due to metal mold reactions are temperature and time dependence under certain casting conditions, from metal mold reaction consideration, using high side melting and pouring temperatures are not recommended and higher solidification rate is desired for shorten

metal mold contacting time at high temperature.

3.8. Summary

- ✧ Metal mold reactions are common and complex problems
- ✧ Surface or interface oxidation is the main form of metal mold reaction
- ✧ Metal mold reaction is a kind surface defect but sometime associates with other casting defects
- ✧ Metal mold reaction should be considered in both thermodynamics and kinetics
- ✧ Metal mold reactions mainly caused by silica containing ceramic materials using in the casting system
- ✧ Metal mold reaction layers of CMSX-4 castings are eutectic phases rich
- ✧ Metal mold reactions of CNV CMSX-4 castings might also induce defects of gases, inclusions, hot tears, and O & Si content errors
- ✧ For metal mold reactions of CNV CMSX-4 casting problem solving the ingot; ceramics used in melting, pouring and gating system including crucible, funnel, thermocouple protection tube and filter; wax pattern; shell mold; cores and casting parameters should be reviewed and controlled
- ✧ Yttria is one of the least reactive refractory materials that can be used to cast reactive alloys, but reaction between aluminum and yttria need to be considered

4. Methodology and Materials

This study will focus on the materials selection in the face coat and binders used in the mold shell. From past in-house studies of metal-mold reactions from CNV 553 J, [52] the silica binder is considered to be the primary suspect for the cause of the reaction in CMSX-4 castings. Additionally, the literature [16] indicates that surface-mold reactions are not experienced with CMSX-4 parts when using SCO (Allison production facilities) facecoats. In the past Chromalloy Nevada (CNV) in-house attempts to mitigate the reaction, it was found that the use of both yttria and zirconia slurry facecoats for CMSX-4 castings still resulted in problems with metal-mold reactions. To better understand the problem and work towards a solution, the present set of experiments was conducted, focusing on seeking a better facecoat on the mold to help keep the molten metal from contact with the silica binder.

Peel-off defects have been observed by visual and stereomicroscope inspection on the shell mold surface of CMSX-4 casting using zirconia slurry facecoat (**Figure 28**)

Porous feature has been observed by visual and stereomicroscope observations on the shell mold surface of CMSX-4 casting using yttria slurry facecoat (**Figure 29**)

It is postulated here that using a non-reactive wash coating on the normal facecoat may help to balance the facecoat strength and surface isolation functions.

For titanium casting, an yttria binder is one of the most inert materials available.

However, it is difficult to work with, as it usually gives very short slurry life (i.e., it wants to gel very rapidly when brought into contact with most any refractory

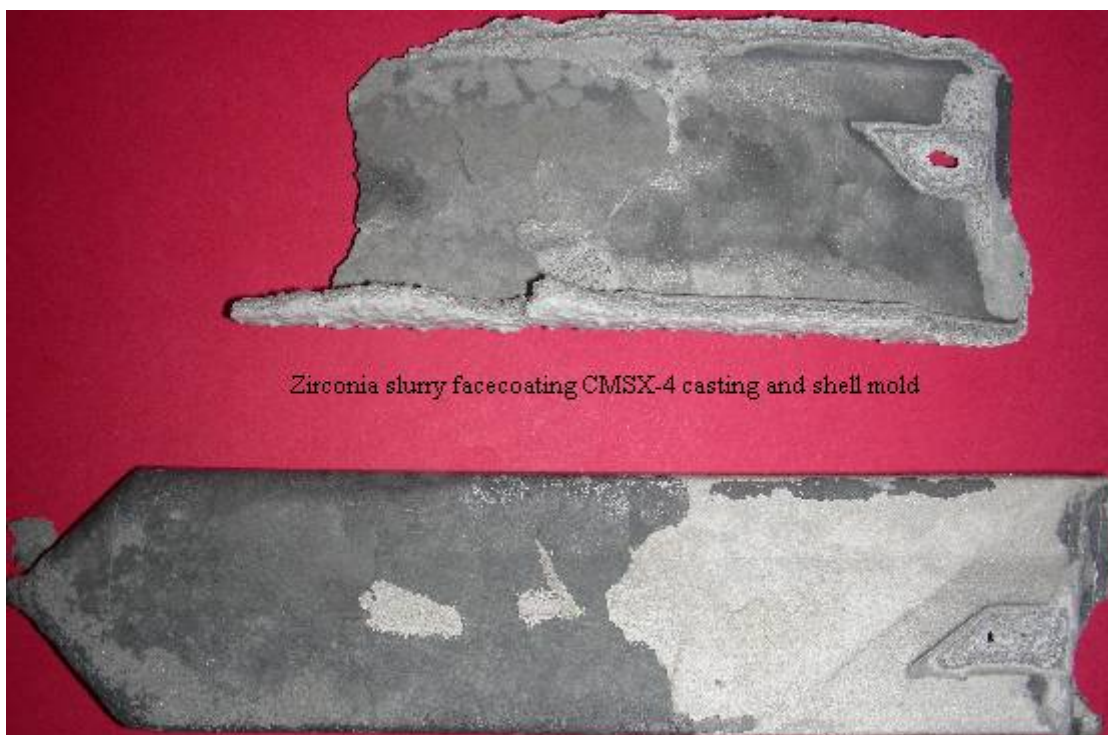


Figure 28. Visual appearance of CMSX-4 casting (Sample 2) and shell mold surface using zirconia slurry facecoat

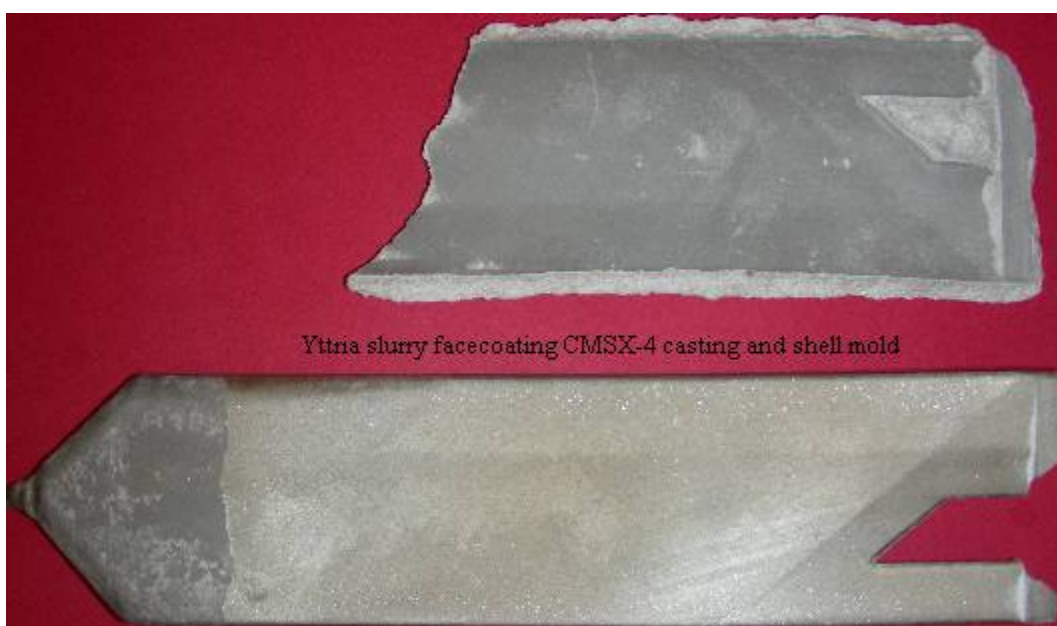


Figure 29. Visual appearance of CMSX-4 casting (Sample 3) and shell mold surface (Sample 9) using yttria slurry facecoat

material). It is also quite expensive vs. most other binders. The yttria bonds will be

somewhat similar in effectiveness to the zirconia binder. It may provide a lower level of reactivity compared to silica, but again, its effectiveness will be highly dependent on the alloy [95].

The first experiment was performed by applying an yttria wash coating on the normal facecoat as described in the literature [93]. After the shell making step, the casting trial was completed normally. After the trial casting using the yttria coating, both the casting and shell were evaluated. The systematic characterization of the metal-mold reaction interface was performed in a commercial laboratory.

4.1. Experimental procedure

As mentioned above, the principal drawbacks of yttria slurries are that the working lifetime is too short, and fine yttria flour is expensive. So instead of a slurry of yttria binder with yttria flour, an yttria aerosol spray coating was instead applied directly to the wax pattern. Then, a yttria binder washing and soaking was applied to the spray coating shell after dewaxing for strengthening (**Figure 30**).

Bonding tests were performed on the (standard) shell molding MOR (Modulus of Rupture) test bars (**Figure 31**).

X-ray diffraction (XRD) was then used to check if the yttria coating well bonded to the normal facecoat after both dewaxing and burnout/firing. A yttria spray coating plate was used as a standard for the XRD test.

The subsequent normal primary coating showed good bonding with the yttria coating, so a complete shell was made for casting trial, which was completed using an argon



Figure 30. NYACOL Yttria binder used as strengthening binder in this project

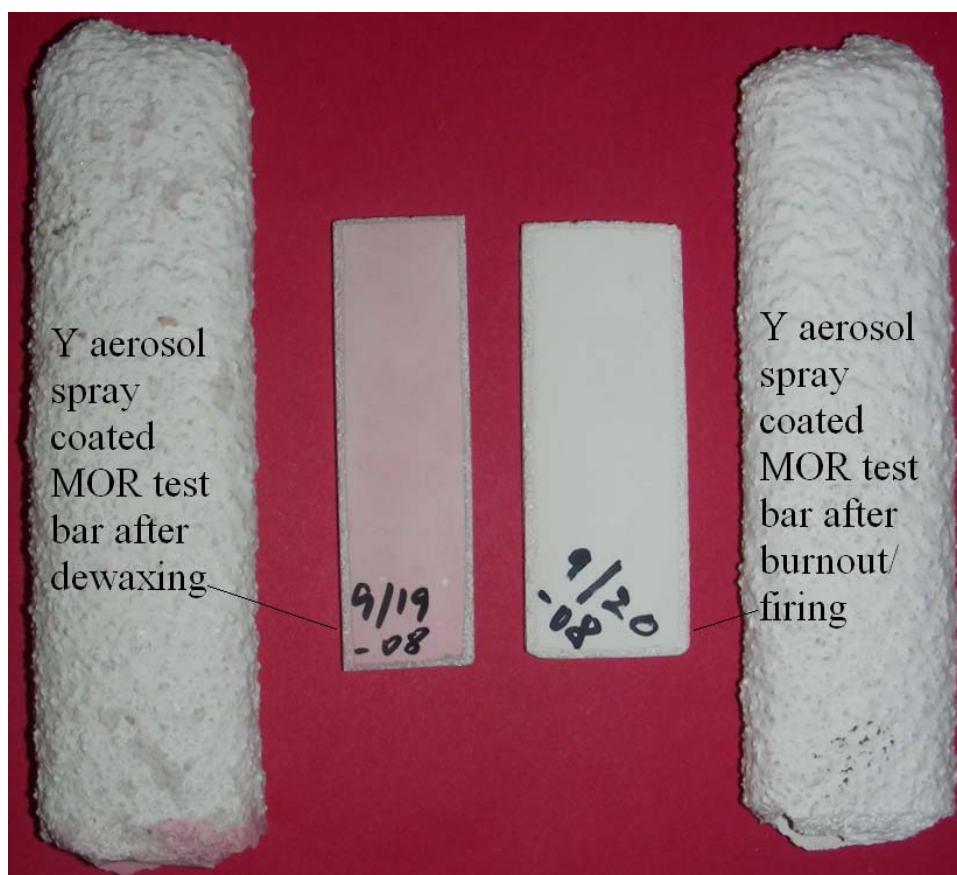


Figure 31. Y_2O_3 Y Aerosol spray coating on zircon facecoat MOR test bars

atmosphere Bridgman casting furnace. Trial castings were produced, with both the cast parts and the shell molds analyzed afterwards using optical and electron techniques for metal mold reaction interface characterization.

Nine characterization samples were prepared by sectioning from their parent parts (**Figure 32**). Characterization was performed both at CNV and at Rocky Mountain Laboratory [96]. Detailed descriptions of the nine samples and their intended purposes are summarized below.

Sample 1: Size ~1/4" x 1/2" from yttria spray coating part.

Try to learn what are the golden layer, dark grey layer and shining spots by AES and EDS.

Sample 2: Size ~1/4" x 1/2" from zirconia slurry facecoating part.

Try to learn what are the golden layer, light black layer and shining spots by AES and EDS.

Sample 3: Size ~1/4" x 1/2" from yttria slurry facecoating part.

Try to learn what are the golden layer, grey layer and shining spots by AES and EDS.

Sample 4: Size ~1/4" x 1/2" from normal zircon slurry facecoating part.

Try to learn what are the golden layer, grey layer and shining spots by AES and EDS.

Sample 5: Size ~1/4" x 1/2" from normal zircon slurry facecoating part after heat

treatment. Try to learn what are the golden layer, grey layer and shining spots by AES and EDS. Also, try to learn why the reaction

layers become harder to remove after heat treatment from the results of Sample 4 and Sample 5.

Sample 6: Size $\sim 1/4"$ x 0.012" (Thickness) yttria spray coating. Try to learn what are the grey layer, metal spots and shining spots by XPS.

Sample 7: Size $\sim 1/4"$ x 0.013" (Thickness) normal zircon face coating. Try to learn what are the grey layer, why this layer is without metal spots and shining spots by XPS

Sample 8: Size $\sim 1/4"$ x 0.189" (Thickness) normal zircon facecoating with alumina backup. Try to learn what are the grey layer, metal spots and shining spots by EDS and XPS.

Sample 9: Size $\sim 1/4"$ x 0.215" (Thickness) yttria facecoating with alumina backup. Try to learn what are the grey layer, metal spots and shining spots by XPS.

4.2. Materials used in the experiment

The yttria aerosol spray (ZYP Y aerosol) was obtained from ZYP coatings Inc. This spray provides easy application of a uniform, thin, protective high-temperature coating that is non-fluorocarbon, non-aqueous-based carrier assures, and is fast drying. The yttria coating is a high-chemical-stability coating for applications where resistance is not demanded. These coatings are used wherever anti-stick, barrier, molten-metal resistant coatings are needed on substrates that do not alone meet the



Figure 32. a) Samples (1-5) sectioning for surface characterization

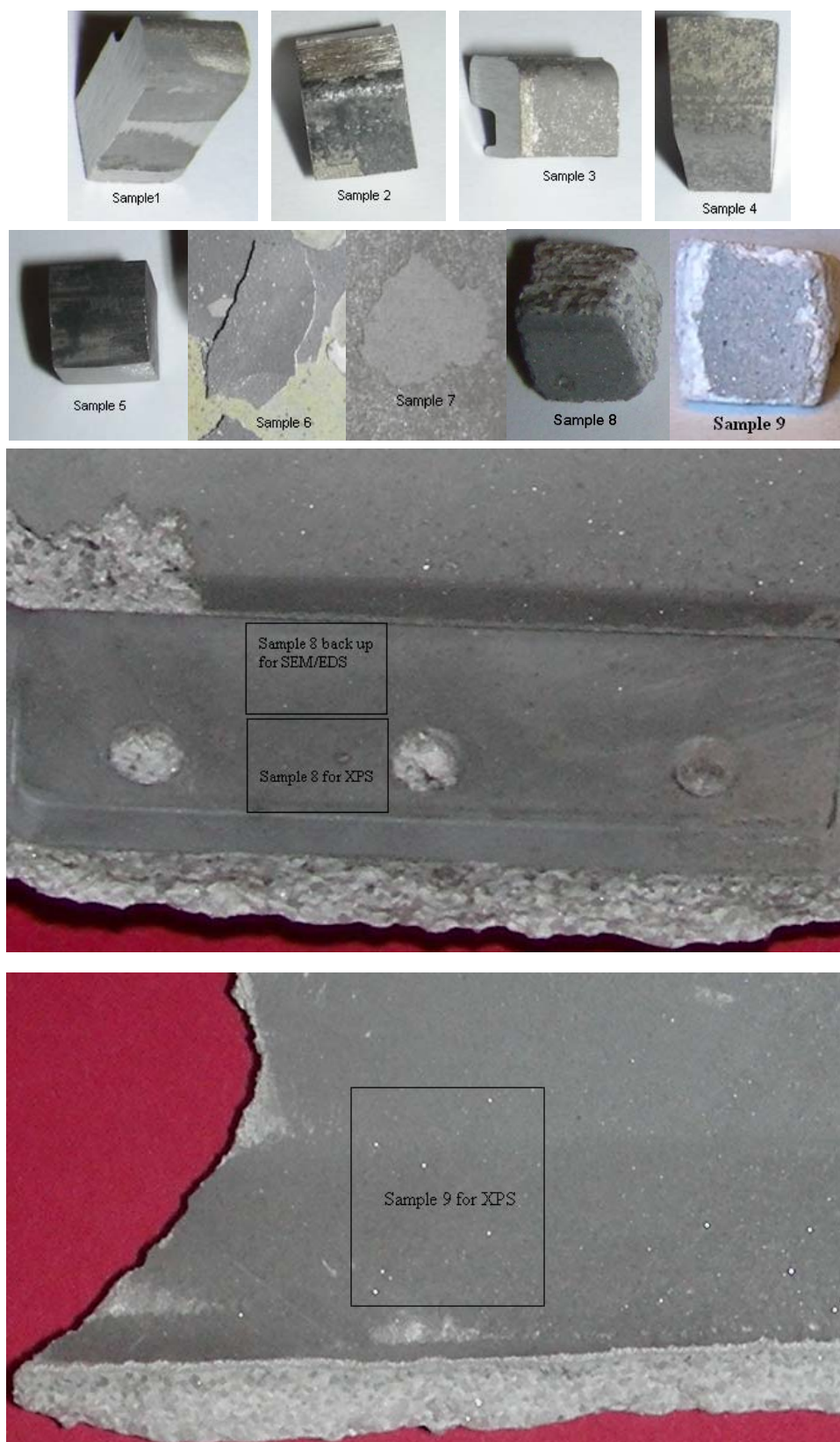


Figure 32. b) Samples for surface characterization



Figure 32. C) Shell molds of CMSX-4 SX castings: Left one (Sample 8) from part with secondary grain defect, Right one (Sample 7) from part with hot tear defect

requirements [97].

NYACOL® colloidal yttria, from NYACOL Nano Technologies, Inc., was used in the yttria spray coating after dewax by washing and soaking method; as a sintering aid, it will give the yttria spray coating good strength after shell mold burnout/firing.

The CMSX-4 casting material was procured from CM group (CMSX-4 VIM refining ingot).

4.3. Characterization Techniques

4.3.1. Optical techniques

Optical microscopy will be used for surface color and morphology observation on both CMSX-4 castings and their shell molds in this project. Optical microscopy at a variety of magnifications was performed using Leica optical microscope with digital camera shown in **Figure 33**.

4.3.2. Electron techniques

4.3.2.1. Scanning Electron Microscopy with X-ray microanalysis (SEM/EDS) [98, 99]

Scanning Electron Microscopy (SEM) will be used for detailed surface morphology by secondary electron imaging of topographic features and compositional contrast by backscattered electron (BSE) imaging of chemical phase difference in this project. Energy Dispersive X-ray Spectroscopy (EDS) will be used for qualitative and quantitative elemental analysis in conjunction with the SEM. X-ray imaging or mapping will be used for the analysis of elemental distribution on sample surfaces.

SEM can produce images of almost any sample at magnifications of 15-300,000X.

The SEM has tremendous depth of field allowing for imaging that cannot be accomplished using optical microscopy. Conductive and nonconductive samples can be imaged. When operated in the backscatter electron (BSE) detection mode, differences in material composition can be observed. Elemental analysis can be

performed on any



Figure 33. Leica Optical Microscope with Digital Camera

feature observed with an integrated Energy Dispersive Spectroscopy (EDS) detector.

EDS is used in conjunction with the SEM providing chemical analysis in areas as small as 1 μm in diameter. EDS detects all elements heavier than Be on the periodic table.

EDS can be performed exactly on any features or particles seen in the SEM images and can “MAP” elements on a surface. Unknown materials can be identified and quantitative analysis can be performed [98].

In SEM, an electron beam is scanned across a sample's surface. When the electrons strike the sample, a variety of signals are generated, and it is the detection of specific

signals, which produces an image or a sample's elemental composition. The three signals, which provide the greatest amount of information in SEM, are the secondary electrons, backscattered electrons, and X-rays.

Secondary electrons are emitted from the atoms occupying the top surface and produce a readily-interpretable image of the surface. The contrast in the image is determined by the sample morphology. A high-resolution image can be obtained because of the small diameter of the primary electron beam.

Backscattered electrons are primary beam electrons, which are 'reflected' from atoms in the solid. The contrast in the image produced is determined by the atomic number of the elements in the sample. The image will therefore show the distribution of different chemical phases in the sample. Because these electrons are emitted from a depth in the sample, the resolution in the image is not as good as for secondary electrons.

Interaction of the primary beam with atoms in the sample causes shell transitions which result in the emission of an X-ray. The emitted X-ray has an energy characteristic of the parent element. Detection and measurement of the energy permits elemental analysis (Energy Dispersive X-ray Spectroscopy or EDS). EDS can provide rapid qualitative, or with adequate standards, quantitative analysis of elemental composition with a sampling depth of 1-2 microns. X-rays may also be used to form maps or line profiles, showing the elemental distribution in a sample surface.

Summary of Instrument Capabilities

✧ Secondary electron imaging of topographic features with magnification up to

100,000X and

- ✧ Spatial resolution better than 50 Å
- ✧ Backscattered electron imaging of chemical phase difference
- ✧ Qualitative and quantitative elemental analysis with EDS
- ✧ X-ray imaging: elemental line scans and maps

Comparison with Related Techniques

- ✧ Auger Electron Spectroscopy (AES) and Electron Spectroscopy for Chemical Analysis (ESCA) are more sensitive to light elements
- ✧ Analysis depth for AES and ESCA is three orders of magnitude less than EDS
- ✧ EDS is only for elemental analysis; ESCA gives chemical state information

Samples/Sample Preparation

Suitable samples include most solids which are stable under vacuum (metals, ceramics, polymers, minerals). Sample must be less than 2 cm in diameter. Sample preparation: non-conducting samples are coated with a thin layer of carbon or gold. Metallographic embedding, polishing, and sectioning is available for samples requiring special preparation.

Limitations

- ✧ Limited detection of elements below Na in the periodic table
- ✧ No detection of elements below C in the periodic table
- ✧ X-ray detection limit ~ 0.1% depending on the element
- ✧ Samples must be compatible with vacuum (no fluids) [99]

Figure 34 shows the JSM-6400 SEM/EDS used in this project. **Figure 35** shows the

Hummer VI-A Sputtering system (Gold coating) used for preparing the samples.

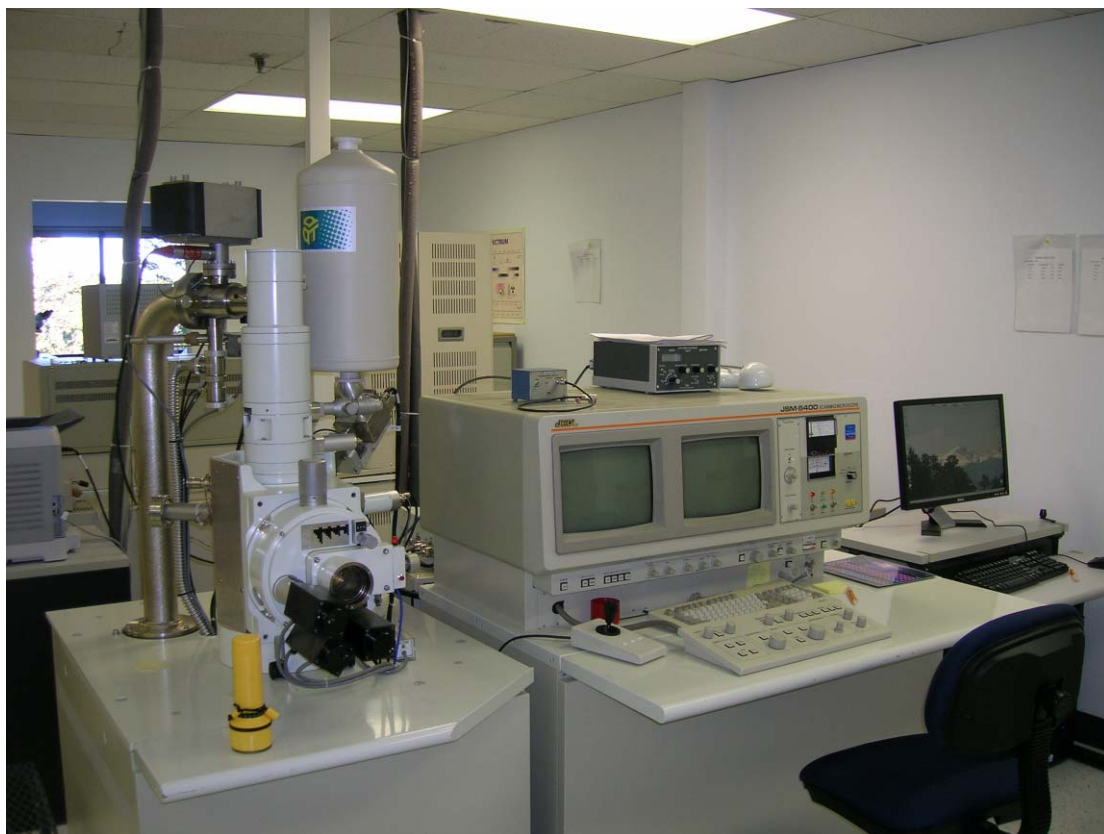


Figure 34. JSM-6400 SEM with iXRF Model 510D EDS



Figure 35. Hummer VI-A Sputtering System (Gold coating)

4.3.2.2. Auger electron spectroscopy (AES)

Auger electron spectroscopy (AES) will be used for chemical surface analysis of casting samples so as to learn the elements on the surfaces and the elemental distribution in depth by depth-profiling. Auger Electron Spectroscopy (AES or Auger) is a chemical surface analysis method. AES measures the chemical composition of the outermost 100 Å of a sample. Measurements can be made at greater depths by ion sputter etching to remove surface layers. All elements except for H and He can be detected at concentrations above 0.1 to 1.0 atom %, depending on the element. In addition, elemental concentration versus depth (up to 2 µm) information can be obtained by ion sputter etching while monitoring every element of interest. Only

conductive samples can be measured with this technique. The sampled area varies from 1 mm down to 2 μm in diameter [98].

General Uses

- ✧ Compositional analysis of the 0- to 3-nm region near the surface for all elements except H and He
- ✧ Depth-compositional profiling and thin film analysis
- ✧ High lateral resolution surface chemical analysis and inhomogeneity studies to determine compositional variations in areas ≥ 100 nm
- ✧ · Grain-boundary and other interface analyses facilitated by fracture
- ✧ · Identification of phases in cross sections

Examples of Applications

- ✧ Analysis of surface contamination of materials to investigate its role in such properties as corrosion, wear, secondary electron emission, and catalysis
- ✧ Identification of chemical-reaction products, for example, in oxidation and corrosion
- ✧ In-depth compositional evaluation of surface films, coatings, and thin films used for various metallurgical surface modifications and microelectronic applications
- ✧ Analysis of grain-boundary chemistry to evaluate the role of boundary precipitation and solute segregation on mechanical properties, corrosion, and stress corrosion cracking phenomena

Samples

- ✧ *Form:* Solids (metals, ceramics, and organic materials) with relatively low vapor pressures ($<10^{-8}$ torr at room temperature). Higher vapor pressure materials can be handled by sample cooling. Similarly, many liquid samples can be handled by sample cooling or by applying a thin film onto a conductive substrate
- ✧ *Size:* Individual powder particles as small as $1\ \mu\text{m}$ in diameter can be analyzed. The maximum sample size depends on the specific instrument; $1.5\ \text{cm}$ ($0.6\ \text{in.}$) in diameter by $0.5\ \text{cm}$ ($0.2\ \text{in.}$) high is not uncommon
- ✧ *Surface topography:* Flat surfaces are preferable, but rough surfaces can be analyzed in selected small areas ($\sim 1\ \mu\text{m}$) or averaged over large areas ($0.5\ \text{mm}$ in diameter)
- ✧ *Preparation:* Frequently none. Samples must be free of fingerprints, oils, and other high vapor pressure materials

Limitations

- ✧ Insensitivity to hydrogen and helium
- ✧ The accuracy of quantitative analysis is limited to $\pm 30\%$ of the element present when calculated using published elemental sensitivity factors. Better quantification ($\pm 10\%$) is possible by using standards that closely resemble the sample
- ✧ Electron beam damage can severely limit useful analysis of organic and biological materials and occasionally ceramic materials
- ✧ Electron beam charging may limit analysis when examining highly insulating

materials

- ✧ Quantitative detection sensitivity for most elements is from 0.1 to 1.0 at. %

Estimated Analysis Time

- ✧ Usually less than 5 min for a complete survey spectrum from 0 to 2000 eV.
Selected peak analyses for studying chemical effects, Auger elemental imaging, and depth profiling generally take much longer

Capabilities of Related Techniques

- ✧ *X-ray photoelectron spectroscopy*: Provides compositional and chemical binding state information, relatively nondestructive
- ✧ *Ion scattering spectroscopy*: Provides superb top atomic layer information, specificity of surface atomic bonding in selected cases, and surface composition and depth profiling information
- ✧ *Secondary ion mass spectroscopy*: High elemental detection sensitivity from part per million to part per billion levels; surface compositional information; depth profiling capability; sensitivity for all elements, including hydrogen and helium
- ✧ *Electron probe*: Analysis to 1- μm depth in conventional operation, quantitative and nondestructive
- ✧ *Analytical electron microscopy*: Chemical analysis in conjunction with high-resolution microscopy [100]

In probing a metallic surface with a view to understanding either its resistance to environmental degradation or, if corroded, to understanding the mechanism of

attack, we will generally be interested in composition as a function of depth, and position. AES can provide this information with a depth resolution of the order of nanometers and a spatial resolution of the order of 10 nm. In many cases information on the chemical or valence state of the surface species can also be obtained. The present review will enable full recognition of the range of information that AES might offer to the investigation of corrosion processes.

AES is an electron spectroscopic method and is closely related to X-ray photoelectron spectroscopy (XPS): each deriving its surface sensitivity from the limited mean free path, in a solid, of the emergent signal. AES is also a vacuum technique and cannot be used for in situ study of corrosion but is not entirely confined to ex situ examination of test pieces. A typical spectrometer is often equipped with a sophisticated preparation chamber. Such a facility can enable high-temperature oxidation using a hot stage, will have a fracture stage, and may be fitted with a retractable electrochemical cell.

AES has been available in commercial form for more than 30 years, a similar history to XPS, and both have reached a mature stage of development. XPS and AES differ from each other in the nature of the energetic beam used to excite an analytical signal from the sample: an x-ray beam for XPS; a finely focused electron beam in the case of AES, with all the attendant facilities for microscopy. Researchers from the field of corrosion are likely to choose XPS for studies in which the surface is expected to be uniform in composition over large areas and for which the main need is information

on surface composition and on the valence state of the elements present, for example, in passivated surfaces of alloy steels. By contrast, AES will be chosen when it is necessary to examine areas of highly localized corrosion, such as cracks and pits. Although AES gives this possibility of excellent microscopy, the use of an electron beam as the excitation source brings with it all the problems of electrostatic charging, as found in the SEM. Unlike the case of the SEM, however, the charging problem cannot be overcome by coating the surface: this would simply mask the chemical information in the surface layer. AES is thus overwhelmingly a technique for the study of metallic surfaces and the thin layers of oxides and minerals that form on them.

EDS is an excellent adjunct facility for a scanning Auger microscope (SAM). When this technique is available on the microscope, the bulk and the surface maps can be generated simultaneously by the same scanning beam. In this case, because there is a perfect register between the pixels of each map, scatter diagrams can be made that include a single element, in surface (SAM) and bulk (EDS) materials. The method of data analysis by use of scatter diagrams was pioneered by Prutton and coworkers who have shown how many different types of images might be combined to give much additional confidence in the data quality

Chemical State Information

Binding energy is defined as the difference in total energy of the system before and after ionization of the atom or ion. Thus, because of the changing ionization state of the atom relative to its neighbors during these transitions, there will be polarization

of the surrounding ions, locking up some energy and modifying the measured binding energies. These, so-called, final-state effects are sensitive to chemical and structural information and give rise to a shift in the kinetic energy of the Auger electron. The chemical shift is similar in magnitude to that observed in XPS and of the order of 2 to 4 eV. In cases where transitions occur between core-like orbitals that are well defined in energy, notably for elements either side of a transition series of the periodic table, the oxide and element can be distinguished better by use of AES compared with XPS because of the additional ionization that occurs on Auger emission. The chemical shift is widely used in studies of the corrosion of copper and zinc, and even more so in the cases of aluminum and silicon. An example of the use of the chemical shift for aluminum is given later in the chapter together with an illustration of chemically sensitive mapping [101].

Figure 36 shows the Perkin Elmer PHI 610 Scanning Auger Microprobe used in this project.

Figure 37 a) shows an AES capability-kinetic energy spectrums and AES map.

Figure 37 b) shows an AES capability-depth profile [102].

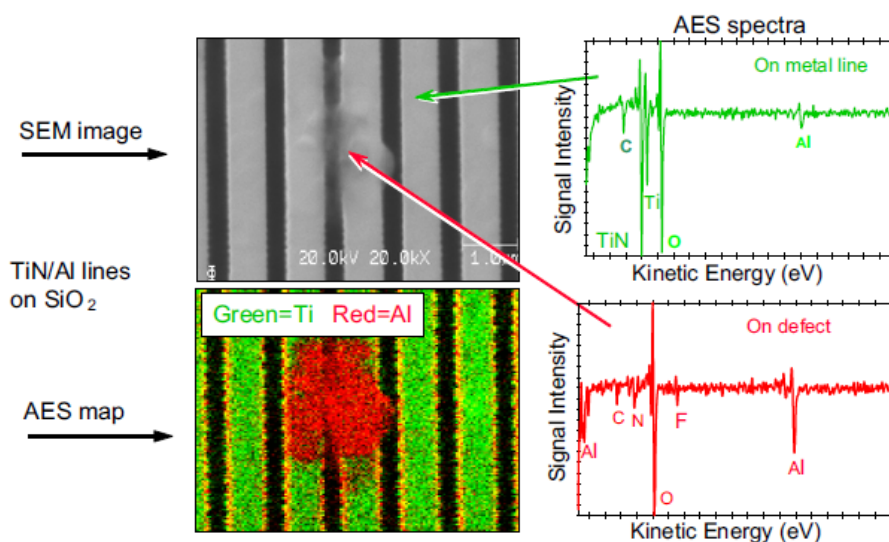


Figure 36. Perkin Elmer PHI 610 Scanning Auger Microprobe

4.3.2.3. X-ray photoelectron spectroscopy (XPS)

Because AES can only be used for conductive samples, so X-ray photoelectron spectroscopy (XPS) will be used for chemical surface analysis on the yttria spray coating and shell mold surfaces after casting process in this project. X-ray photoelectron spectroscopy (XPS) also called Electron Spectroscopy for Chemical

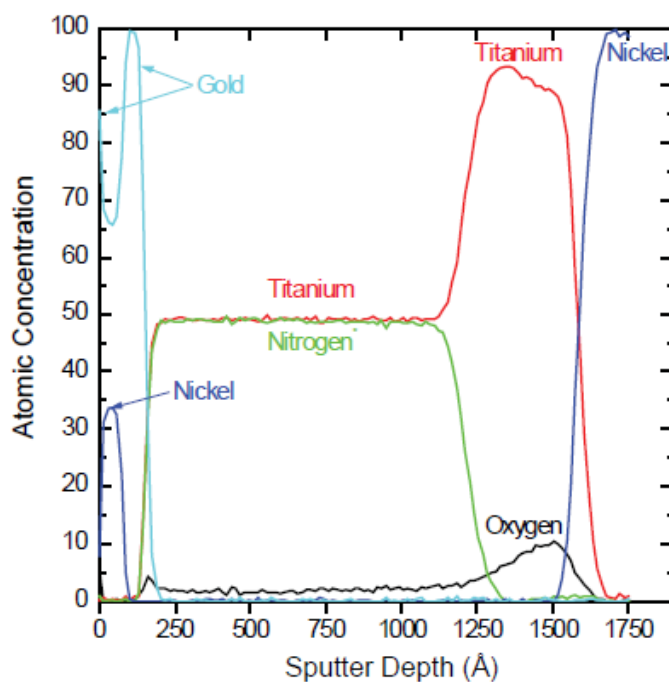
Thin Contamination Layer



Auger analysis shows the thin residue is an Al flake, probably originating from the etch chamber.

Figure 37. a) AES kinetic energy spectrum and AES mapping capability [102]

Decorative Coating Defect



AES sputter profiles provide compositional information as a function of depth

Figure 37. b) AES depth-profiling capability [102]

Analysis (ESCA) is a chemical surface analysis method. XPS measures the chemical composition of the outermost 100 Å of a sample. Measurements can be made at greater depths by ion sputter etching to remove surface layers. All elements except for H and He can be detected at concentrations above 0.05 to 1.0 atom %, depending on the element. In addition, chemical bonding information can be determined from detailed analysis. Conductive and nonconductive samples can be measured and the technique is well suited for polymeric materials. The sampled area varies from 1 mm down to 30 µm in diameter [98].

General Uses

- ✧ Elemental analysis of surfaces of all elements except hydrogen
- ✧ Chemical state identification of surface species
- ✧ In-depth composition profiles of elemental distribution in thin films
- ✧ Composition analysis of samples when destructive effects of electron beam techniques must be avoided

Examples of Applications

- ✧ Determination of oxidation states of metal atoms in metal oxide surface films
- ✧ Identification of surface carbon as graphitic or carbide

Samples

- ✧ *Form:* Solids (metals, glasses, semiconductors, low vapor pressure ceramics)
- ✧ *Size:* ≤6.25 cm³ (≤0.4 in.³)
- ✧ *Preparation:* Must be free of fingerprints, oils, or other surface contamination

Limitations

- ✧ Data collection is slow compared with other surface analysis techniques, but analysis time can be decreased substantially when high resolution or chemical state identification is not needed
- ✧ Poor lateral resolution
- ✧ Surface sensitivity comparable to other surface analysis techniques
- ✧ Charging effects may be a problem with insulating samples. Some instruments are equipped with charge-compensation devices
- ✧ The accuracy of quantitative analysis is limited

Estimated Analysis Time

- ✧ Requires an overnight vacuum pumpdown before analysis
- ✧ Qualitative analysis can be performed in 5 to 10 min
- ✧ Quantitative analysis requires 1 h to several hours, depending on information desired

Capabilities of Related Techniques

- ✧ *Auger electron spectroscopy*: Compositional analysis of surfaces. Faster, with better lateral resolution than XPS. Has a depth-profiling capability. Electron beam can be very damaging; bonding and other chemical state information are not easily interpreted
- ✧ *Low-energy ion-scattering spectroscopy*: Sensitive to the top atom layer of the

surface and has profiling capabilities. Quantitative analysis requires use of standards; no chemical state information; poor mass resolution for high-Z elements

- ✧ *Secondary ion mass spectroscopy*: The most sensitive of all surface analysis techniques. Can detect hydrogen, and depth profiling is possible. Has pronounced matrix effects that can cause orders of magnitude variations in elemental sensitivity and make quantitative analysis difficult [93]

XPS is a very successful surface analytical tool for corrosion research but also for the investigation of corrosion failures in industry, related to various environments.

Although XPS requires a sample transfer from the electrolyte to the ultrahigh vacuum (UHV) with a loss of the contact to the electrolyte and the control of the electrode potential, it provides reliable data on the chemical situation of the surface. This information is required to get a sound base for the interpretation of the mechanisms of corrosion processes and their kinetics. XPS involves the ionization of atoms on solid surfaces (or species in the gas phase) by absorption of photons. The use of an x-ray source (AlK α or MgK α) permits the ejection of electrons from all electronic levels, especially core levels (within the energy range of the x-ray beam). The energy spectrum of the ejected electrons is characteristic for the elements involved in this process. In 1954 Kai Siegbahn and his group developed a high-resolution electron spectrometer, which permitted the precise determination of the energy of XPS signals, i.e. the energy of the core levels where the electrons come from. In 1958 the same

Swedish group detected the chemical shift of XPS signals, i.e. the influence of the charge of atoms and their chemical environment on their energy. This discovery was a decisive step to develop this process to an analytical method for the study of the chemistry of solid surfaces and surface layers. Therefore the method was called electron spectroscopy for chemical analysis (ESCA), synonymous with XPS. In 1981 Kai Siegbahn received the Nobel Prize in physics for his pioneering work. Up to the mid-1970s XPS was a surface method applied to very fundamental studies of solids in contact with vacuum and low-pressure gas phase. When commercial spectrometers became available with an efficient and fast entry lock for specimens to the UHV, it developed to a widely applied method for fundamental and applied studies. Nowadays XPS is an essential method to study surfaces that have been exposed to gaseous and liquid environments as, for example, in catalysis, electrode kinetics, materials science, and corrosion. It is indispensable for many fields in research and industry including the optimization and control of products.

XPS has several advantages in comparison to other methods. It is a very soft method. Most specimens are not affected by the x-rays and they may be examined with quasi in situ conditions with no change of the composition of their surface and even with conservation of the oxidation state of the specimens. For this purpose an appropriate specimen preparation and transfer is an important aspect to avoid any uncontrolled changes due to the exposure of the specimen to the laboratory atmosphere. Other methods using electrons or ions as a probing beam like AES or ion scattering spectroscopy (ISS) might be more harmful. An important feature is the

chemical shift of XPS signals, which provides information on the oxidation state and the chemical binding of the species. The information depth of XPS is related to the escape depth of the photoelectrons, which is in the range of a few nm, thus sampling near surface layers and thin anodic films of this thickness. XPS has been widely used since the mid-1970s to solve various problems in research and industry [94].

Figure 38 shows the KRATOS Analytical XPS Instrument, Model: Kratos Axis HSi used in this project.

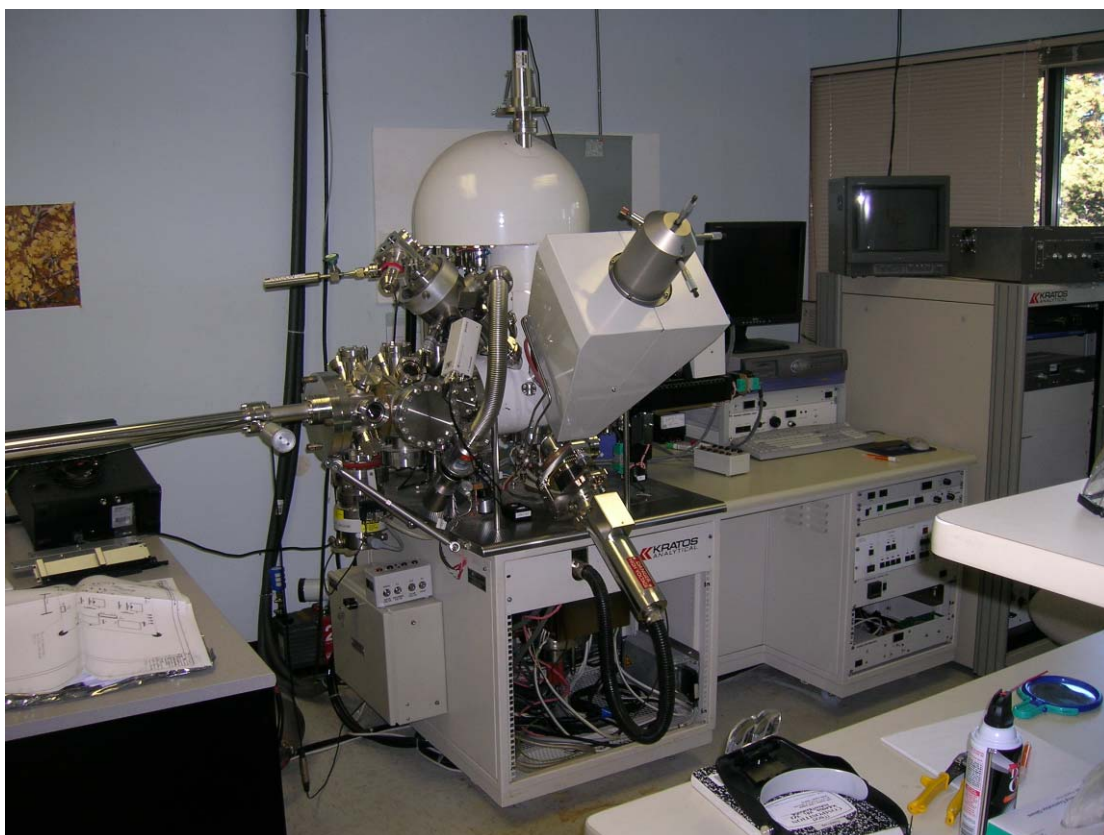


Figure 38. KRATOS Analytical XPS Instrument, Model: Kratos Axis His

3.3.3.4 X-ray diffraction (XRD)

X-ray diffraction (XRD) will be used for yttria coating identification on the shell

mold MOR bar after dewaxing in this project. X-ray diffraction techniques are some of the most useful in the characterization of crystalline materials, such as metals, intermetallics, ceramics, minerals, polymers, plastics, or other inorganic or organic compounds. X-ray diffraction techniques can be used to identify the phases present in samples from raw starting materials to finished product and to provide information on the physical state of the sample, such as grain size, texture, and crystal perfection. Most x-ray diffraction techniques are rapid and nondestructive; some instruments are portable and can be transported to the sample.

The sample may be as small as an airborne dust particle or as large as an airplane wing.

In general, x-ray analysis is restricted to crystalline materials, although some information may be obtained on amorphous solids and liquids. Similar information can often be obtained using electron diffraction or neutron diffraction, but the sample limitations are usually more severe and the equipment considerably more elaborate and costly. Samples are acceptable in many forms, depending on the availability of the material and the type of analysis to be performed. Single crystals from a few microns to a few inches in diameter or loose or consolidated aggregate of many small crystals can be used. Although the overall size of the sample may be large, the actual area of the sample examined in a given experiment rarely exceeds 1 cm^2 (0.16 in.^2) and may be as small as $10 \text{ }\mu\text{m}^2$. The type of information desired may range from the question of sample crystallinity or its composition to details of the crystal structure or the state of orientation of the crystallites. Crystal structure analysis is

usually performed only on samples of single crystals, which are often approximately 100 μm in diameter. Phase identification can be conducted on virtually all single crystal or powder samples. Also useful are measurements of the physical state of a sample that detect differences from the ideal crystal. The most common cause of crystal defects is deformation due to local or external applied stresses. Deformation or strain analysis is useful, especially in metallurgy [93].

Figure 39 shows Philips Analytical (PANalytical) X'Pert X-ray Diffractometer used in this project.



Figure 39. Philips Analytical (PANalytical) X'Pert X-ray Diffractometer

4.4. Characterization of metal mold reaction interfaces

The instrument specifications and capabilities of SEM/EDS, XPS and AES used in

this project are shown in [Appendix 2](#).

4.4.1. Characterization of metal mold reaction layers on castings

Auger Electron Spectroscopy (AES) was performed on Sample 1, Sample 3 and Sample 4. AES is an elemental analysis technique which is capable of detecting all elements except for H and He and has a nominal detection limit of ~0.1 atom%. Spectral interferences may prohibit the detection of some elements in relatively low concentrations. The sampling volume of the measurement has a depth of ~10 nm and an analysis area ~5-10 μm in diameter. The quantification method assumes that the sampling volume is homogeneous, which is rarely the case; thus, tables of relative elemental compositions are provided as a means to compare similar samples and to identify contaminants and are not meant to provide accurate compositional data. Accurate quantification of data can be achieved through the use of well-characterized reference materials of similar composition to the unknown sample. Compositional profiles (also called Sputter Depth Profiles (SDP)) were obtained by combining AES analysis with simultaneous sputter etching with a 2.0 keV Ar^+ ion beam. Depth scales are referenced to the sputter rate for SiO_2 . Depth scales are reported on this relative scale since all elements/compounds sputter at different rates. Relative sputter rates are useful for comparison of similar samples. More accurate sputter rates can be determined using a reference material of known or measurable thickness that is compositionally similar to the unknown sample. Sputter etching can cause apparent compositional changes in multi-element systems. All elements have different sputter

rates, thus “differential sputtering” can deplete the film of one or more of the constituent elements. Scanning Electron Microscopy in conjunction with Energy Dispersive Spectroscopy (SEM/EDS) was performed on Sample 1, Sample 2, Sample 3 and Sample 5. SEM images depict topographic features of the sample surface. SEM imaging was performed at 20 keV and 10 keV. EDS is an elemental analysis technique capable of detecting all elements except for H, He, Li, and Be with a detection limit of ~0.1 %. Spectral interferences may prohibit the detection of some elements in relatively low concentrations. The sampling volume is dependent on the accelerating voltage of the SEM, with a nominal analysis volume approximated by a sphere ~1 μm in diameter at 20 keV. Lower accelerating voltages yield smaller sampling volumes. Quantification accuracy is excellent when the sampling volume is homogeneous and the compounds do not contain carbon or nitrogen [96].

3.4.2. Characterization of metal-mold reaction layers on shell molds

X-ray Photoelectron Spectroscopy (XPS) also referred to as Electron Spectroscopy for Chemical Analysis (ESCA) was performed on Sample 6, Sample 7, Sample 8, and Sample 9. XPS is an elemental analysis technique which is capable of detecting all elements except for H and He and has a nominal detection limit of ~0.1 atom%. Spectral interferences may prohibit the detection of some elements in relatively low concentrations. Samples were measured at a 90° Take-Off-Angle (TOA) yielding a sampling depth of ~10 nm. The analysis area was ~500 μm in diameter. Analyses

were performed with a monochromatic Al $K\alpha$ x-ray source. Charge neutralization of the sample surface was achieved with the use of a low-energy electron flood gun. Energy scales of the spectra are referenced to the C 1s C-C/C-H signal at 284.5 eV. The quantification method assumes that the sampling volume is homogeneous, which is rarely the case; thus, tables of relative elemental compositions are provided as a means to compare similar samples and to identify contaminants and are not meant to provide accurate compositional data. Accurate quantification of data can be achieved through the use of well-characterized reference materials of similar composition to the unknown sample.

Scanning Electron Microscopy in conjunction with Energy Dispersive Spectroscopy (SEM/EDS) was performed on Sample 8 Backup. Sample 8 Backup was coated with ~20nm of gold (Au) to facilitate analysis [96].

5. Results and discussion

5.1. Results of mold making and CMSX-4 casting trial

The mold making results are shown in **Figure 40**, **Figure 41**, **Figure 42**, and **Figure 43**. Similarly, the results of the casting trial using the yttria face coating and binder are shown in **Figure 44**, **Figure 45**, **Figure 46**, **Figure 47**, and **Figure 48**. The yttria casting trial still showed metal mold reaction surface feature, but had some improvement over the previous castings.

Comparing **Figures 45** and **Figure 46**, the shell mold with yttria aerosol spray coating and yttria binder washing and soaking showed better quality than the shell mold with yttria aerosol spray coating but without yttria binder washing and soaking.

Figure 47 a) showed a white colored dross on the top surface of the pouring basin of CMSX-4 casting trial. **Figure 47 b)** showed more white colored dross on the surface of pouring basin of CMSX-4 casting with secondary gain defect. Similarly, **Figure 47 c)** showed no dross on the surface of pouring basin of a CMSX-4 casting with a hot tear defect.



Figure 40. Wax pattern assembly after Y aerosol spray coating



Figure 41. Wax pattern assembly after Y aerosol spray coating, normal zircon facecoating and stuccoing



Figure 42. Four side view of R & D test shell after dewaxing



Figure 43. a) Bottom filtration b) Shell mold after burnout/firing c) Washing shell mold after dye penetration inspection

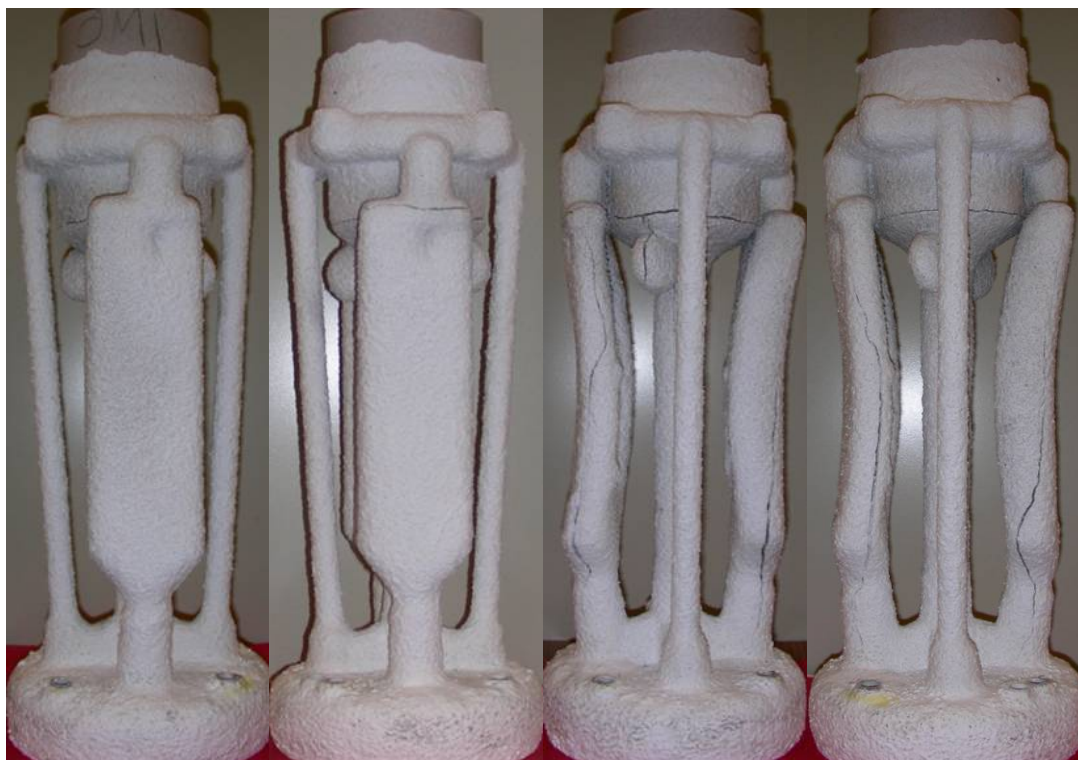


Figure 44. Four side view of shell mold after casting



Figure 45. Visual appearance of CMSX-4 casting trial using shell mold with yttria aerosol spray coating and yttria binder washing and soaking.

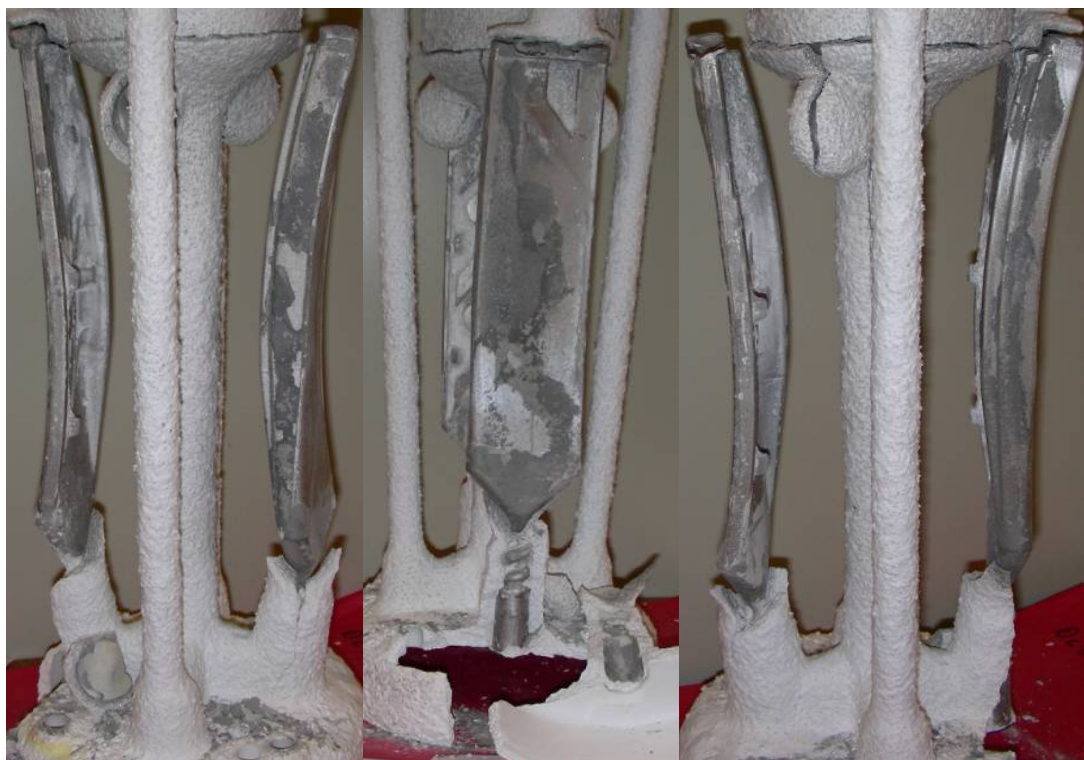


Figure 46. Visual appearance of CMSX-4 casting trial using shell mold with yttria aerosol spray coating but without yttria binder washing and soaking



Figure 47. a) Visual appearance of top surface of pouring basin of CMSX-4 casting trial showed some dross.



Figure 47. b) more dross on the surface of pouring basin of CMSX-4 casting with secondary grain defect

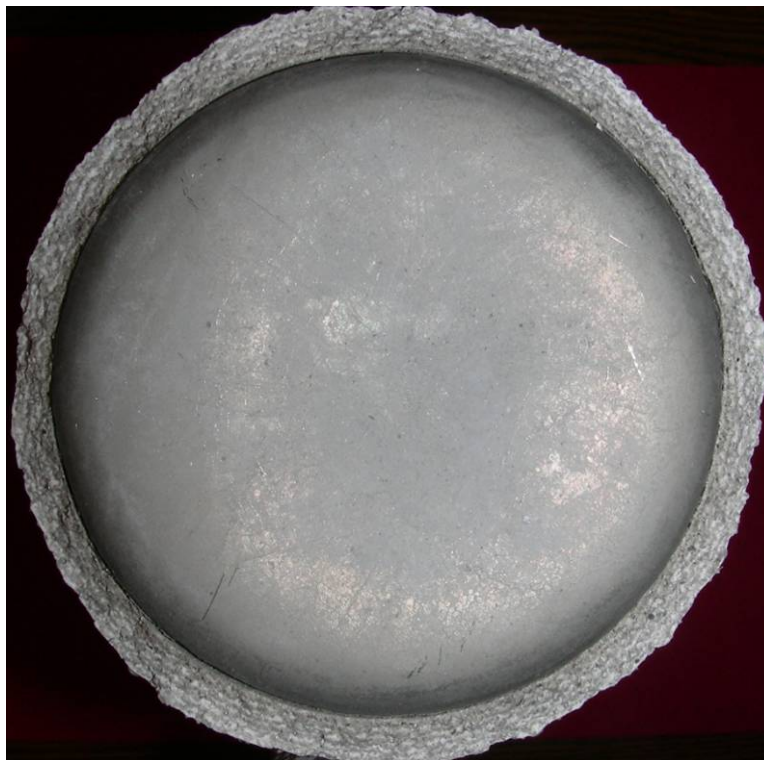


Figure 47. c) No dross on the surface of pouring basin of CMSX-4 casting with hot tear defect.



Figure 48. Visual appearance of gating system of CMSX-4 casting trial

5.2. Results of examinations by optical microscopy

Optical images of samples 1-9 are shown the **Figure 49** through **Figure 66**.

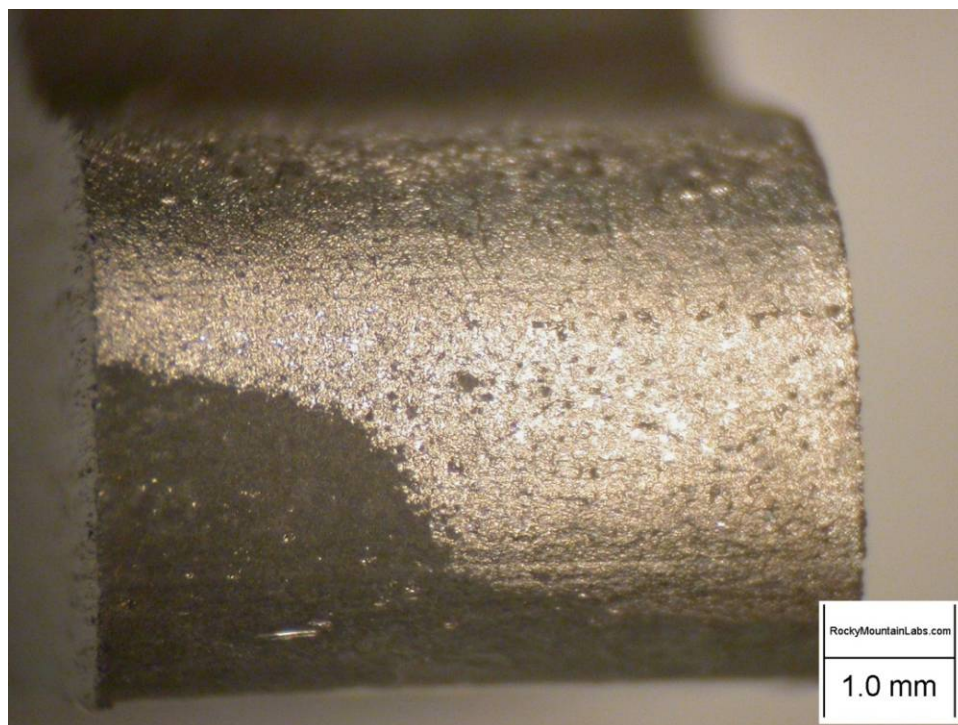


Figure 49. 20X optical image of Sample 1

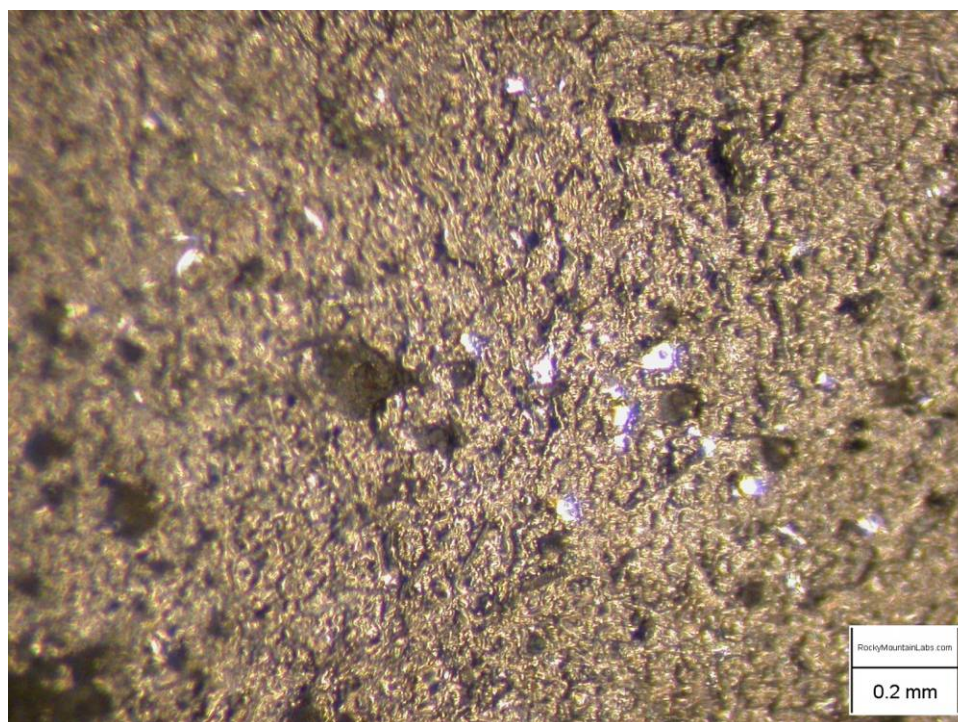


Figure 50. 80X optical image of Sample 1

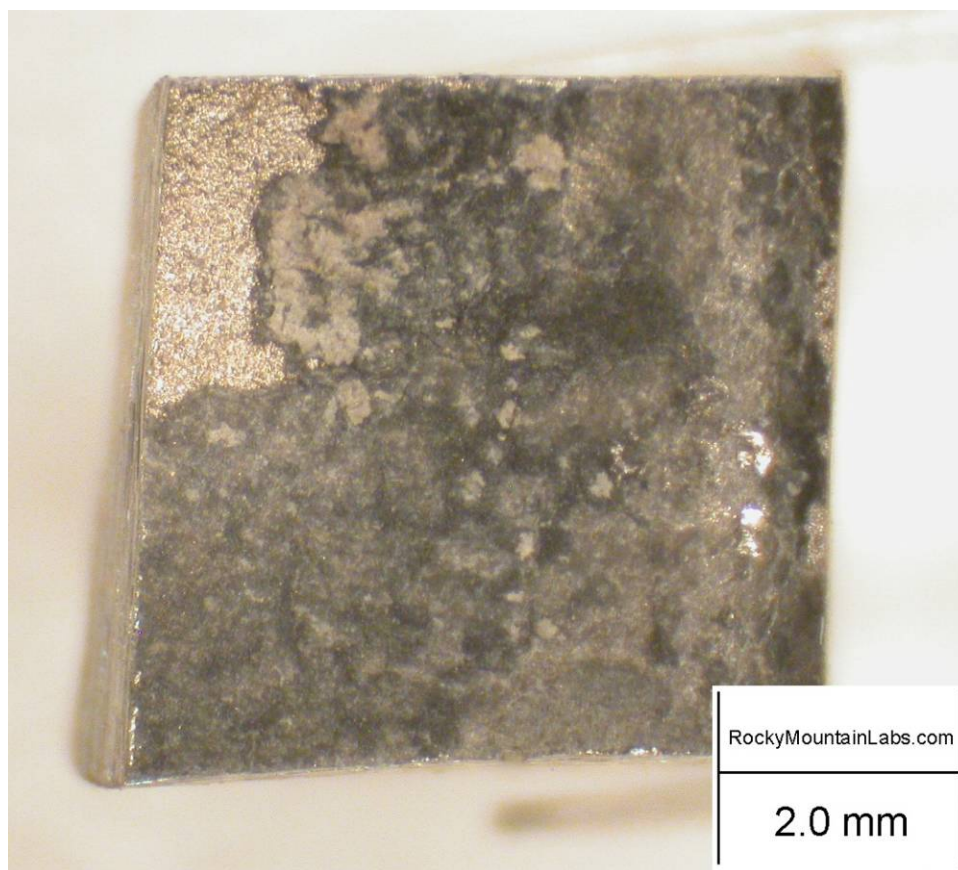


Figure 51. 13.4X optical image of Sample 2

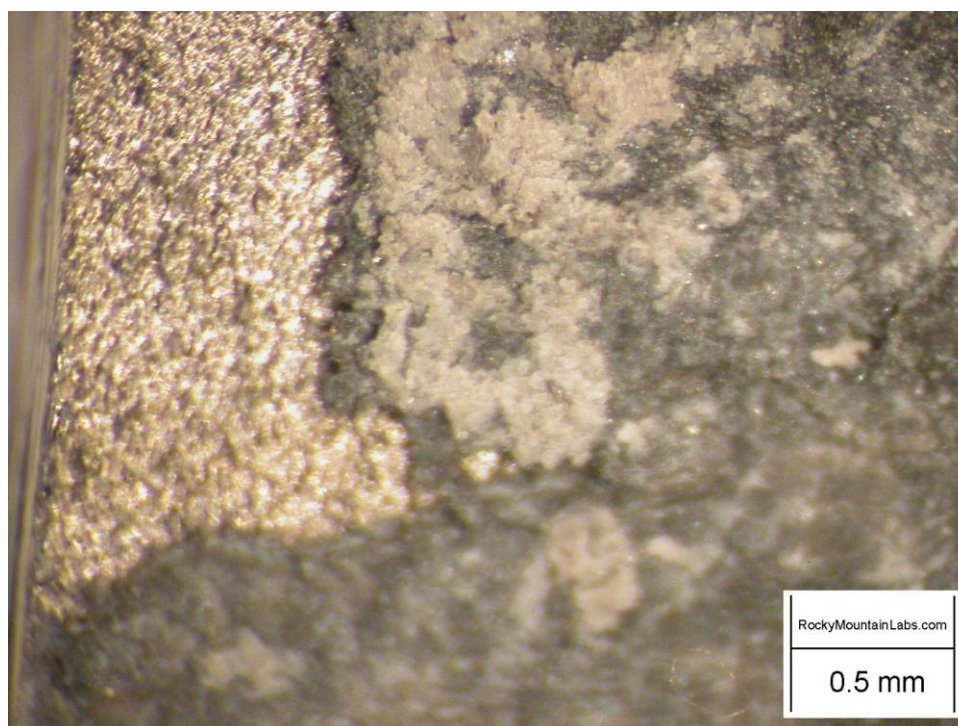


Figure 52. 50X optical image of Sample 2

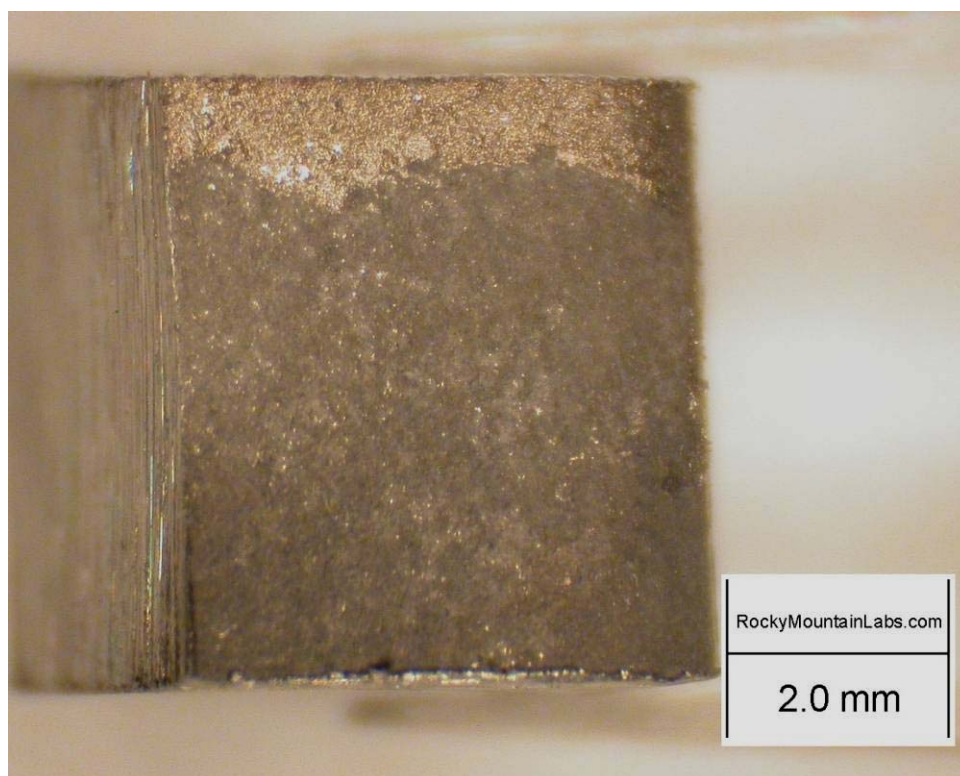


Figure 53. 13.4X optical image of Sample 3

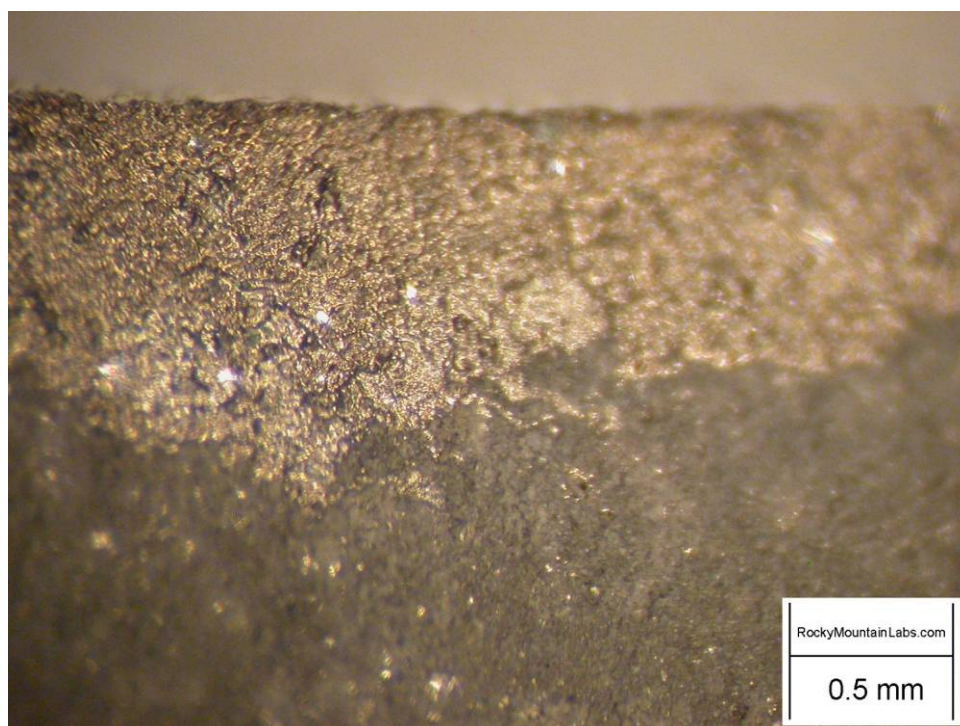


Figure 54. 50X optical image of Sample 3

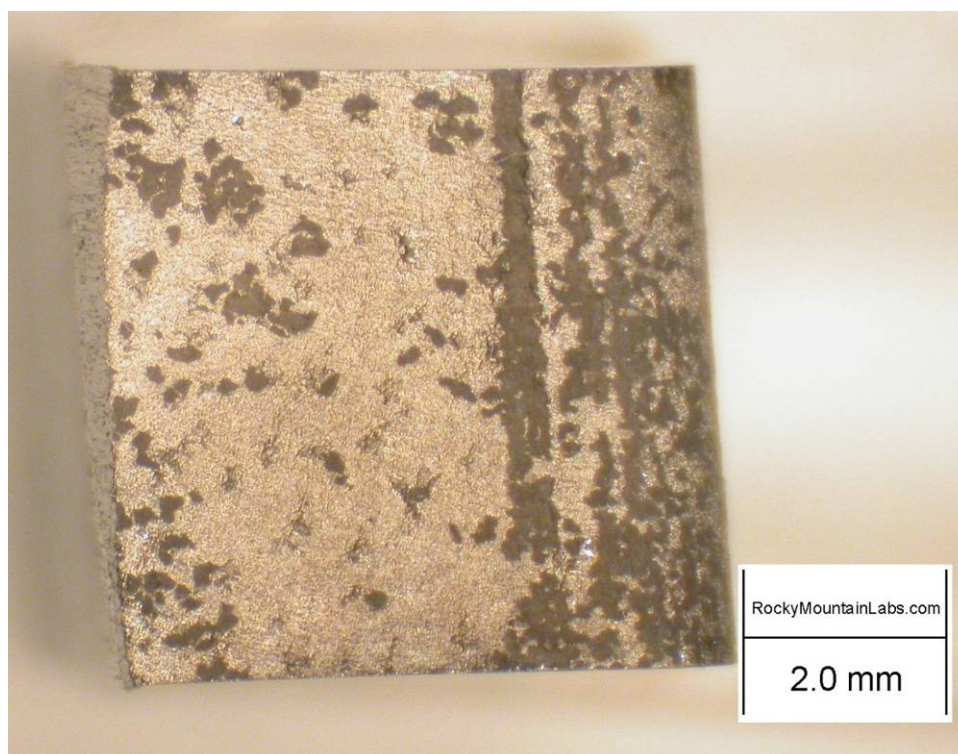


Figure 55. 13.4X optical image of Sample 4 Backup

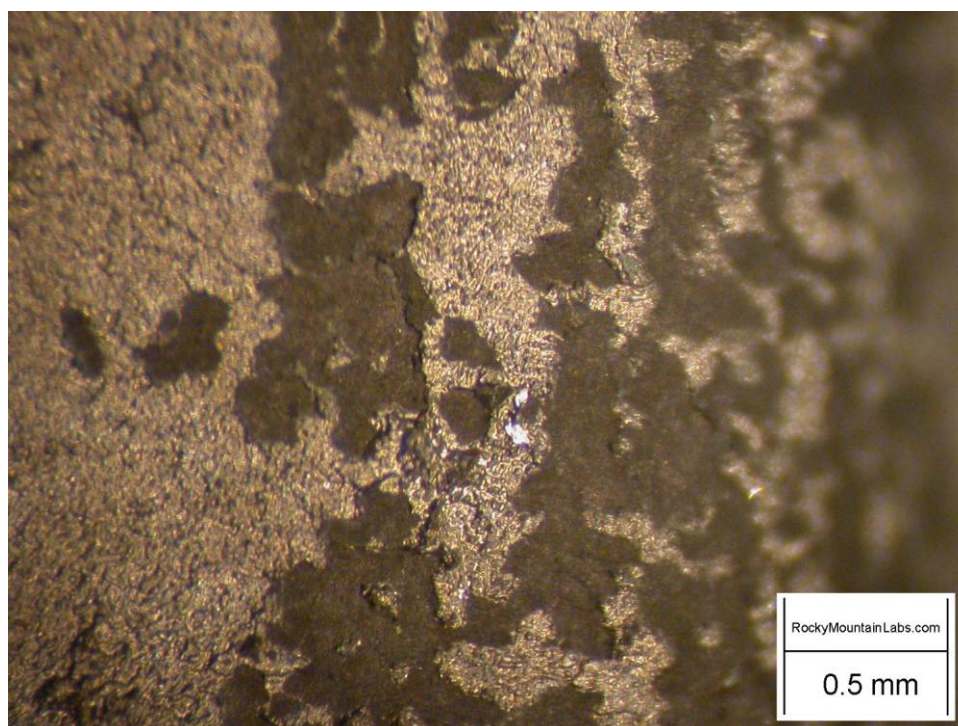


Figure 56. 50X optical image of Sample 4 Backup

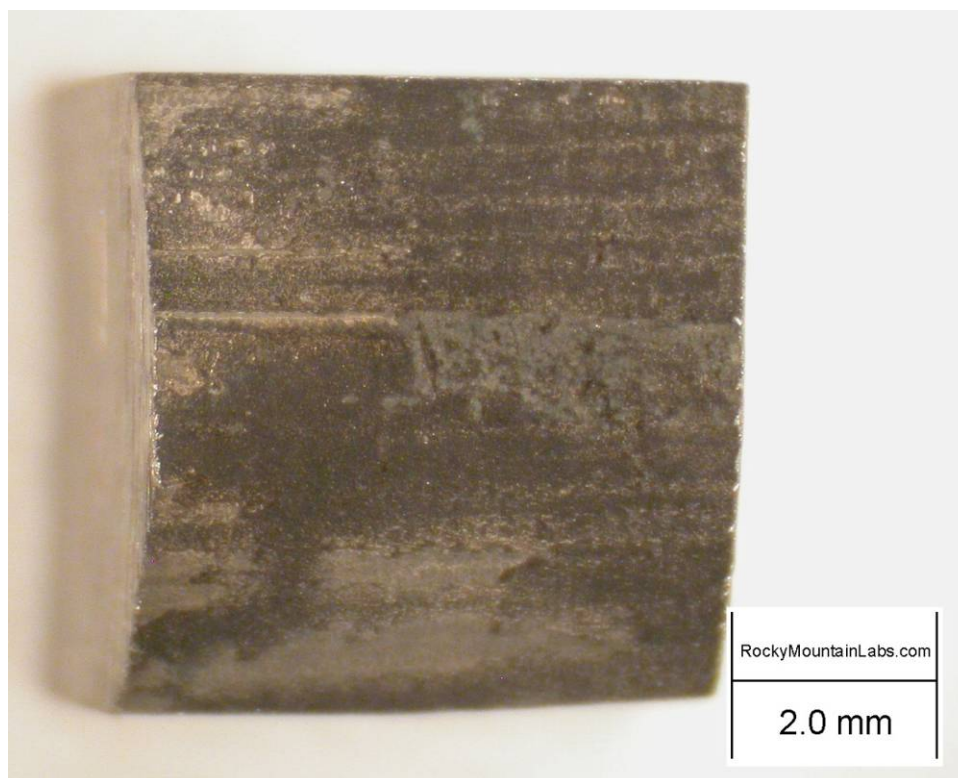


Figure 57. 13.4X optical image of Sample 5

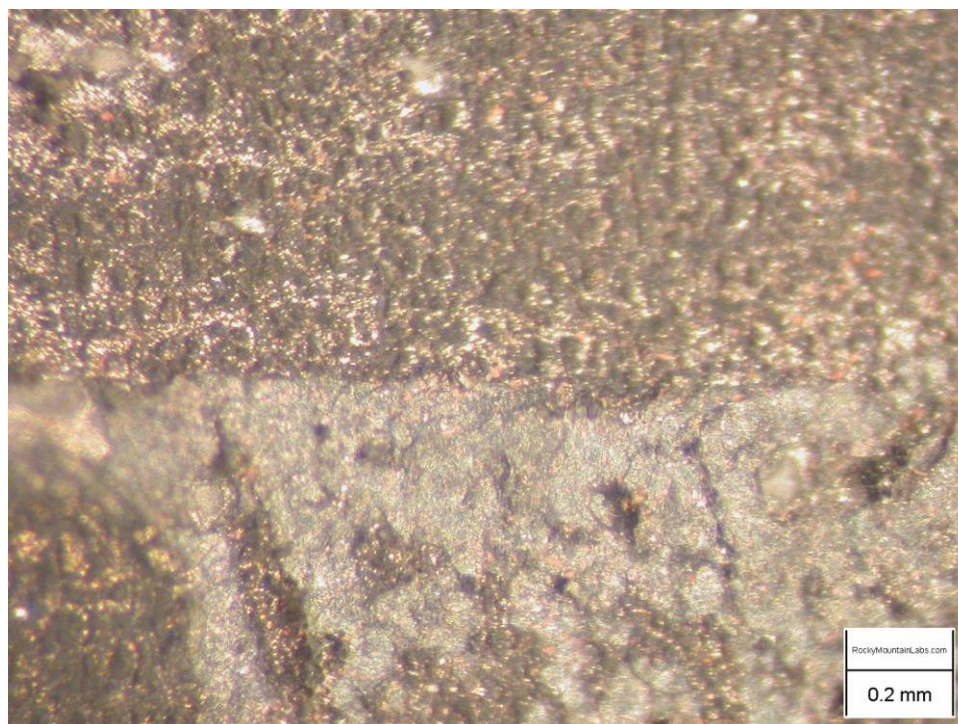


Figure 58. 80X optical image of Sample 5

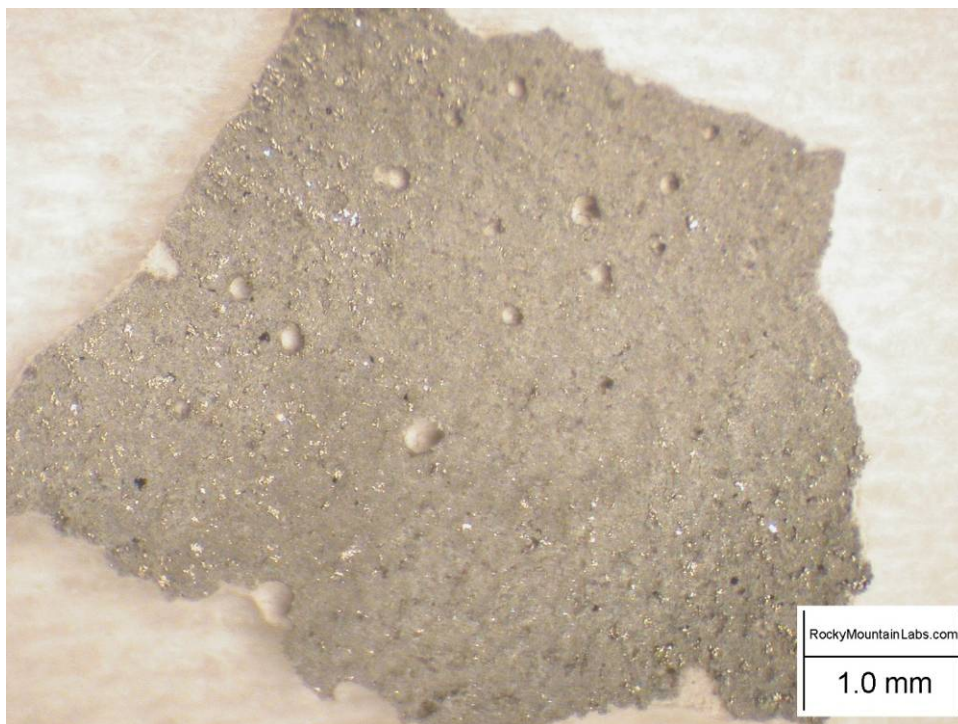


Figure 59. 24X optical image of Sample 6

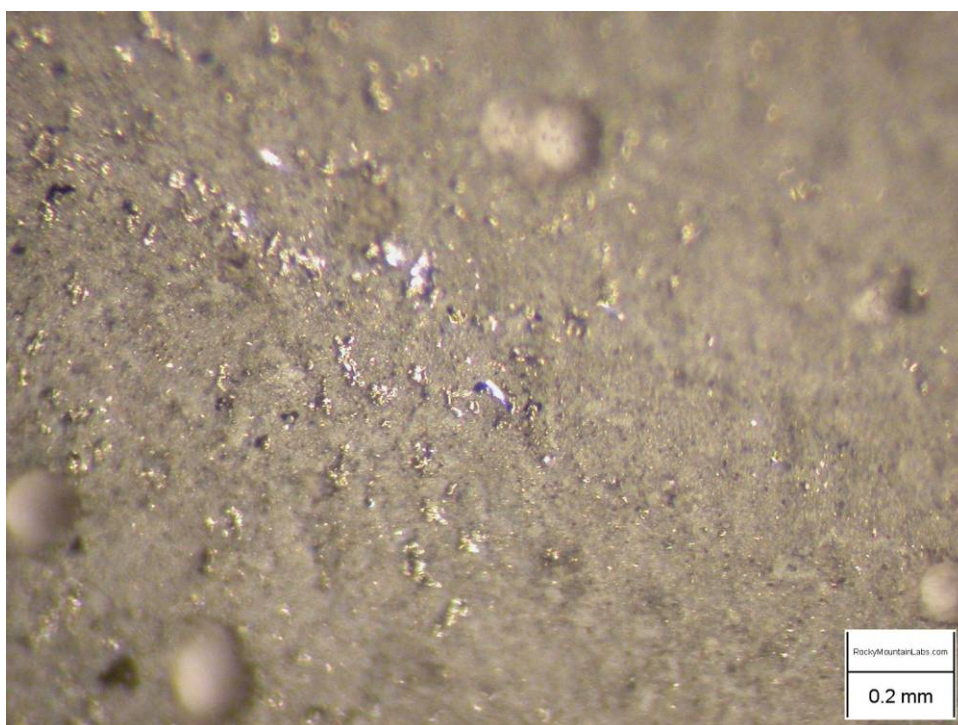


Figure 60. 80X optical image of Sample 6



Figure 61. 13.4X optical image of Sample 7

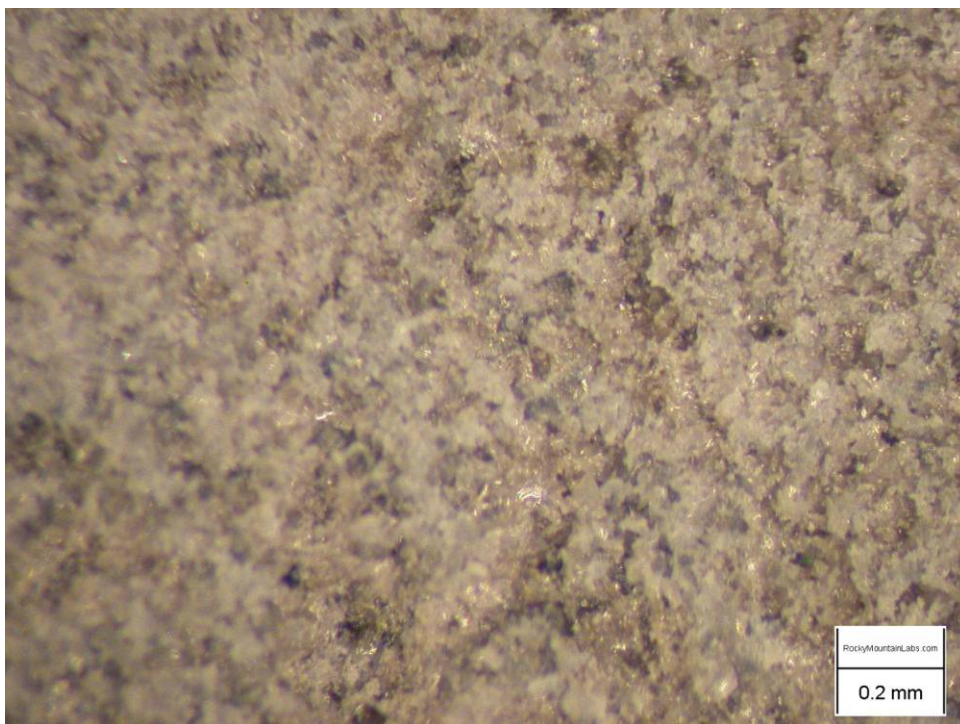


Figure 62. 80X optical image of Sample 7

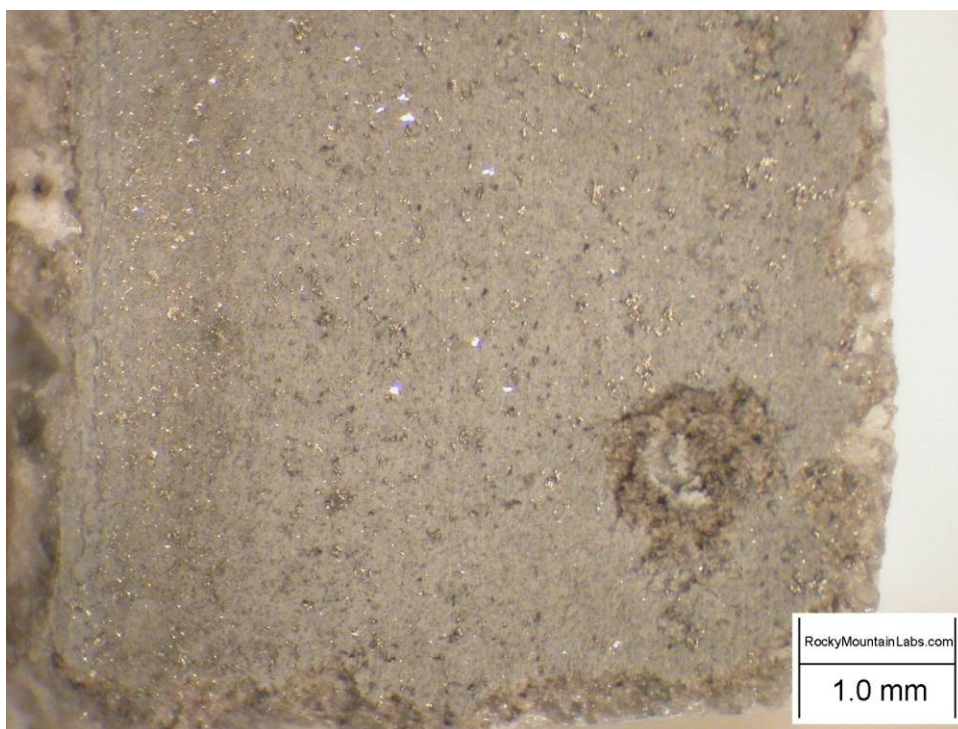


Figure 63. 24X optical image of Sample 8

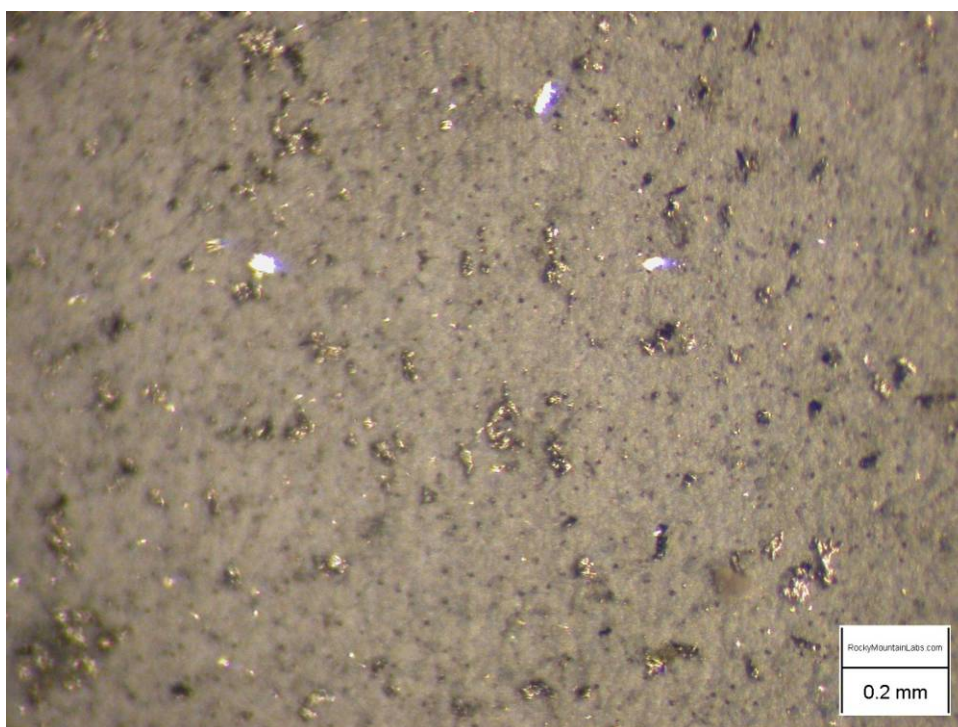


Figure 64. 80X optical image of Sample 8

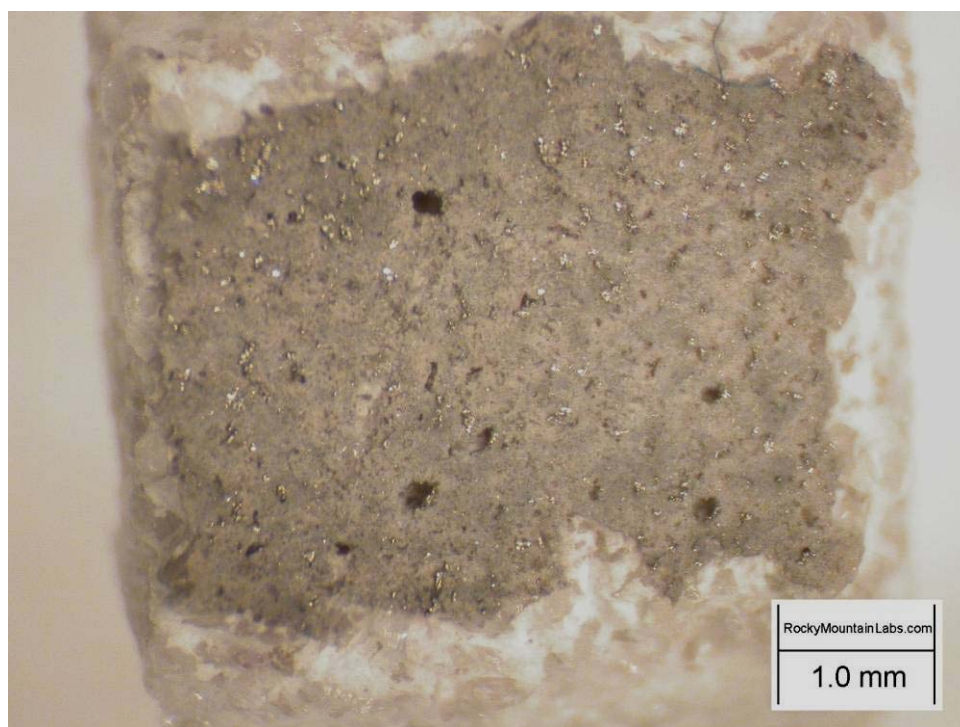


Figure 65. 24X optical image of Sample 9

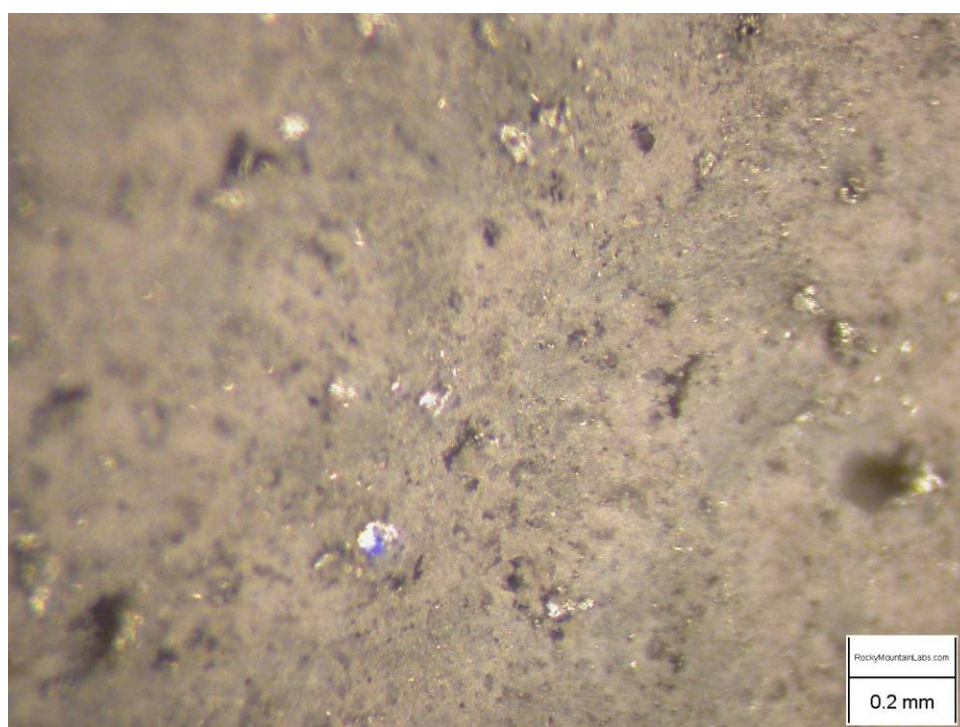


Figure 66. 80X optical image of Sample 9

5.3. Results of Analytical Examinations

5.3.1. XRD results

Figure 67 shows the result of Y_2O_3 identification on the Y_2O_3 Y Aerosol spray coating MOR test bar (after dewaxing) by XRD. The XRD pattern B is much closer to pattern A, indicating a good bonding condition between the Y_2O_3 aerosol spray coating and the normal facecoating.

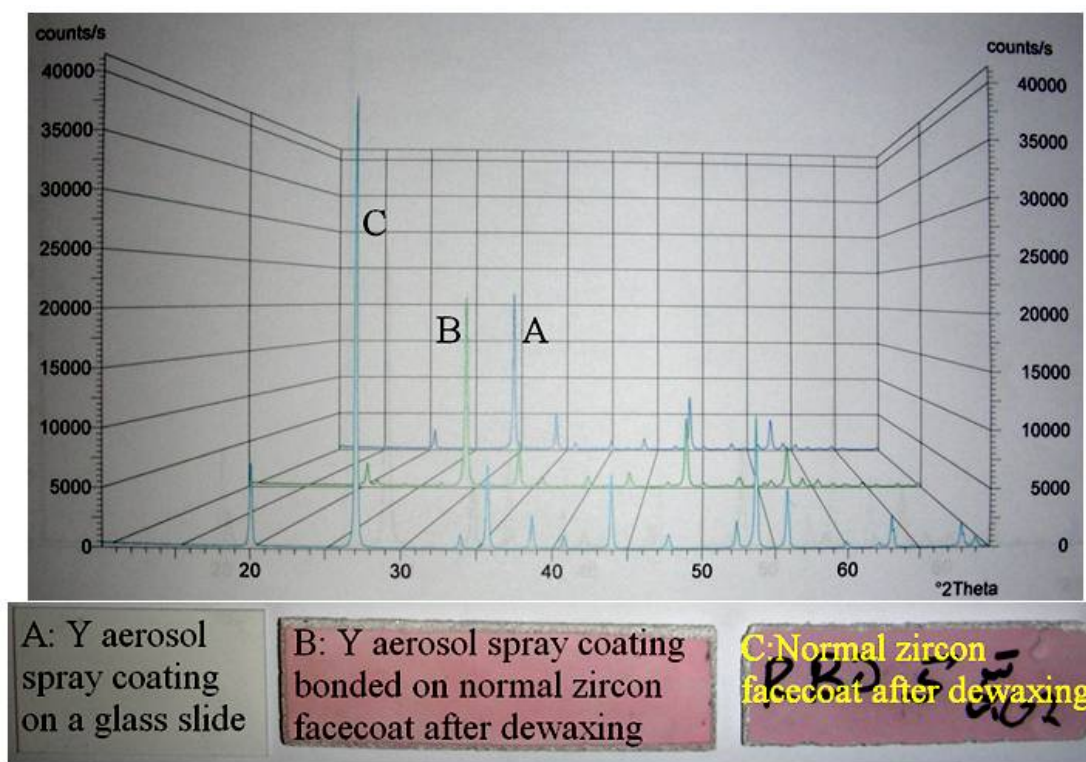


Figure 67. Y_2O_3 identification on the Y_2O_3 Y Aerosol spray coating MOR test bar after dewaxing by XRD

5.3.2. SEM/EDS results

Table 10 shows a summary of the relative elemental surface composition of samples as determined by EDS analysis (atom %). **Figure 68** through **Figure 107** show detailed results of SEM/EDS analysis.

Area	C	O	Al	Si	Ca	Ti	Cr	Co	Ni	Y	Zr	Hf	Mo	Ta	W	Re
1-Bulk	1.1	7.1	15	-	-	3.0	12	8.5	50	-	-	-	0.7	3.1	0.1	-
1-Shiny	-	-	3.1	-	-	0.8	22	14	26	-	-	-	3.5	7.4	13	11
1-Dark	-	57	32	2.8	4.5	0.1	0.2	0.2	1.5	1.9	-	-	-	-	-	-
2-Light	-	57	32	2.8	4.5	0.1	0.2	0.2	1.5	-	-	-	-	-	-	1.9
2-Dark	-	68	3.2	0.9	1.4	-	-	-	0.3	-	26	0.6	-	-	-	-
2-Gold	-	13	11	-	0.4	3.1	10	8.1	51	-	0.3	-	0.2	3.0	-	-
3-Dark	5.3	43	27	-	0.3	0.5	1.4	2.1	15	3.8	-	0.4	-	0.9	0.1	0.1
3-Gold	5.8	4.5	13	-	-	1.7	5.4	7.7	59	-	-	-	0.2	3.0	0.2	0.2
3-Dark	-	57	42	-	-	-	-	-	0.2	0.6	-	-	-	-	-	-
5-Light	11	39	33	-	-	1.8	1.1	1.4	9.3	-	-	-	-	3.2	-	-
5-Dark	-	42	38	-	-	0.4	1.2	2.0	15	-	-	-	-	0.5	0.2	-
5-Light	8.5	39	27	-	-	0.6	2.2	2.2	20	-	-	-	-	1.1	0.4	-
8-Light	16	-	-	-	-	29	-	-	-	-	-	-	-	53	-	-
8-Light	0.4	16	6.1	-	-	36	-	-	-	-	-	-	-	38	-	-

Table 10. Relative elemental surface composition of samples as determined by EDS analysis (atom %).

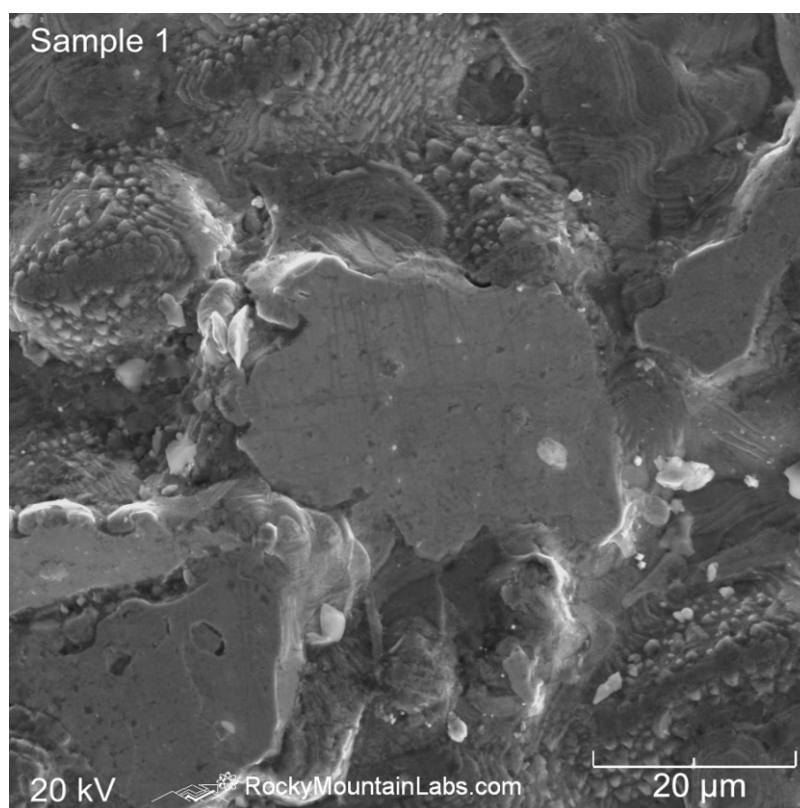


Figure 68. 1500X SEM image of shiny spot on Sample 1

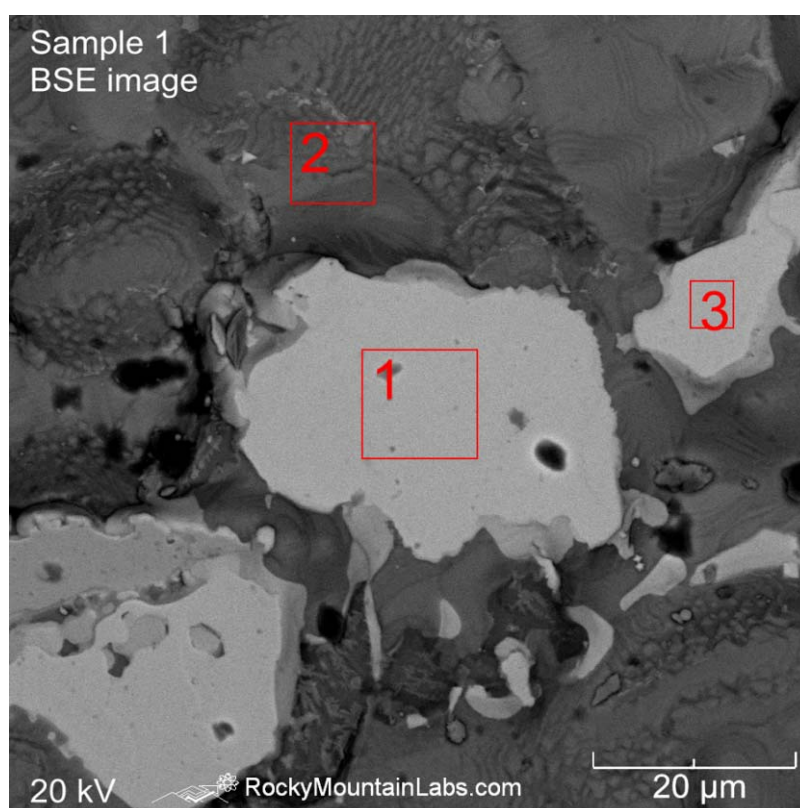


Figure 69. 1500X BSE image of shiny spot on Sample 1

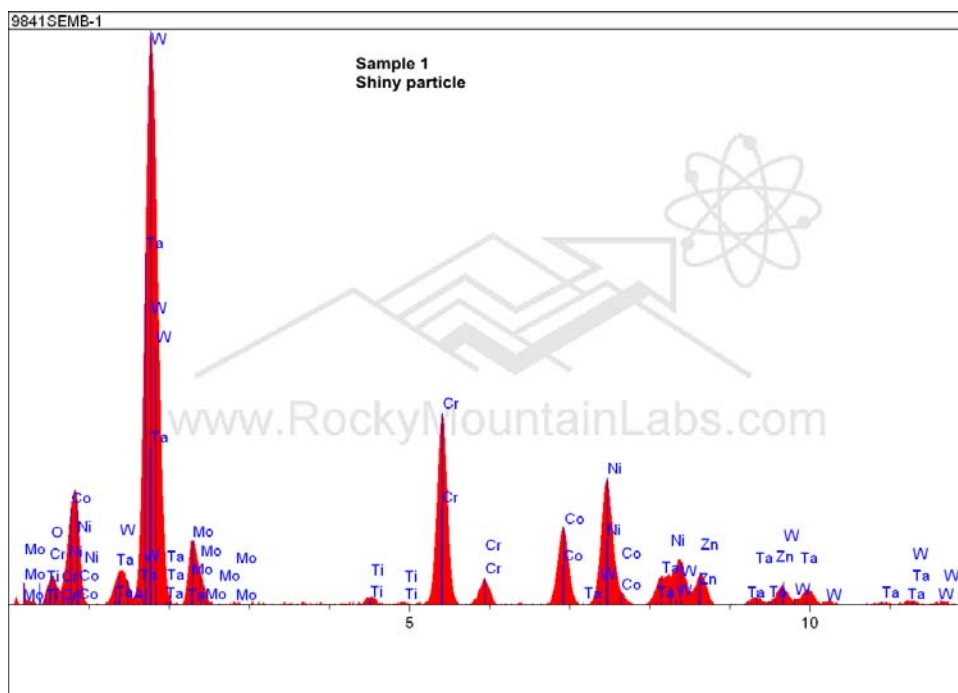


Figure 70. EDS spectrum of Area 1 in **Figure 69**.

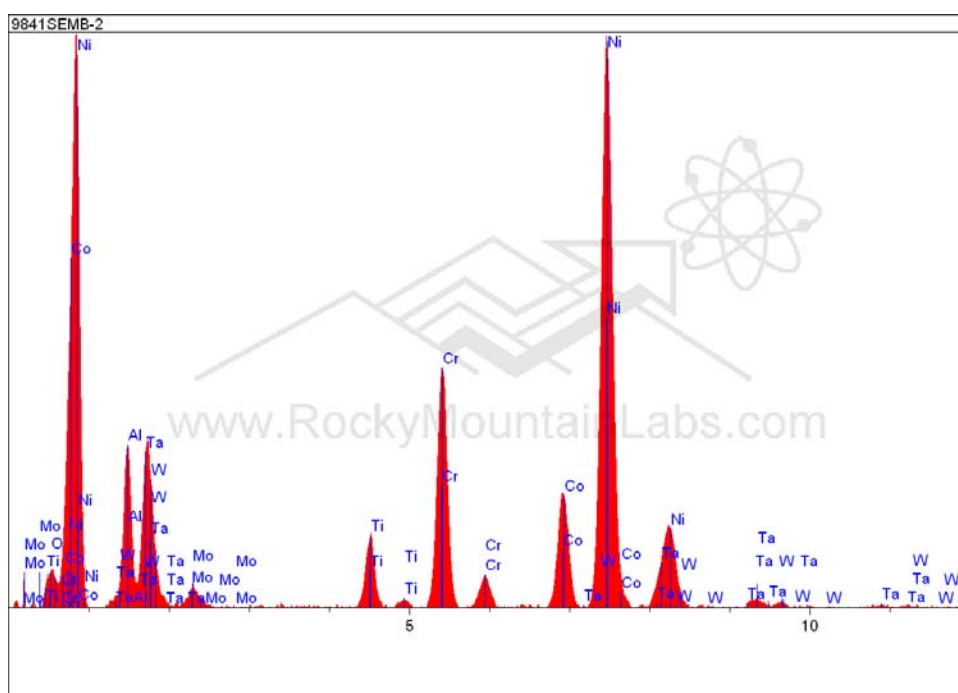


Figure 71. EDS spectrum of Area 2 in **Figure 69**.

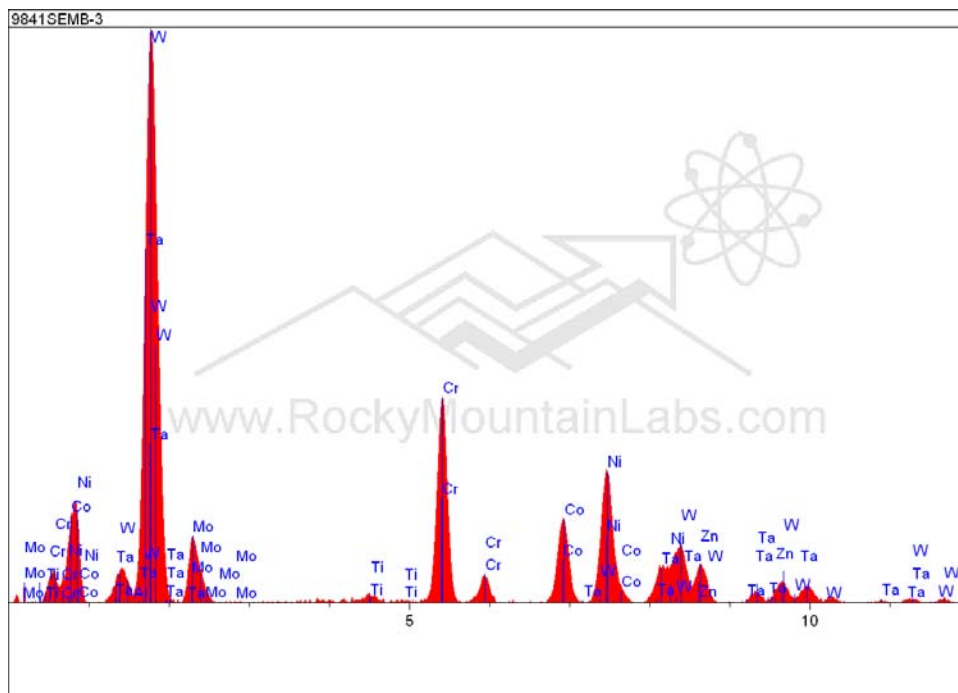


Figure 72. EDS spectrum of Area 3 in **Figure 69**.

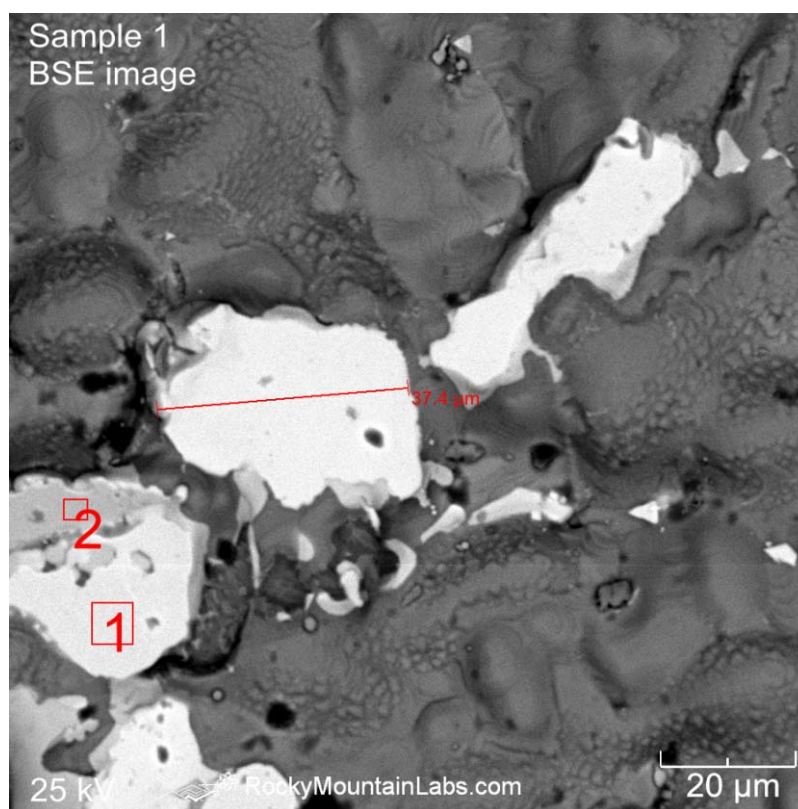


Figure 73. 1000X BSE image of shiny spots on Sample 1

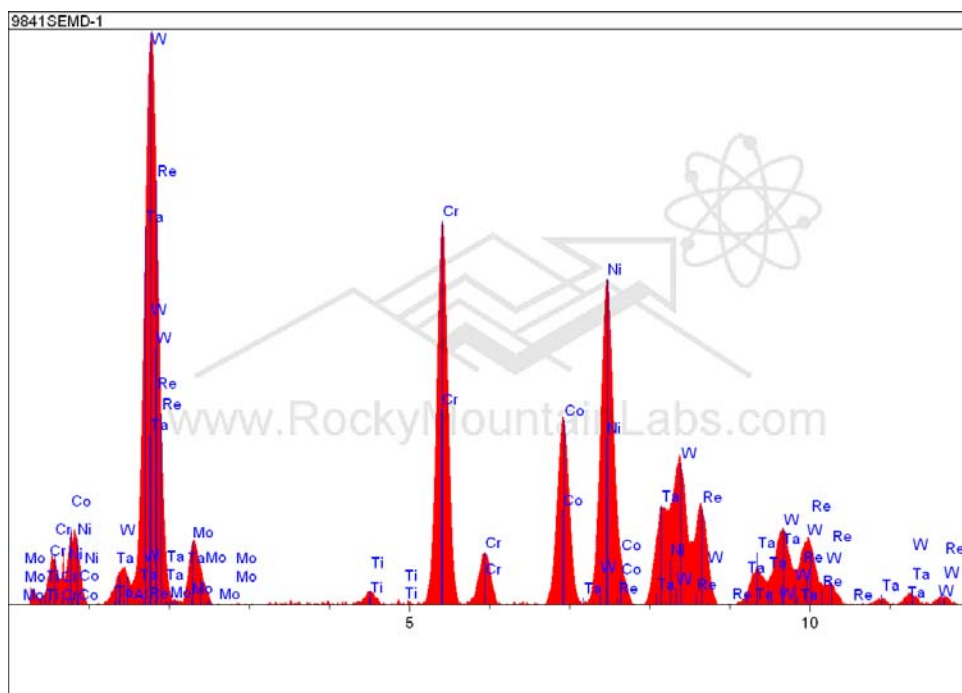


Figure 74. EDS spectrum of Area 1 in **Figure 73**.

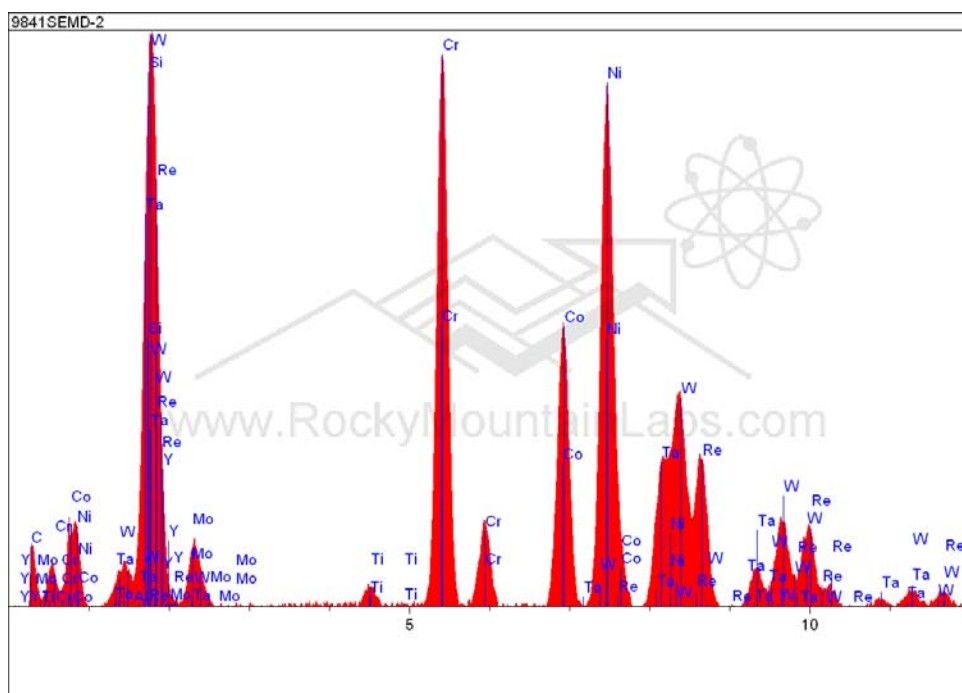


Figure 75. EDS spectrum of Area 2 in **Figure 73**.

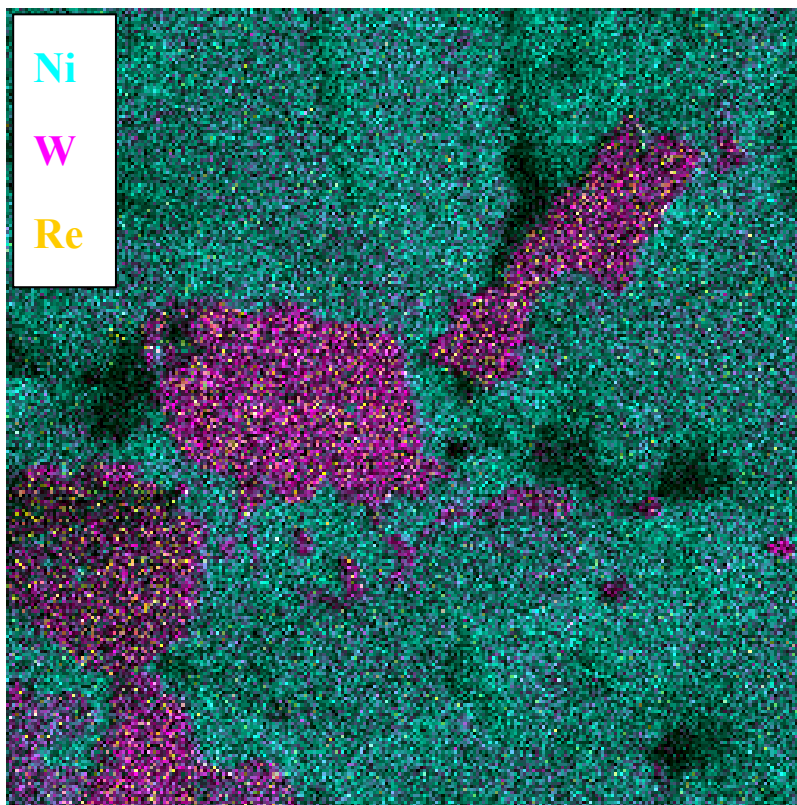


Figure 76. EDS map of Area in **Figure 73**.

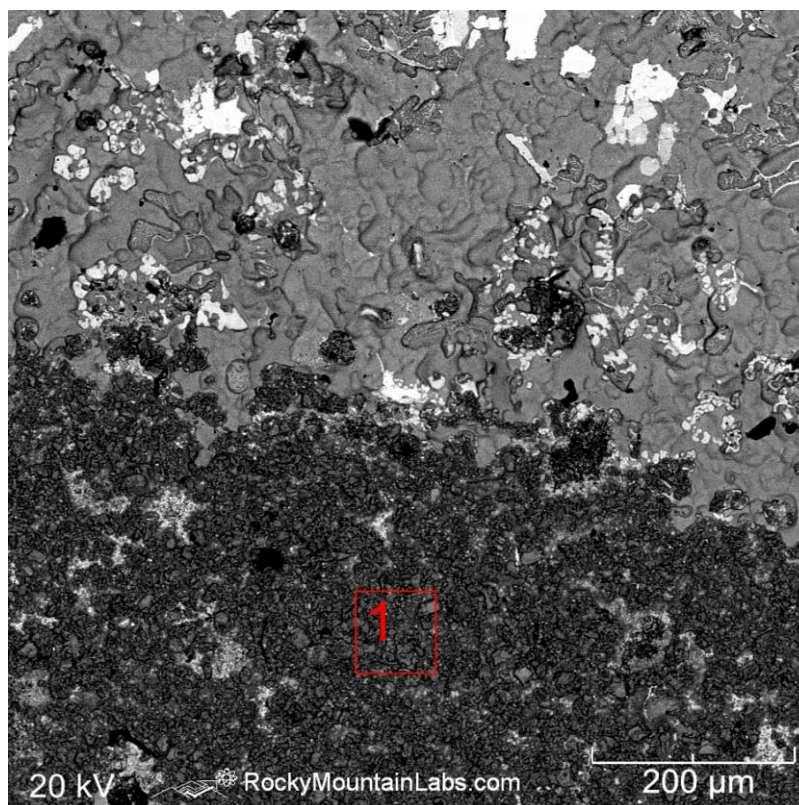


Figure 77. 150X BSE image of dark and golden area on Sample 1

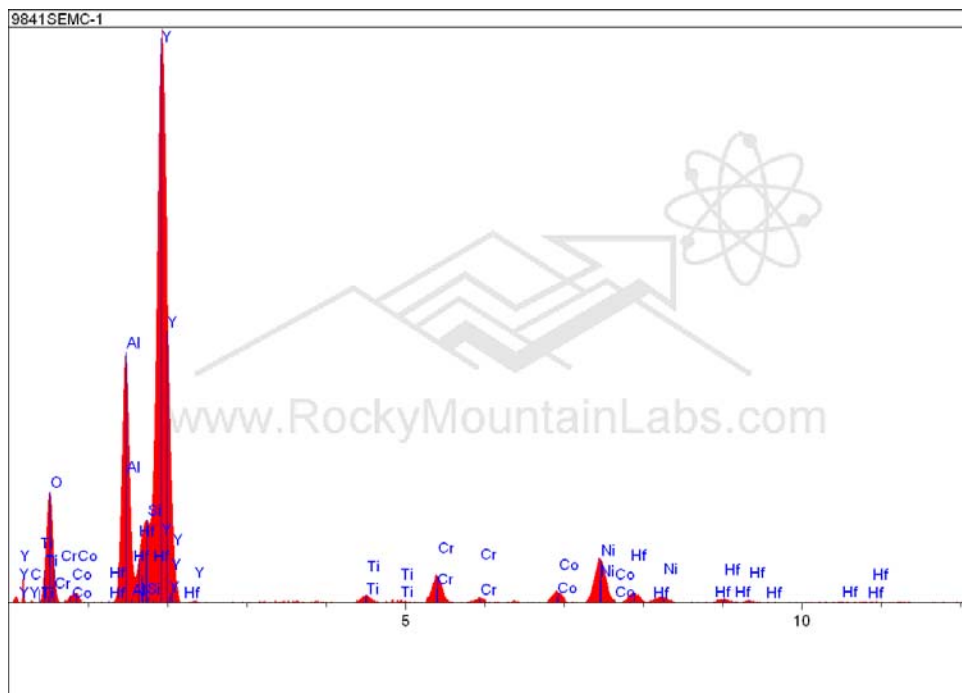


Figure 78. EDS spectrum of Area 1 in **Figure 77**.

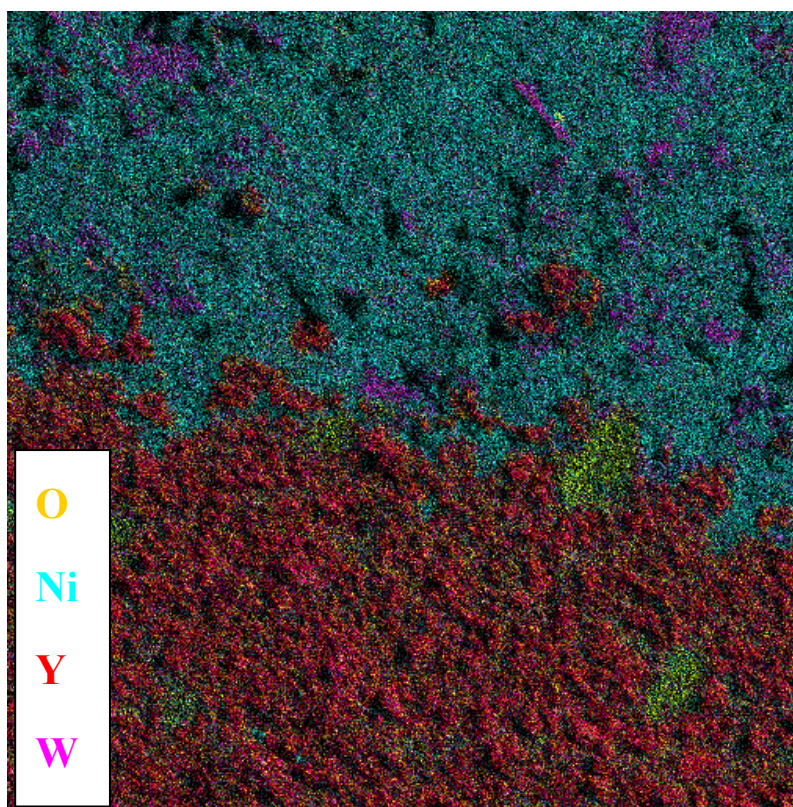


Figure 79. EDS map of Area in **Figure 77**.

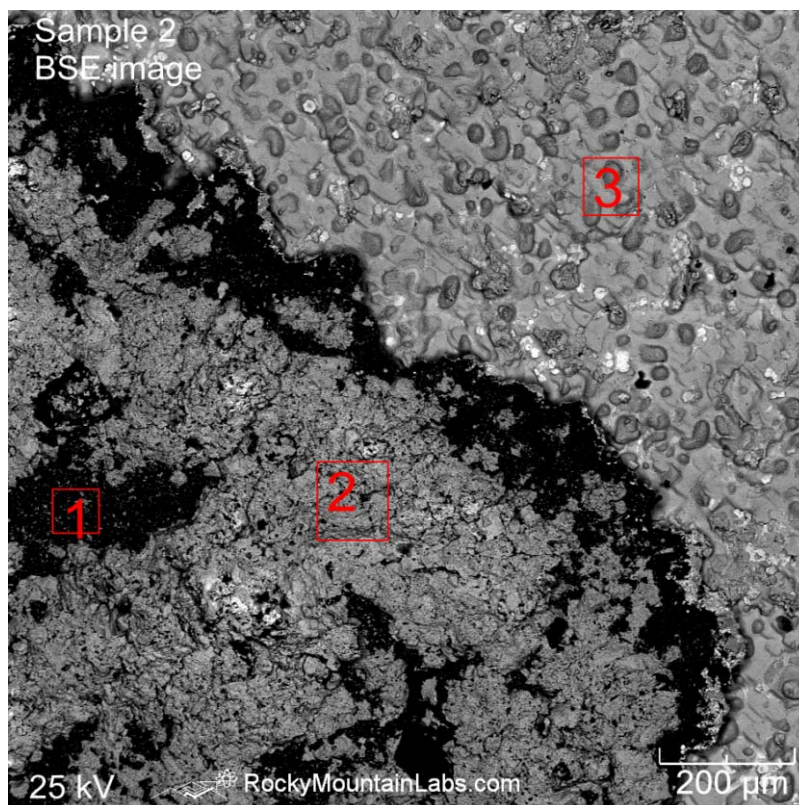


Figure 80. 100X BSE image of Sample 2

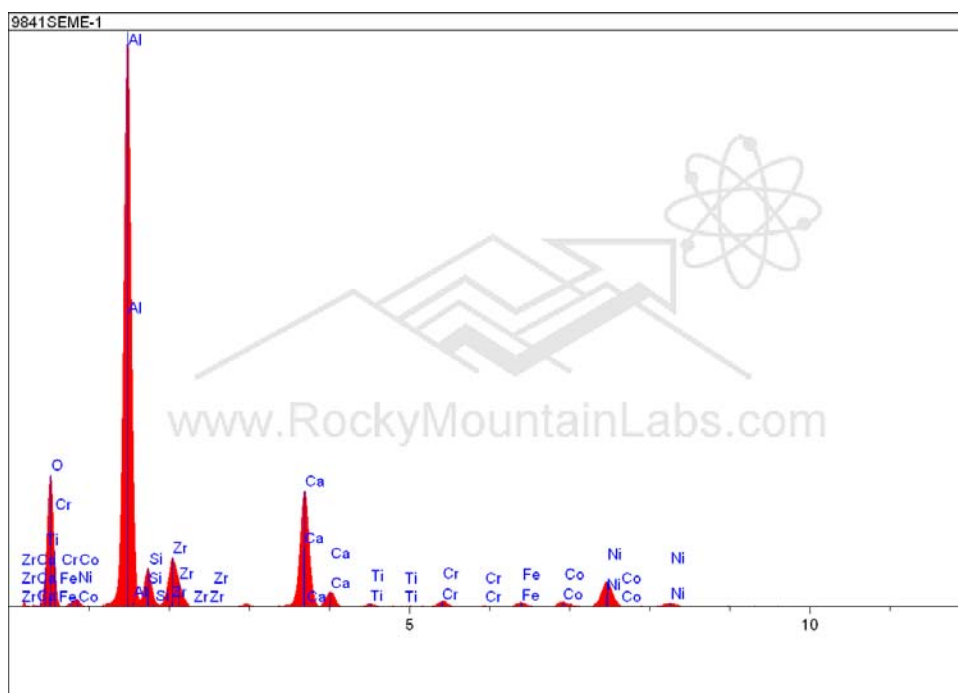


Figure 81. EDS spectrum of Area 1 in **Figure 80.**
(Optically light colored area)

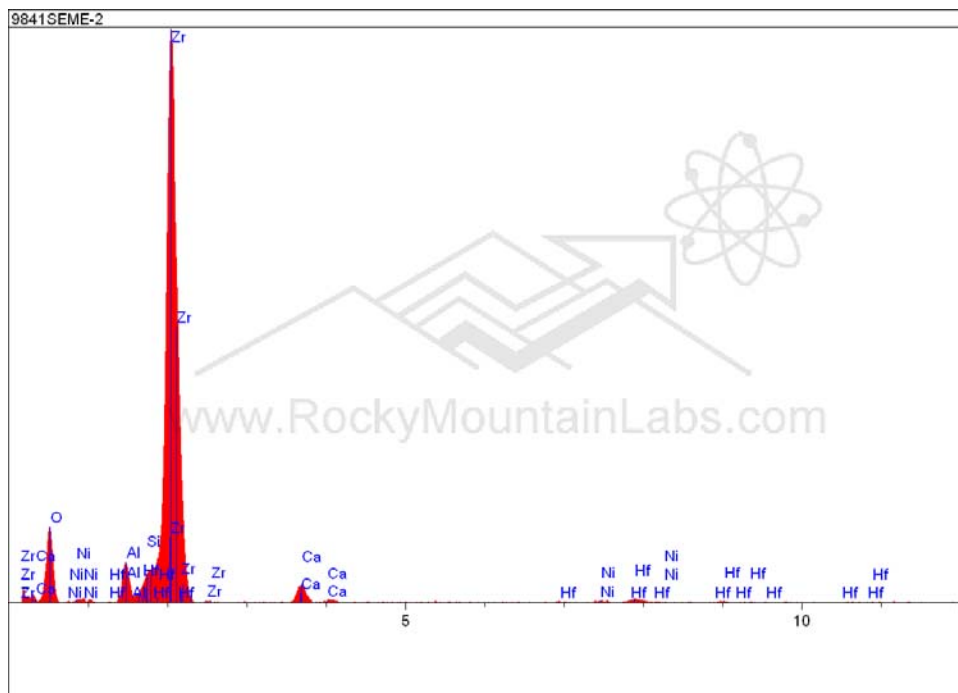


Figure 82. EDS spectrum of Area 2 in **Figure 80.**
(Optically dark colored area)

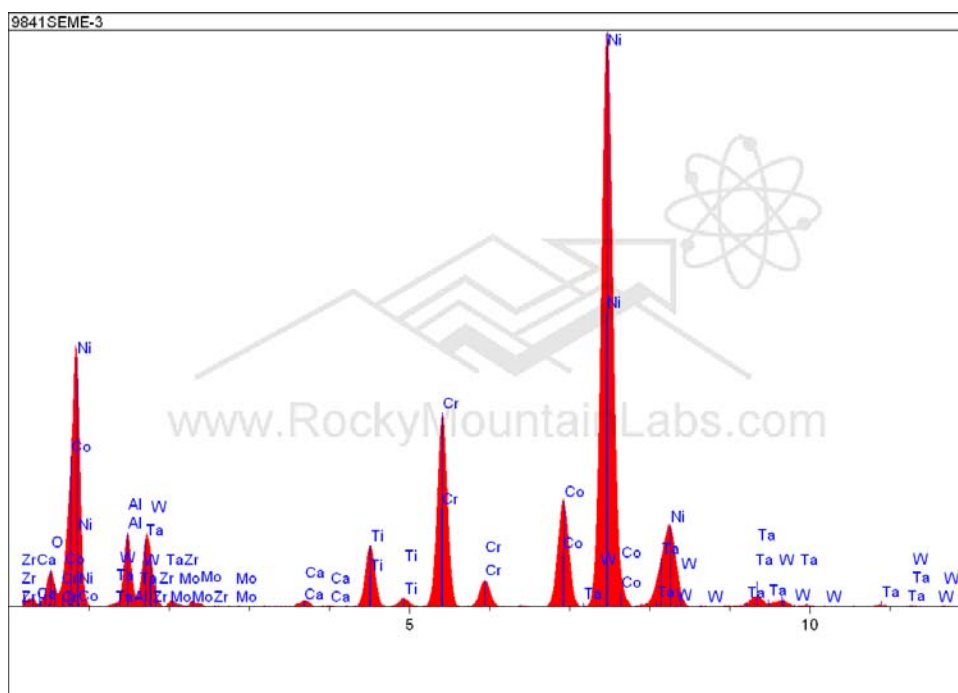


Figure 83. EDS spectrum of Area 3 in **Figure 80.**
(Optically gold colored area)

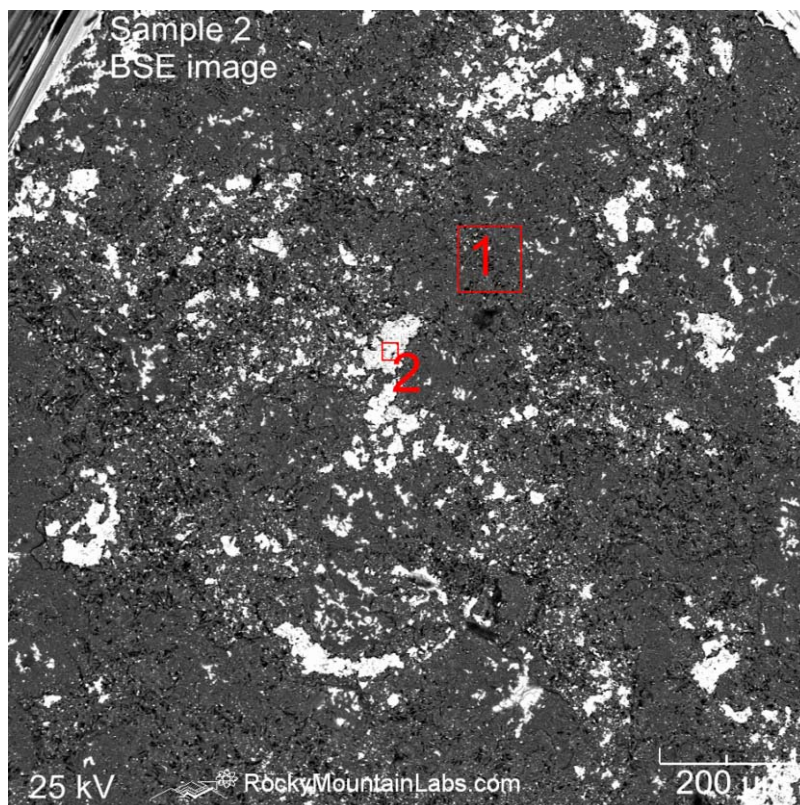


Figure 84. 100X BSE image of Sample 2

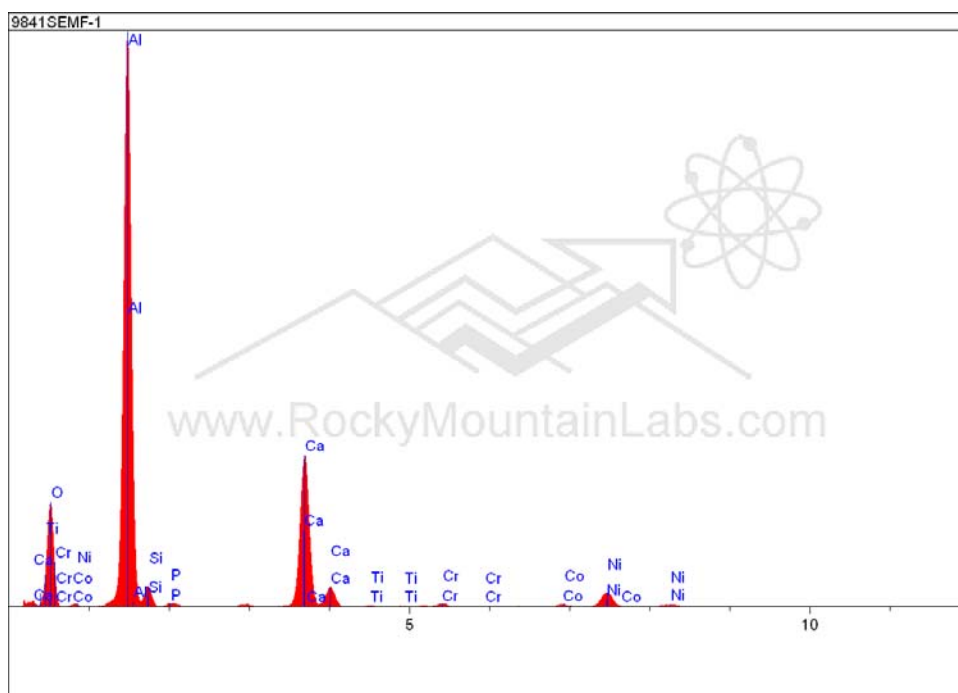


Figure 85. EDS spectrum of Area 1 in **Figure 84.**
(Optically light colored area)

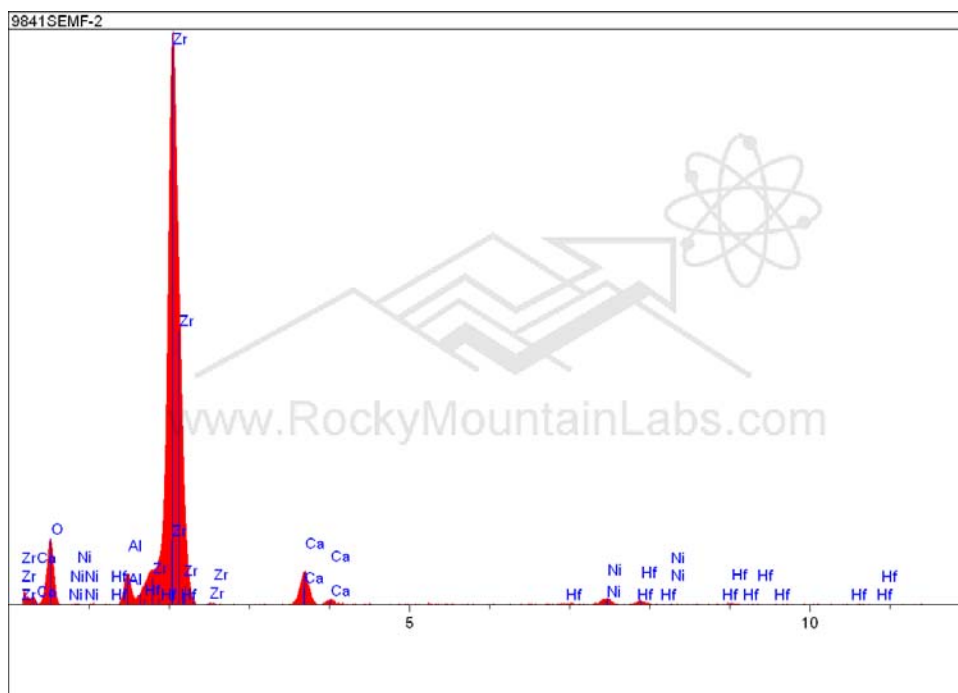


Figure 86. EDS spectrum of Area 2 in **Figure 84.**
(Optically dark colored area)

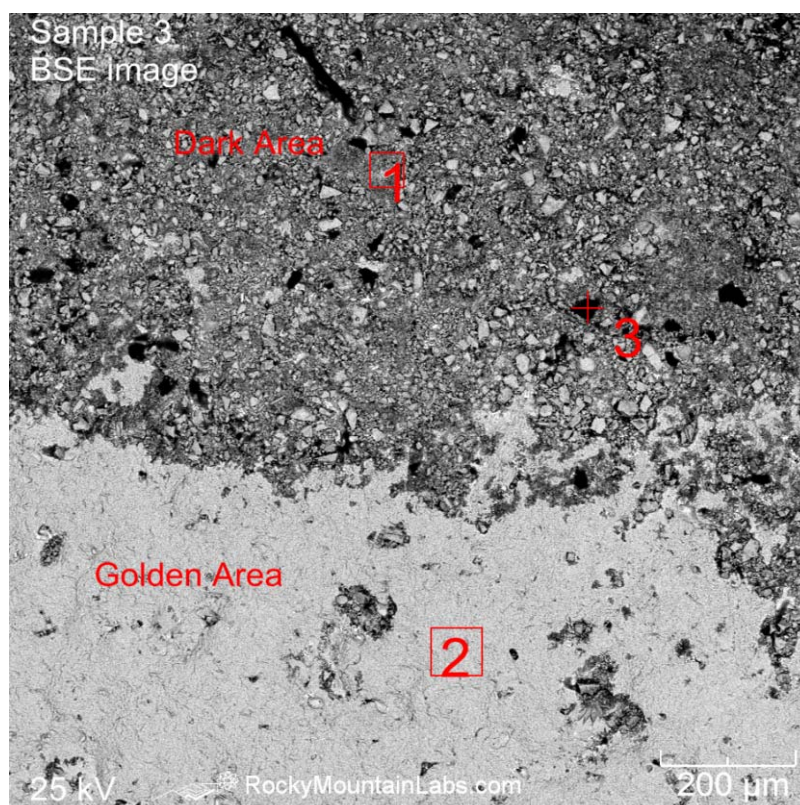


Figure 87. 100X BSE image of Sample 3

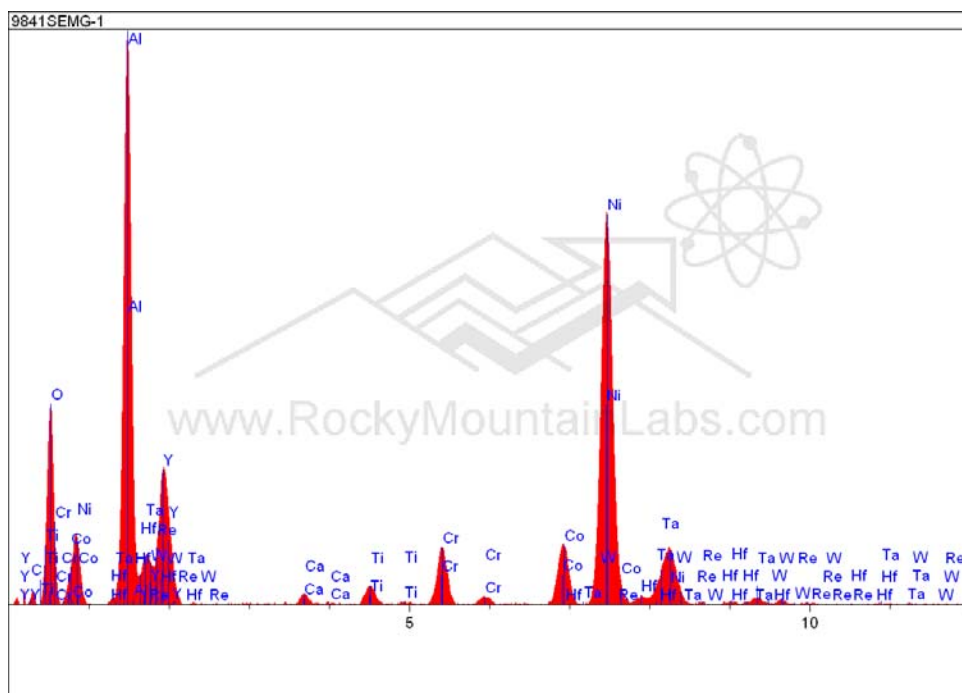


Figure 88. EDS spectrum of Area 1 in **Figure 87.**
(Optically dark colored area)

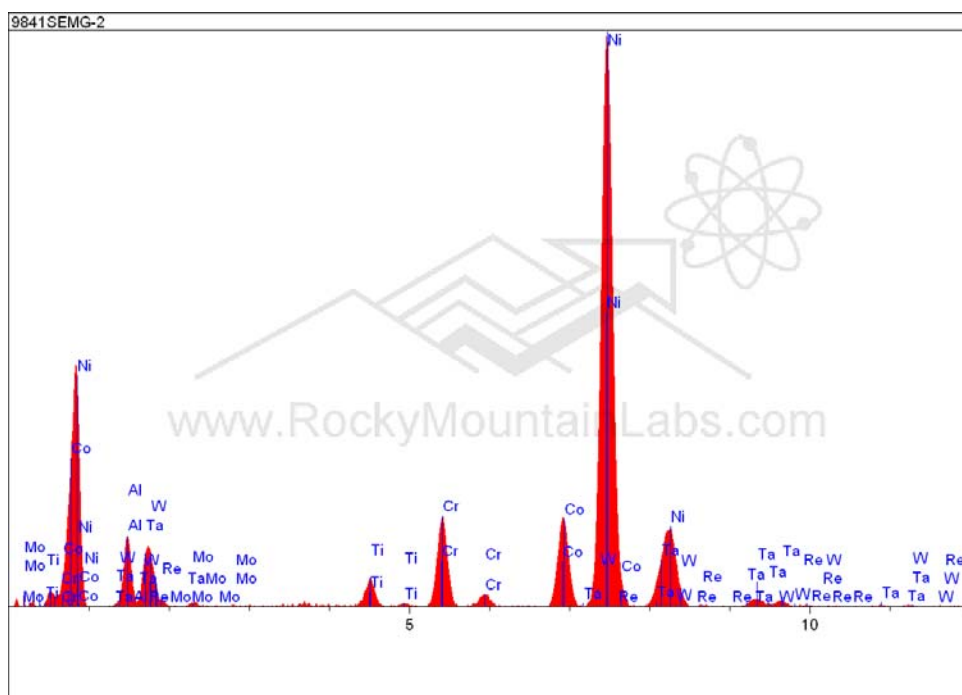


Figure 89. EDS spectrum of Area 2 in **Figure 87.**
(Optically gold colored area)

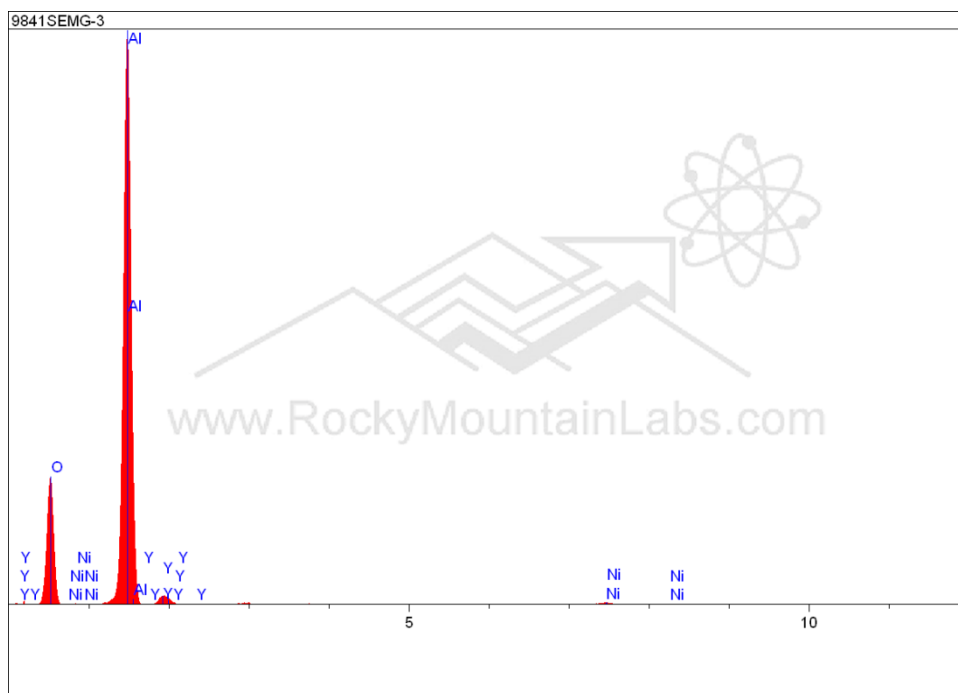


Figure 90. EDS spectrum of Point 3 in **Figure 87**.

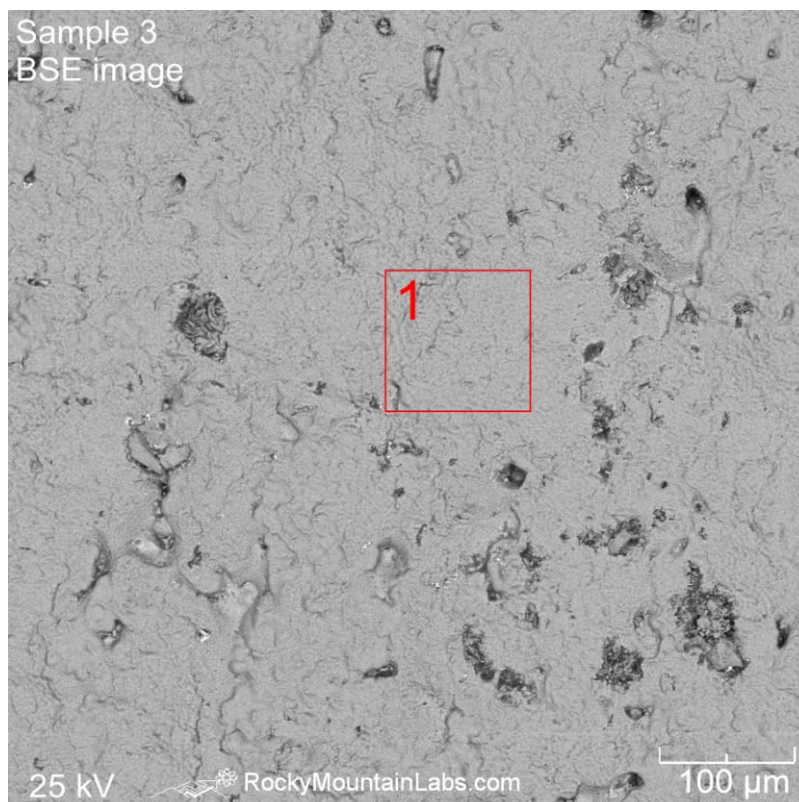


Figure 91. 200X BSE image of gold colored area on **Sample 3**

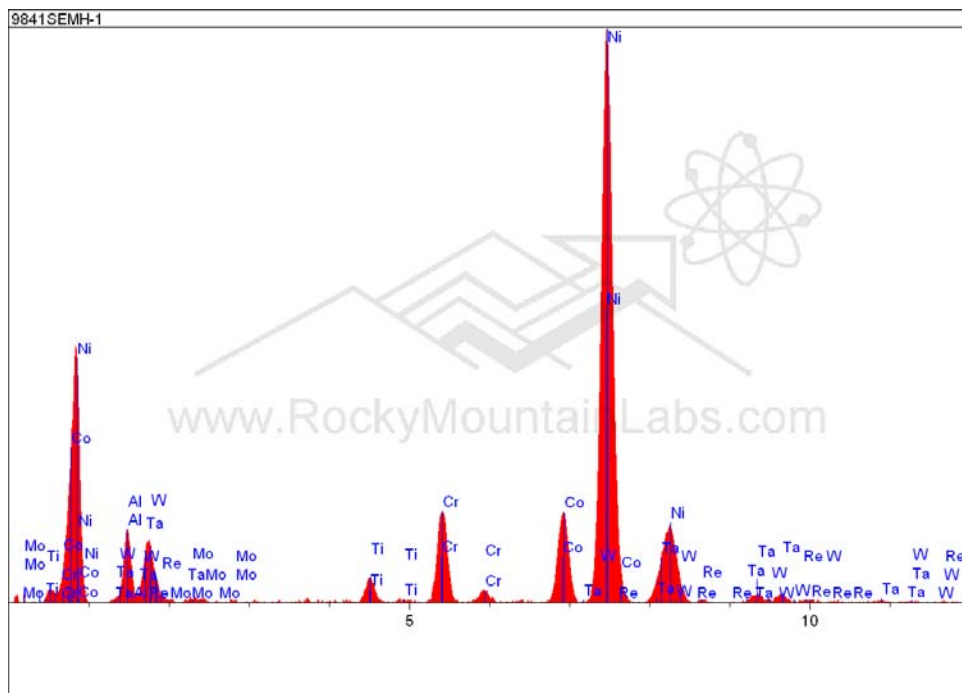


Figure 92. EDS spectrum of Area 1 in **Figure 90**.

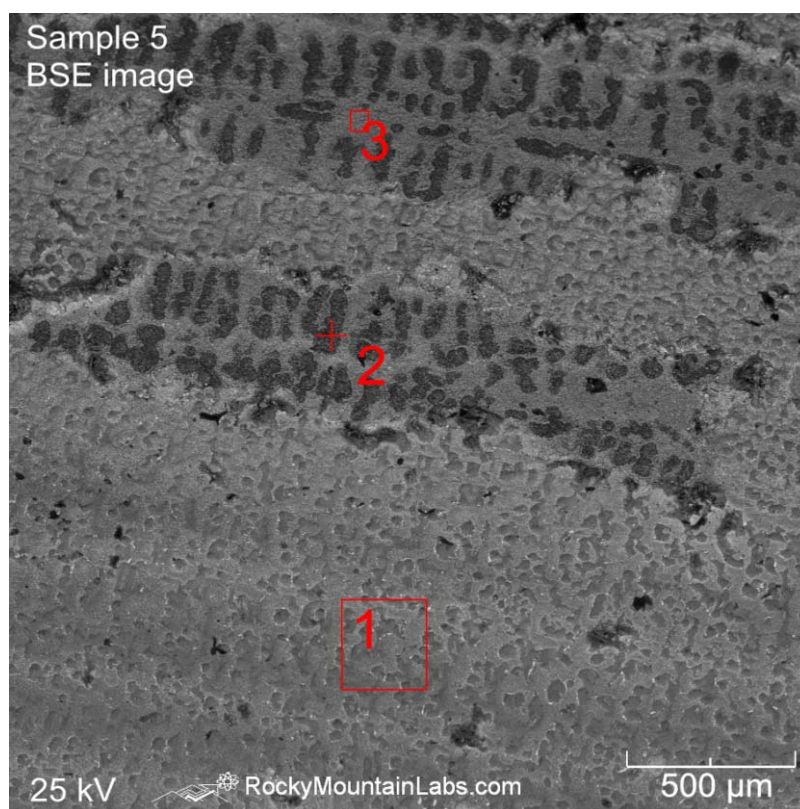


Figure 93. 50X BSE image of Sample 5

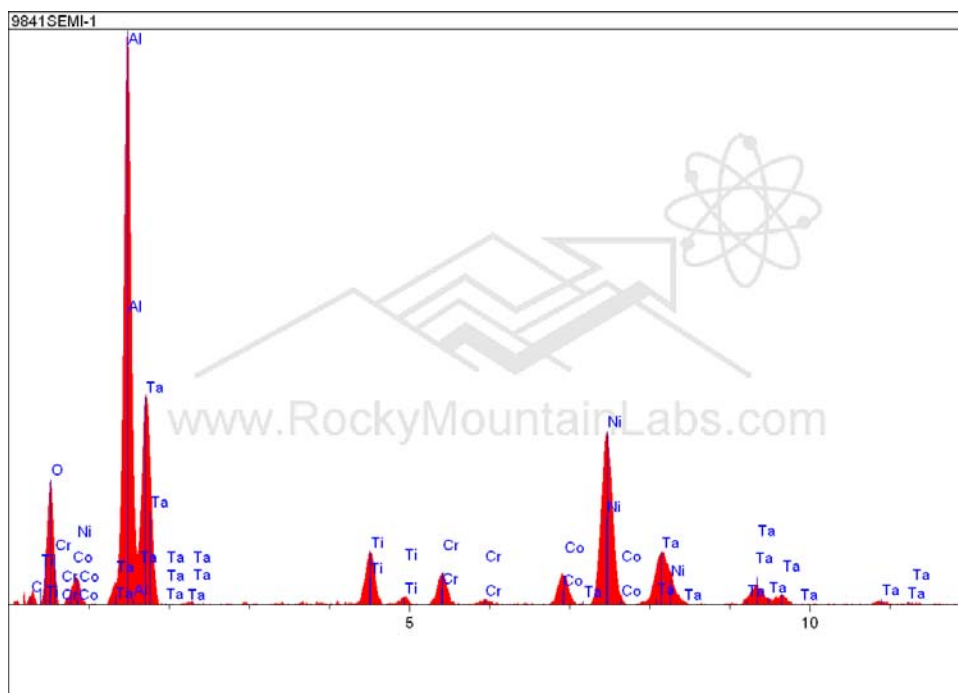


Figure 94. EDS spectrum, Area 1 in **Figure 93**.

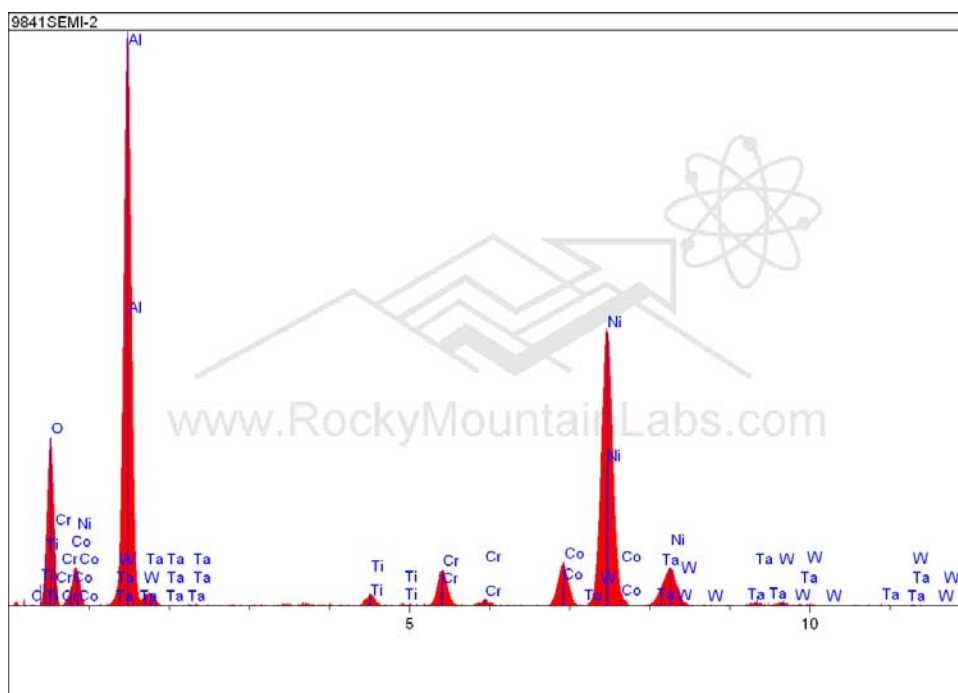


Figure 95. EDS spectrum, Point 2 in **Figure 93**.

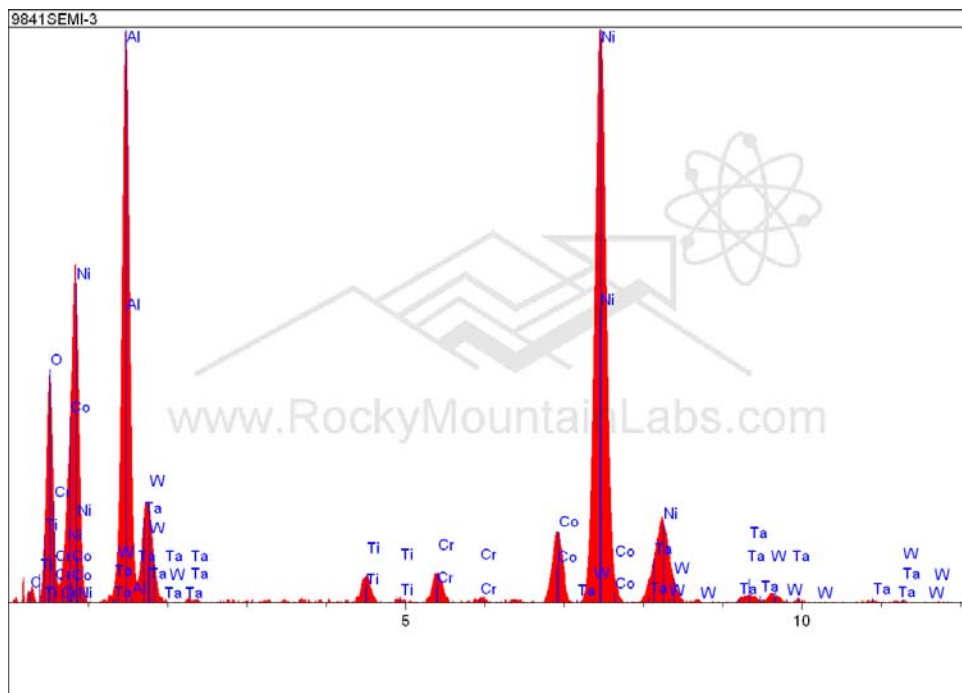


Figure 96. EDS spectrum, Area 3 in **Figure 91**.

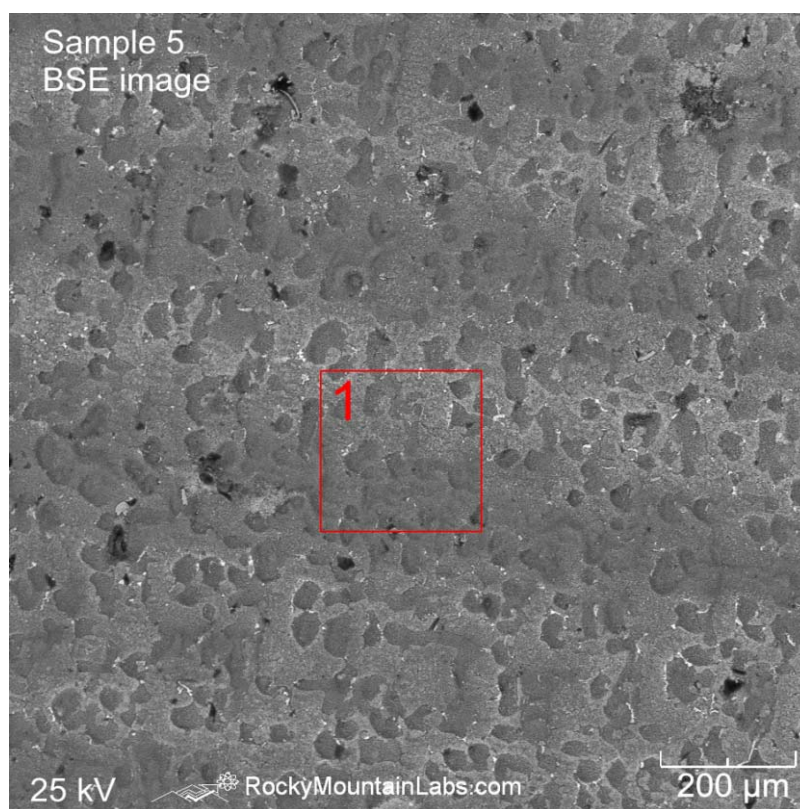


Figure 97. 100X BSE image of Sample 5

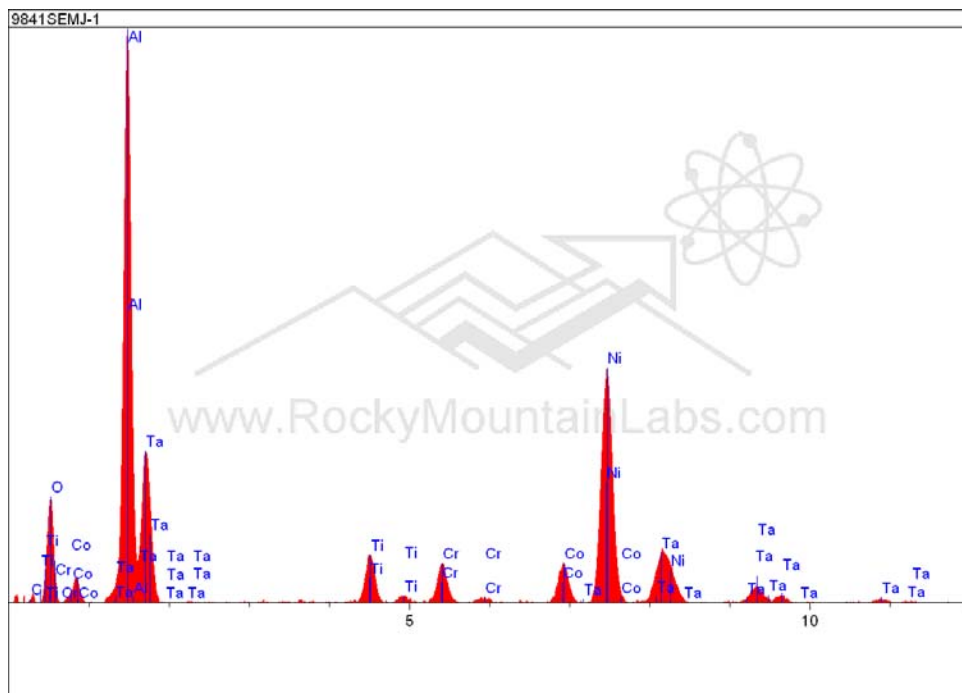


Figure 98. EDS spectrum of Area 1 in **Figure 97**.

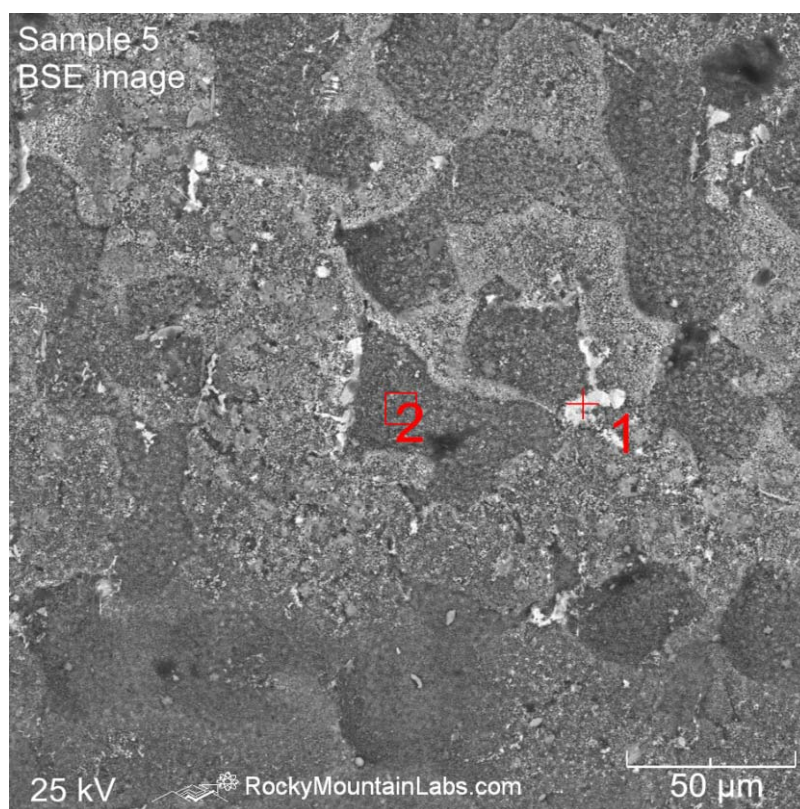


Figure 99. 500X BSE image of Sample 5

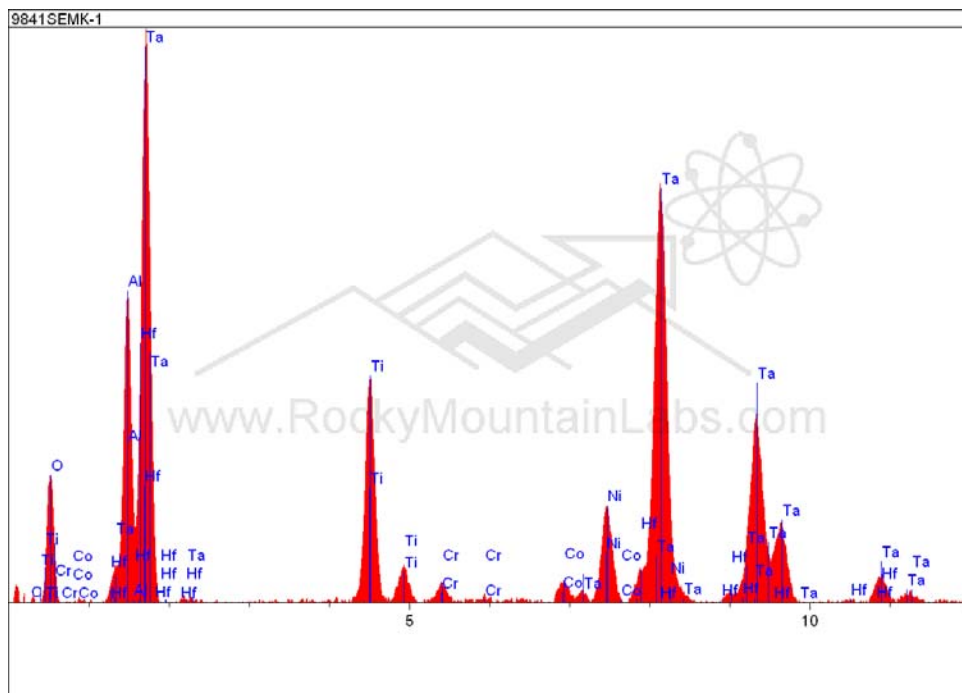


Figure 100. EDS spectrum of Point 1 in Figure 99.

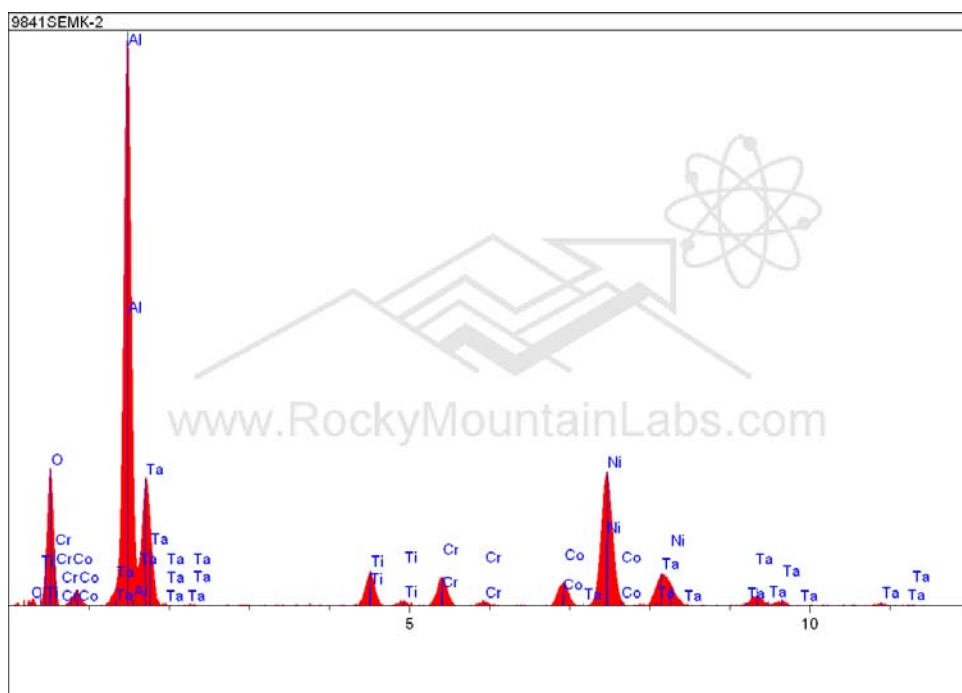


Figure 101. EDS spectrum of Area 2 in Figure 99.

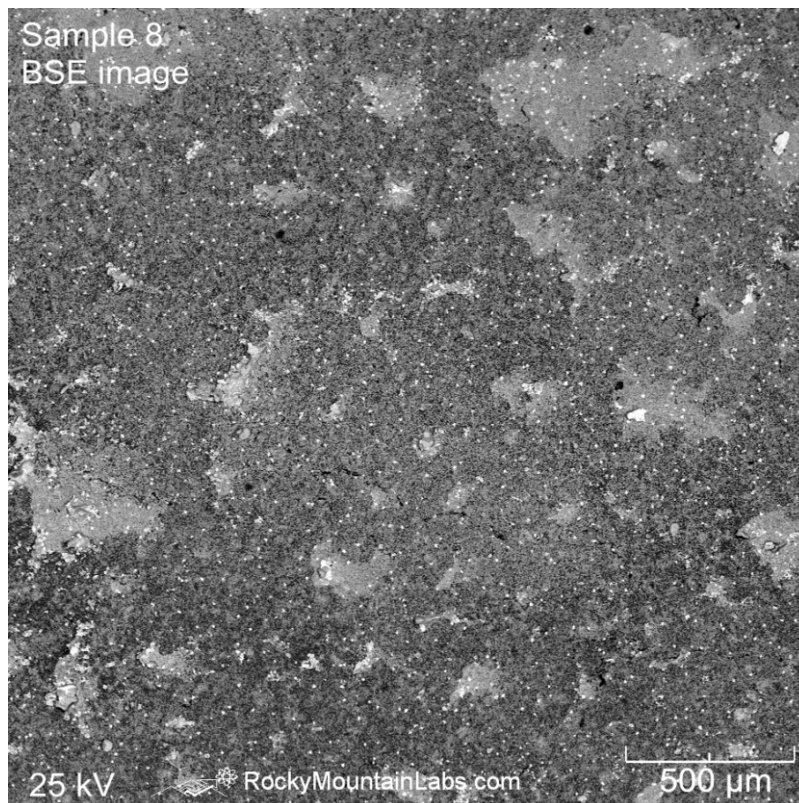


Figure 102. 50X BSE image of Sample 8 Back up

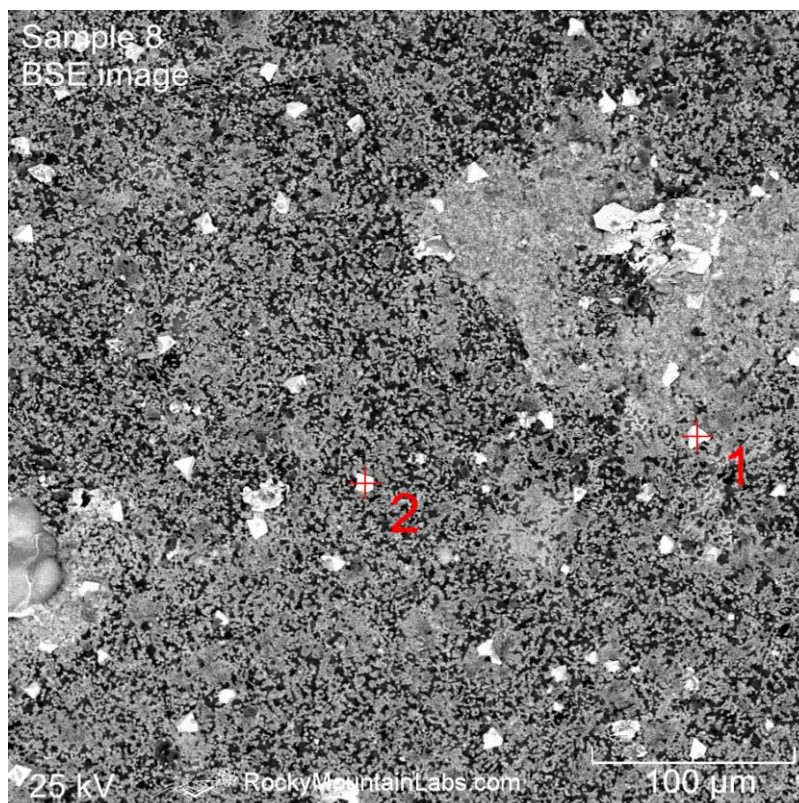


Figure 103. 300X BSE image of Sample 8 Back up

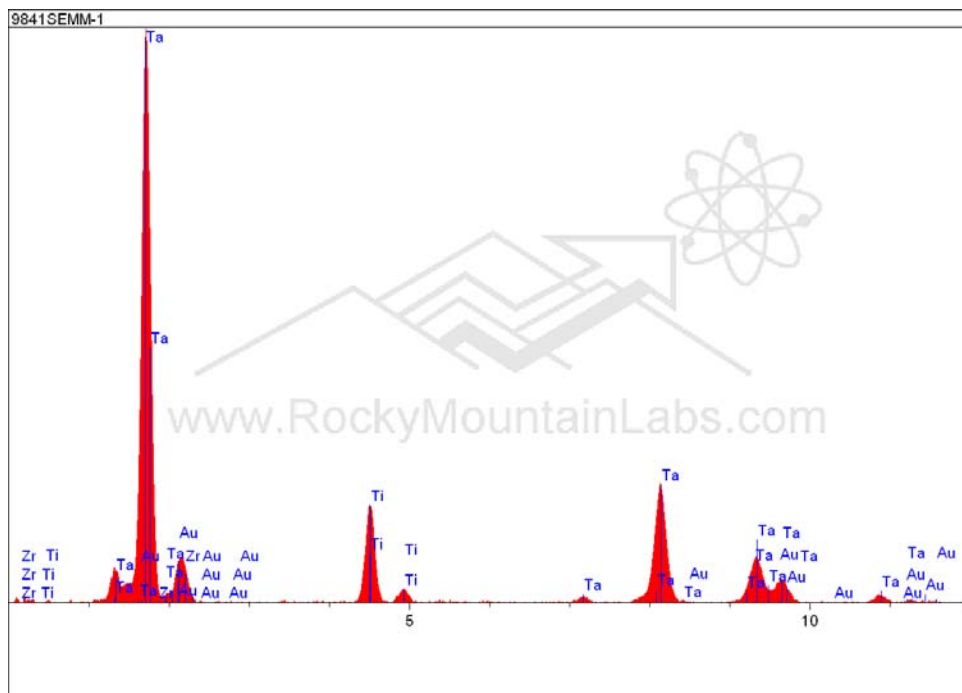


Figure 104. EDS spectrum of Point 1 in **Figure 103**.

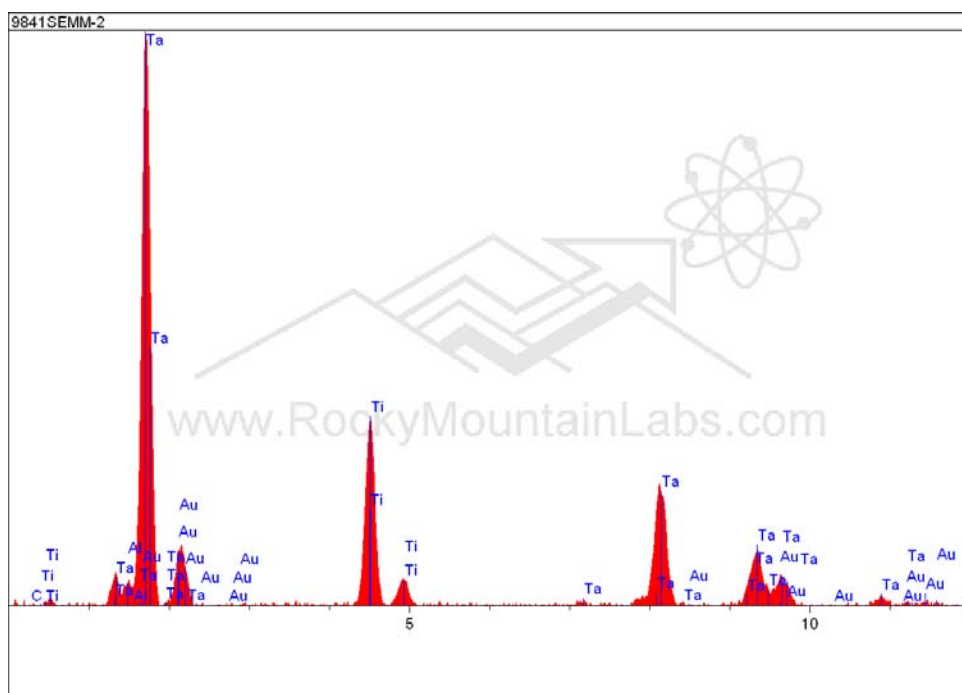


Figure 105. EDS spectrum of Point 2 in **Figure 103**.

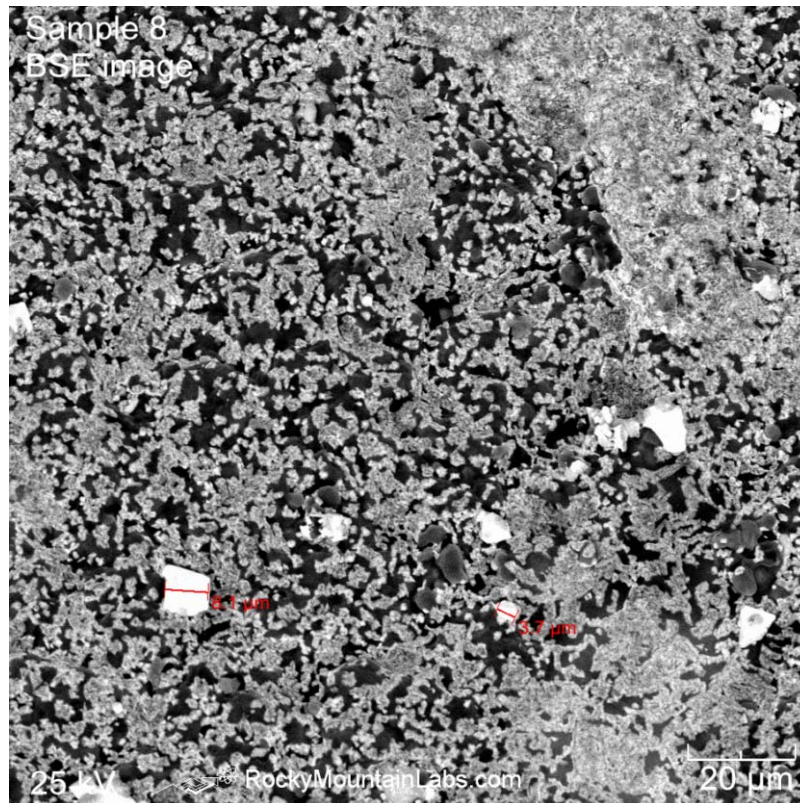


Figure 106. 800X BSE image of Sample 8

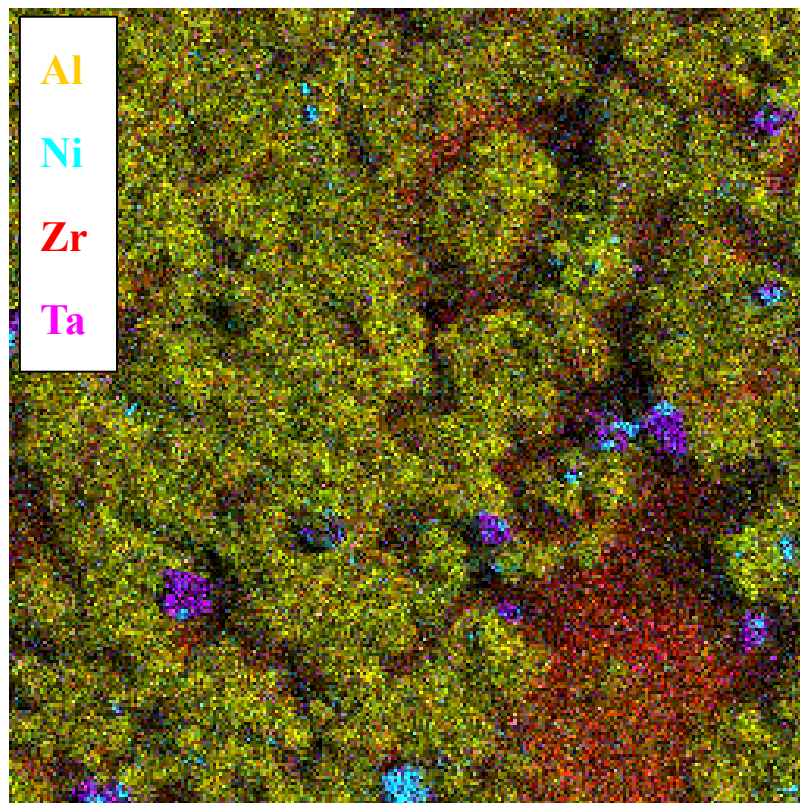


Figure 107. EDS map of area in **Figure 106.**

5.3.3. AES results

Table 11 shows a summary of the relative elemental surface composition of samples as determined by AES analysis (atom %). **Figure 108** through **Figure 124** show detailed results of the AES analysis.

Area	C	O	Al	Si	Ti	Cr	Co	Ni	Cu	Zn	Zr	Hf	Mo	Ta	W	Re
1-Shiny	48	17	2.6	4.8*	2.7	2.4	1.7	3.2	-	0.6	2.9	-	5.5	3.3	5.0	-
1-Shiny [†]	2.2	-	-	-	1.3	12	9.8	13	-	-	-	-	-	8.5	-	22
3-Gold	43	21	8.1	7.0	2.5	1.2	2.1	5.8	1.0	2.2	-	-	-	1.3	1.3	-
4-Gold	41	20	13	3.8*	4.6	1.2	2.1	3.3	1.4	5.6	1.9	-	-	1.4	-	-
4-Grey	49	12	15	4.0*	2.1	-	1.0	0.9	1.7	11	2.0	-	-	-	-	-
4-Shiny	31	14	38	-	2.1	0.5	1.4	2.0	1.5	4.6	2.8	1.3	-	-	-	-
4-Shiny [†]	0.8	25	56	-	-	-	-	1.3	-	-	-	17	-	-	-	-

Table 11. Relative elemental surface composition of samples as determined by AES analysis (atom %). [†]Surveys taken after depth profile, *The detection and/or quantification of silicon is questionable due to spectral interferences

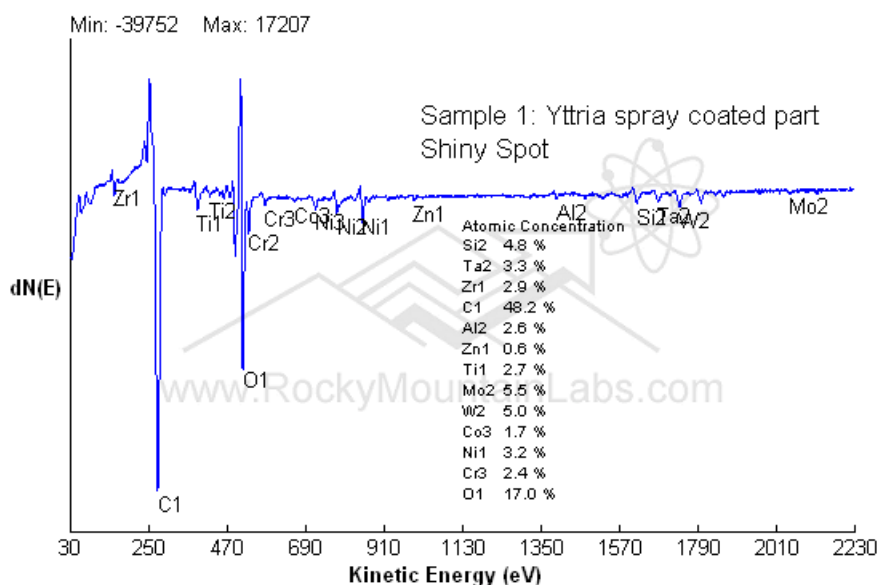


Figure 108. AES surface survey of shiny spot on Sample 1

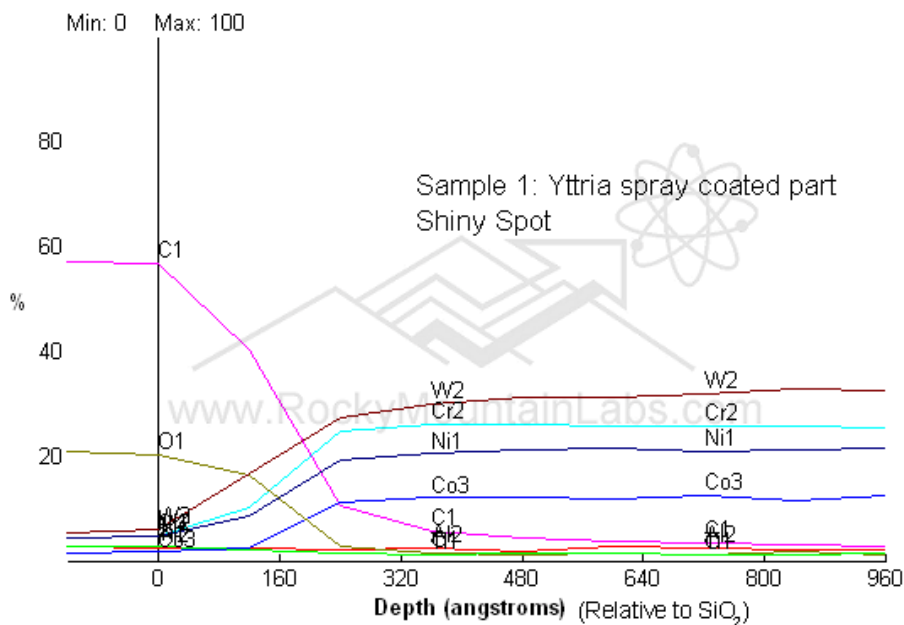


Figure 109. AES sputter depth profile of shiny spot on Sample 1

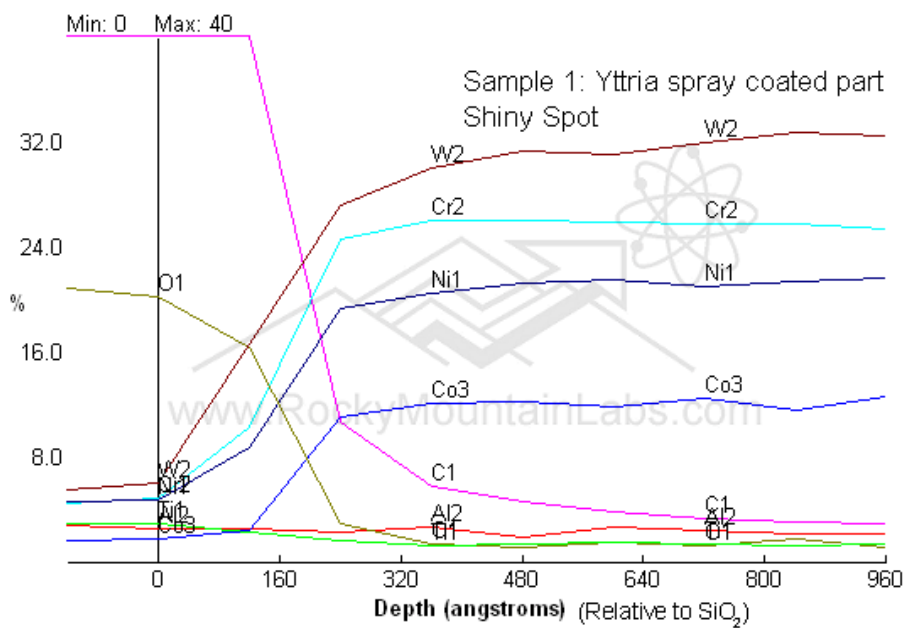


Figure 110. AES sputter depth profile of shiny spot on Sample 1, 0-40% plot

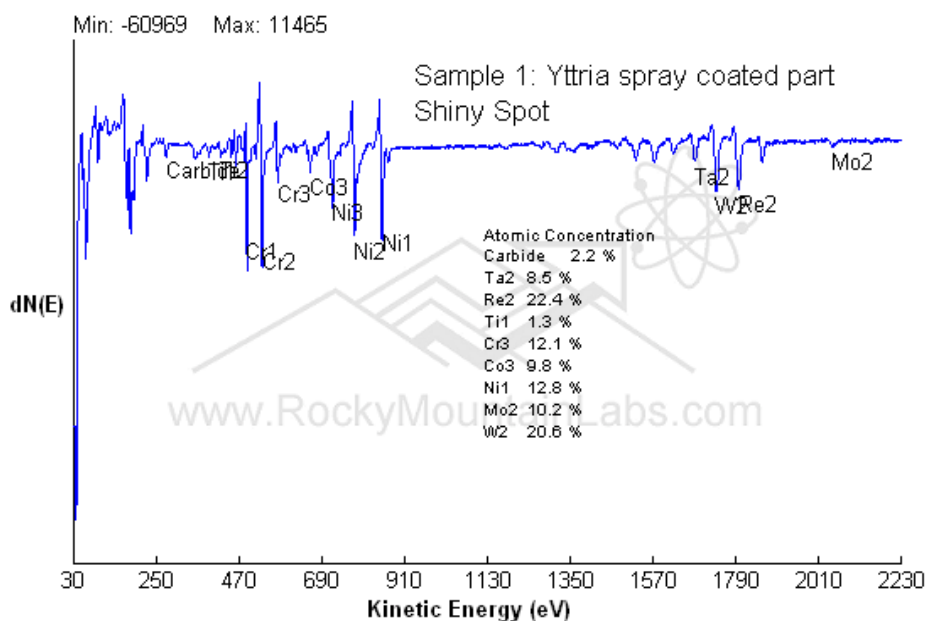


Figure 111. AES sub-surface survey of shiny spot on Sample 1

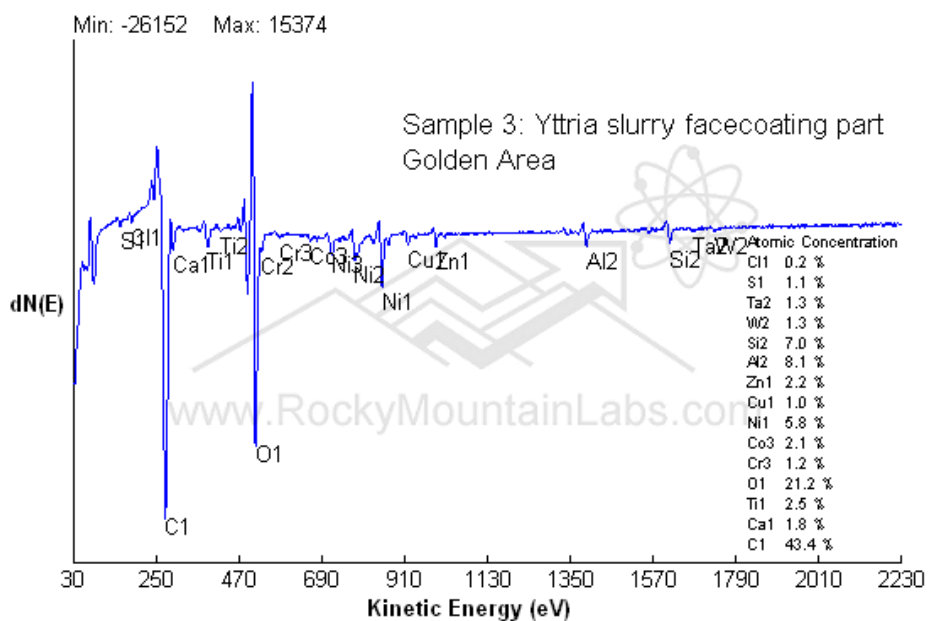


Figure 112. AES surface survey of gold colored area on Sample 3

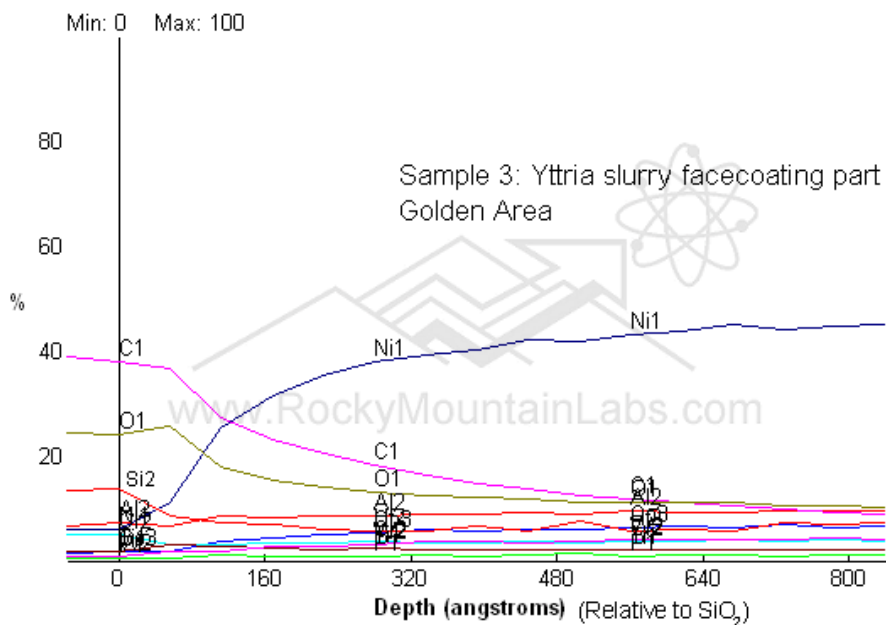


Figure 113. AES sputter depth profile of gold colored area on Sample 3

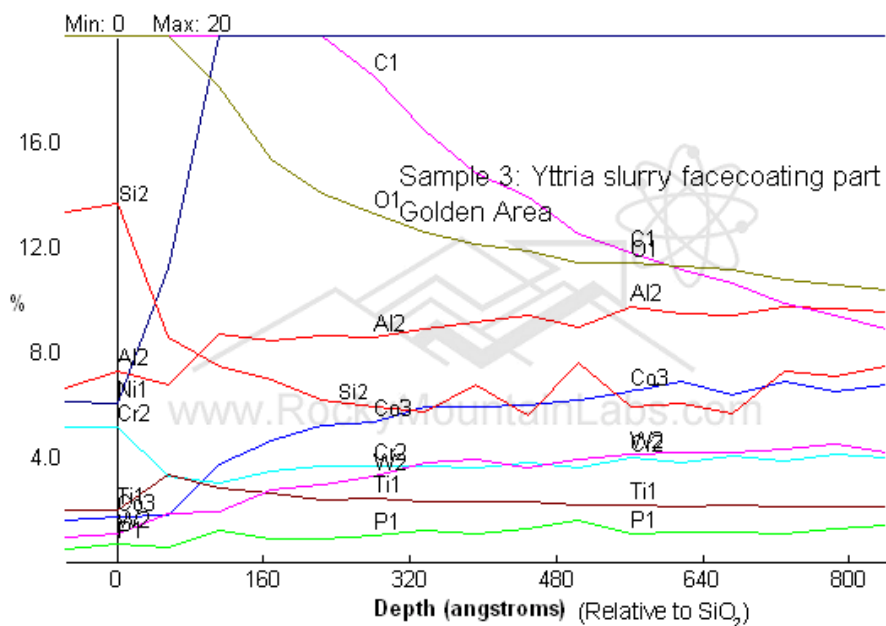


Figure 114. AES sputter depth profile of gold colored area on Sample 3, 0-20% plot

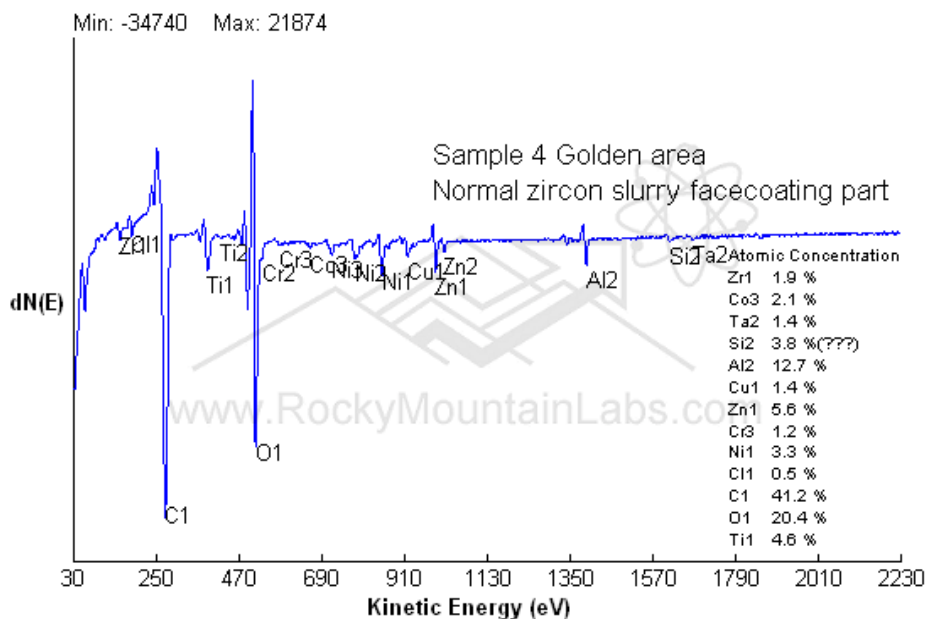


Figure 115. AES surface survey of gold colored area on Sample 4

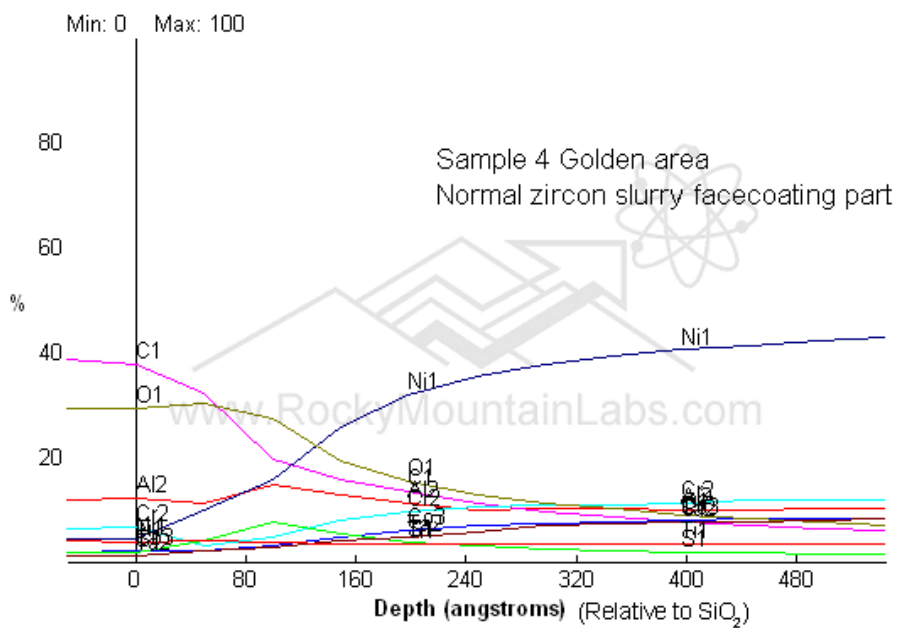


Figure 116. AES sputter depth profile of gold colored area on Sample 4

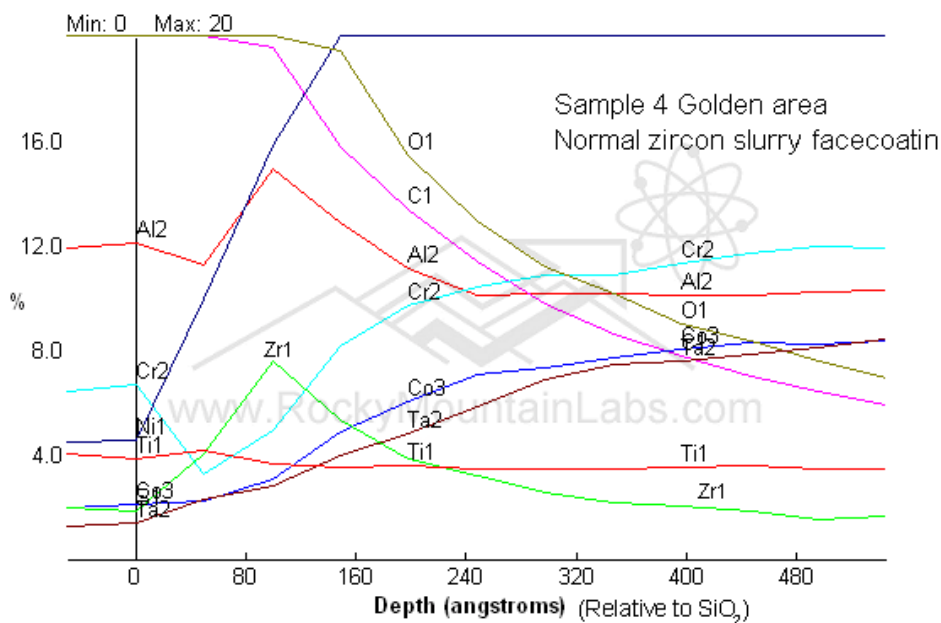


Figure 117. AES sputter depth profile of gold colored area on Sample 4, 0-20% plot

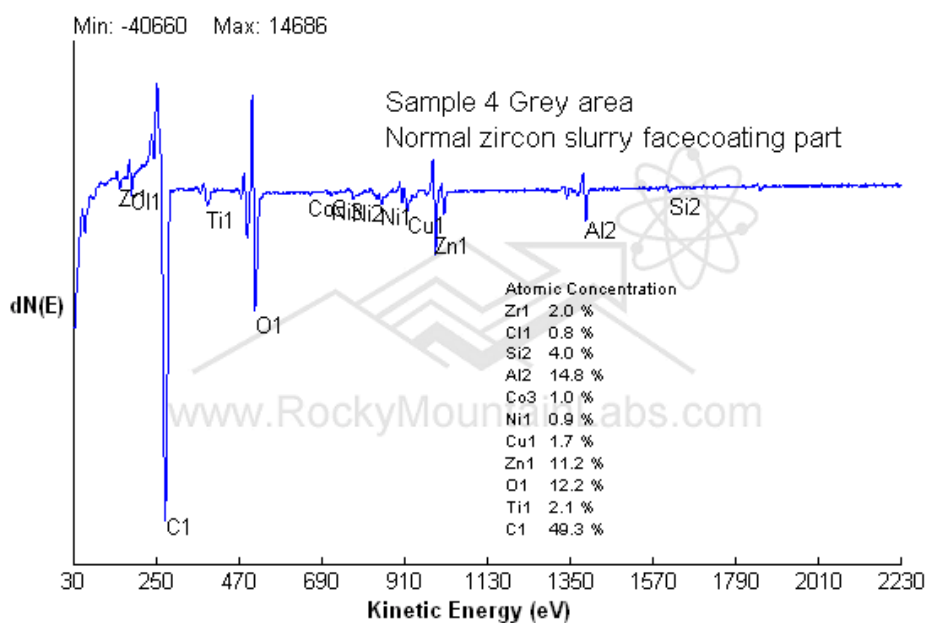


Figure 118. AES surface survey of grey colored area on Sample 4

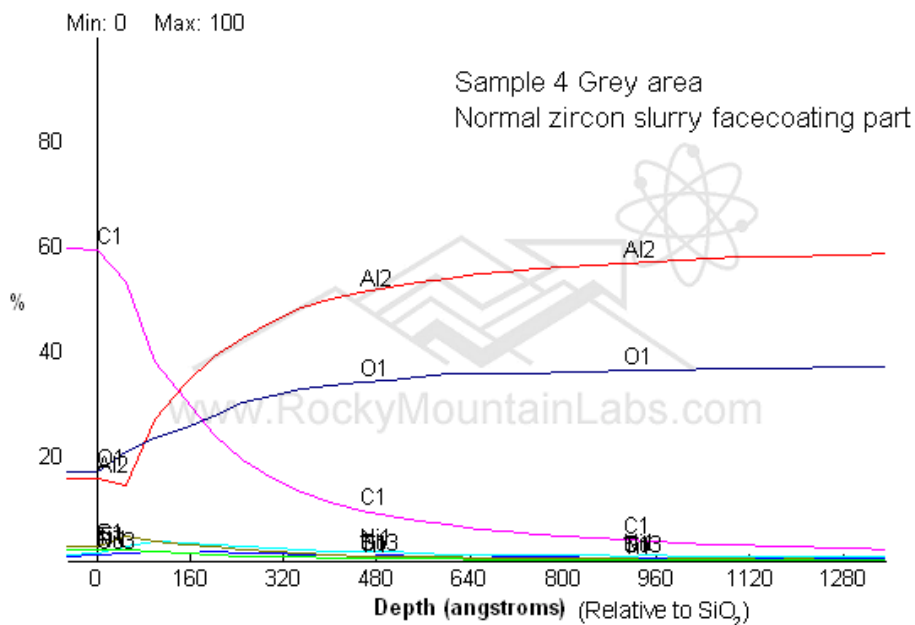


Figure 119. AES sputter depth profile of grey colored area on Sample 4

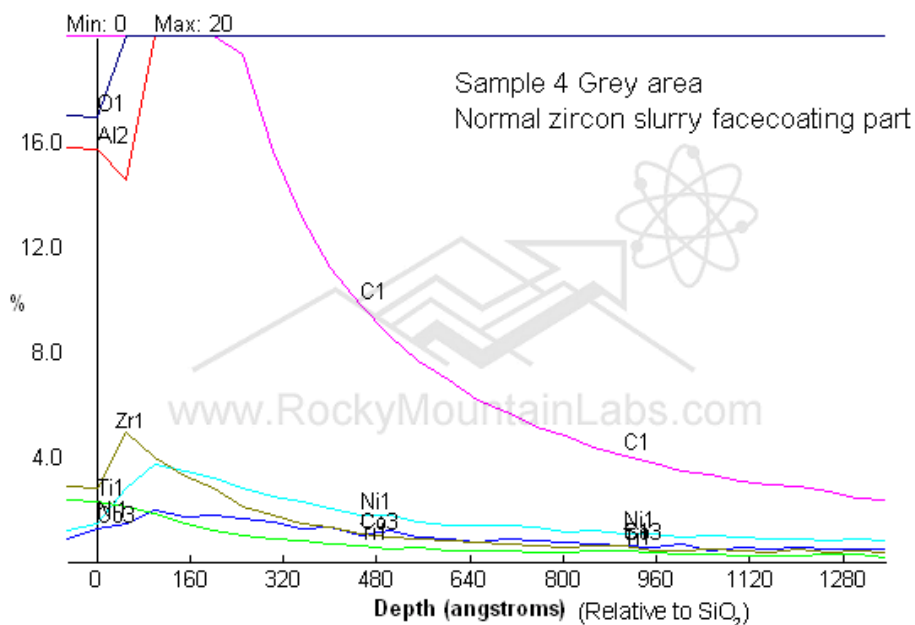


Figure 120. AES sputter depth profile of grey colored area on Sample 4, 0-20% plot

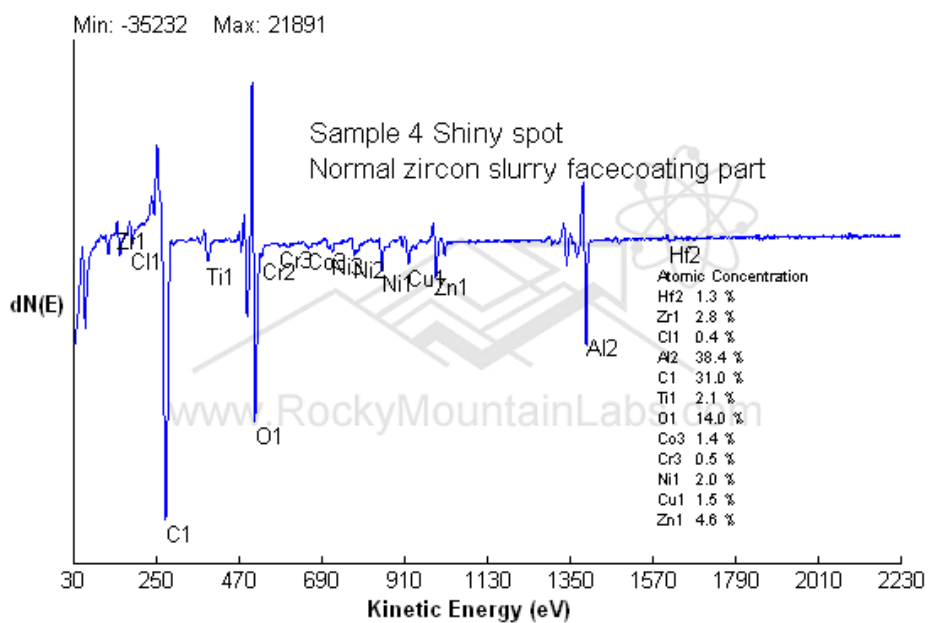


Figure 121. AES surface survey of shiny spot on Sample 4

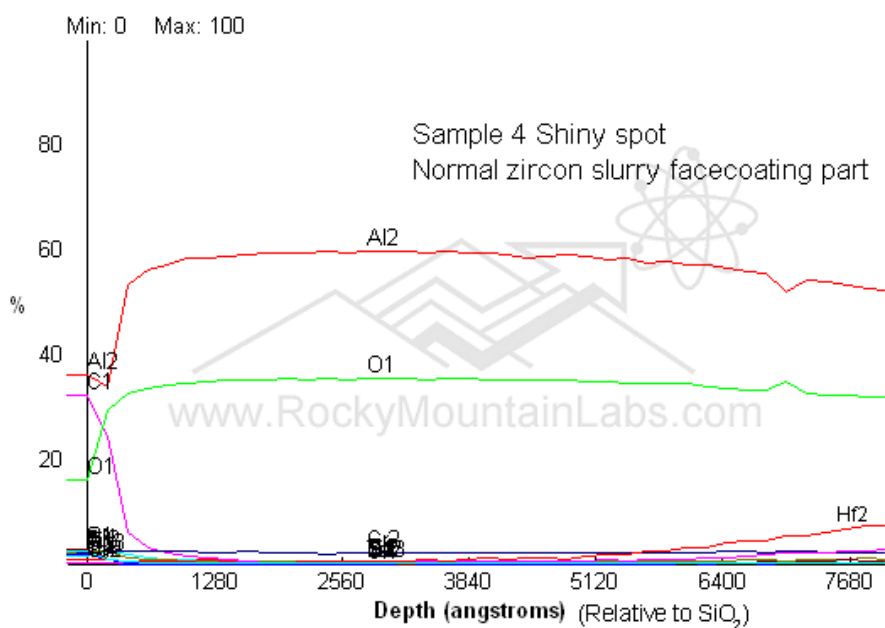


Figure 122. AES sputter depth profile of shiny spot on Sample 4

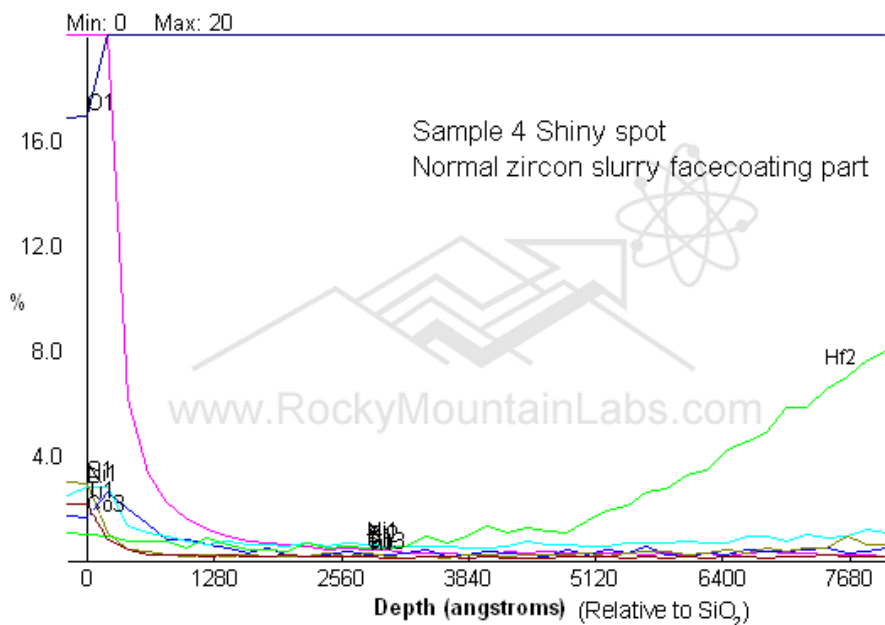


Figure 123. AES sputter depth profile of shiny spot on Sample 4, 0-20% plot

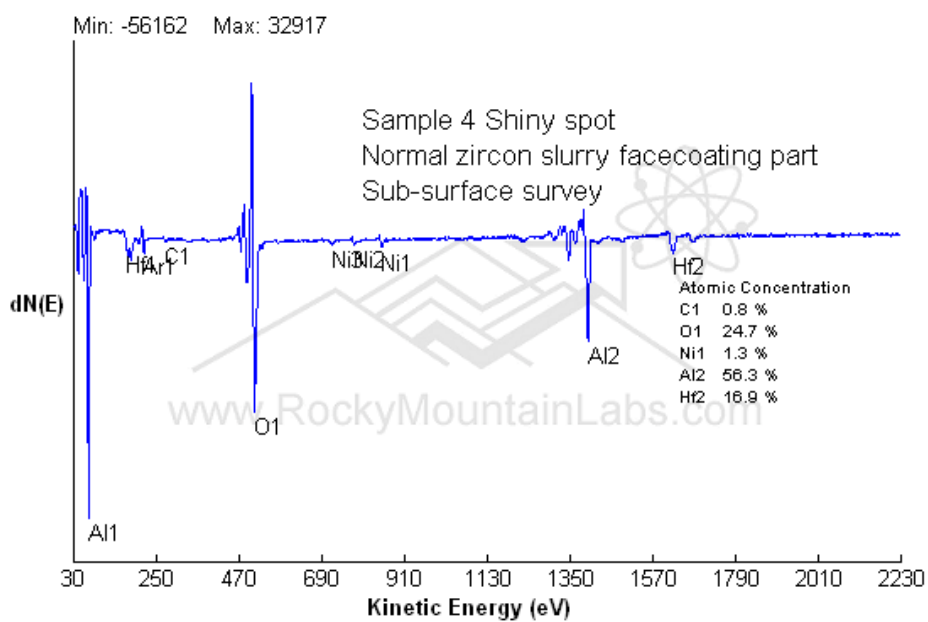


Figure 124. AES sub-surface survey of shiny spot on Sample 4

5.3.4. XPS results

Table 12 shows a summary of the relative elemental surface composition of samples as determined by AES analysis (atom %). **Figure 125** through **Figure 128** show detailed results of AES analysis.

Sample	C	O	F	Na	Mg	Al	Si	Ti	Co	Ni	Y	Zr	Hf
6	19	52	0.4	-	-	13	-	0.1	-	0.6	11	0.8	3.2
7	18	56	-	2.1	0.2	5.8	10	-	-	-	-	8.3	-
8	17	55	2.8	1.2	-	13	-	-	-	-	-	0.9	9.9
9	26	50	0.9	0.1	-	7.0	0.9	-	0.3	-	6.1	0.9	8.0

Table 12. Relative elemental surface composition of samples as determined by XPS analysis (atom %).

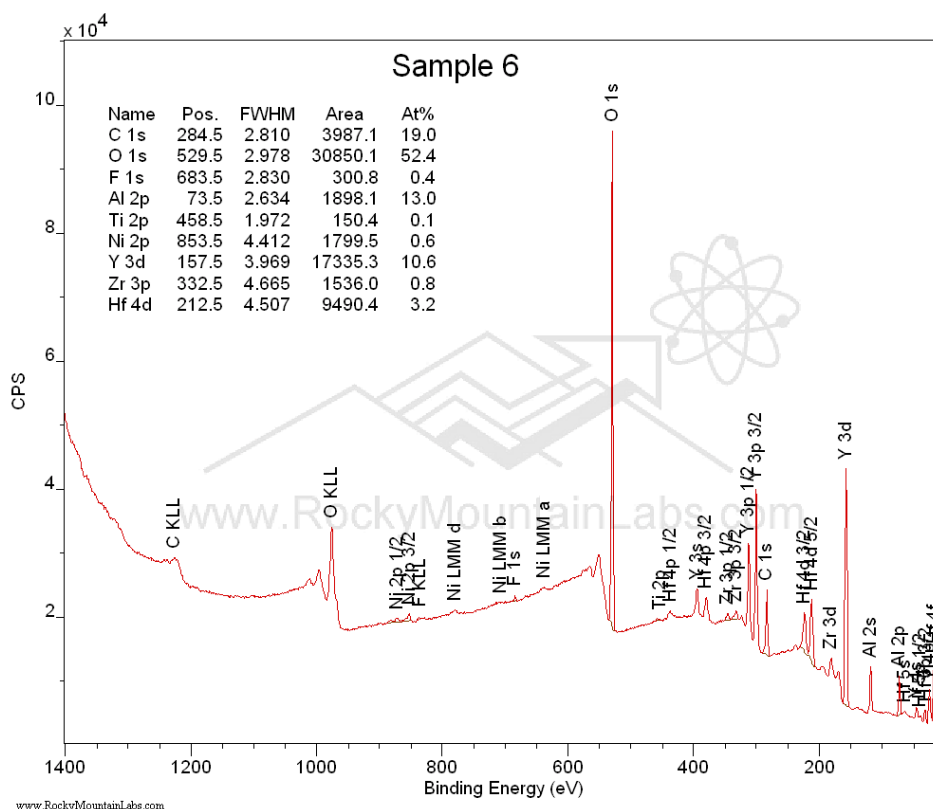


Figure 125. XPS surface survey of Sample 6

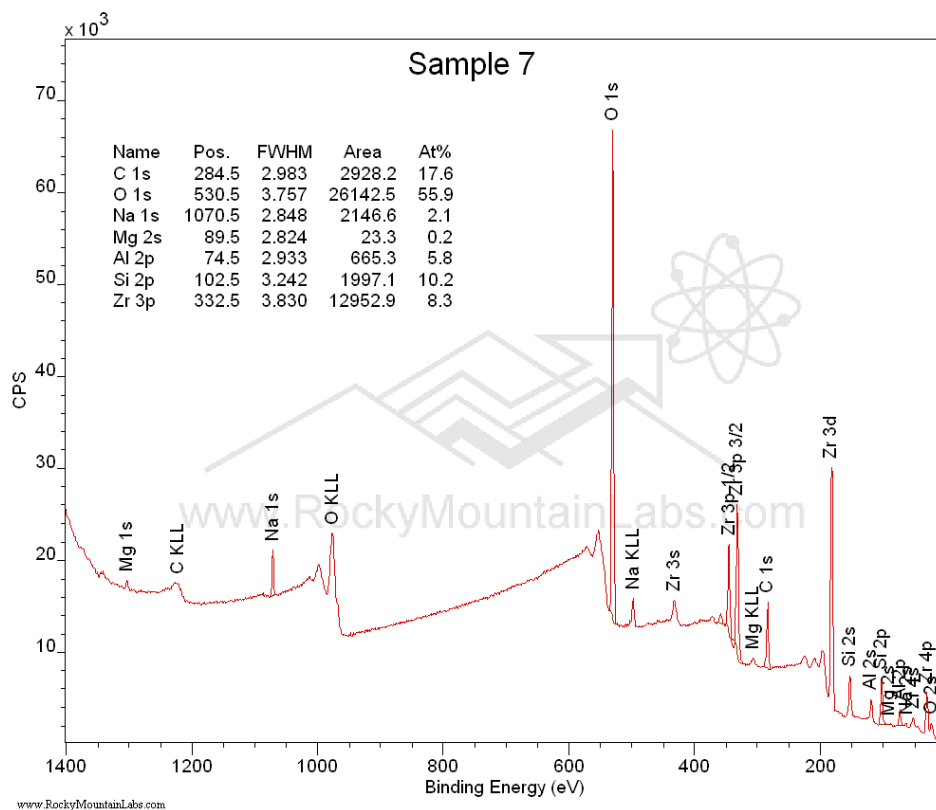


Figure 126. XPS surface survey of Sample 7

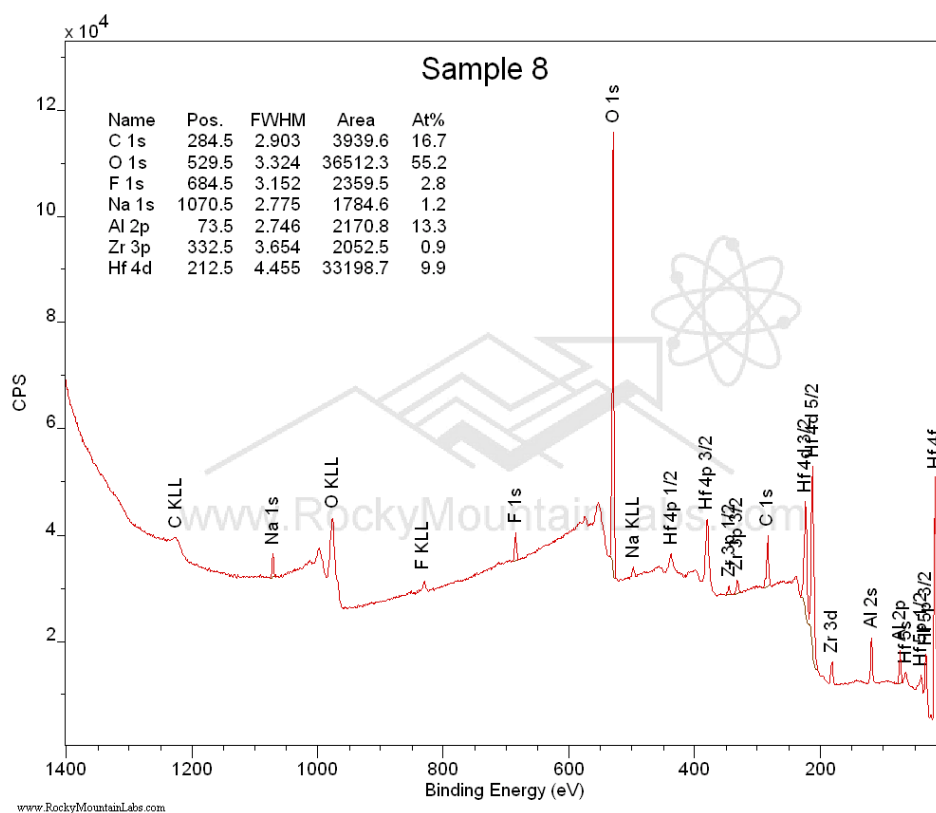


Figure 127. XPS surface survey of Sample 8

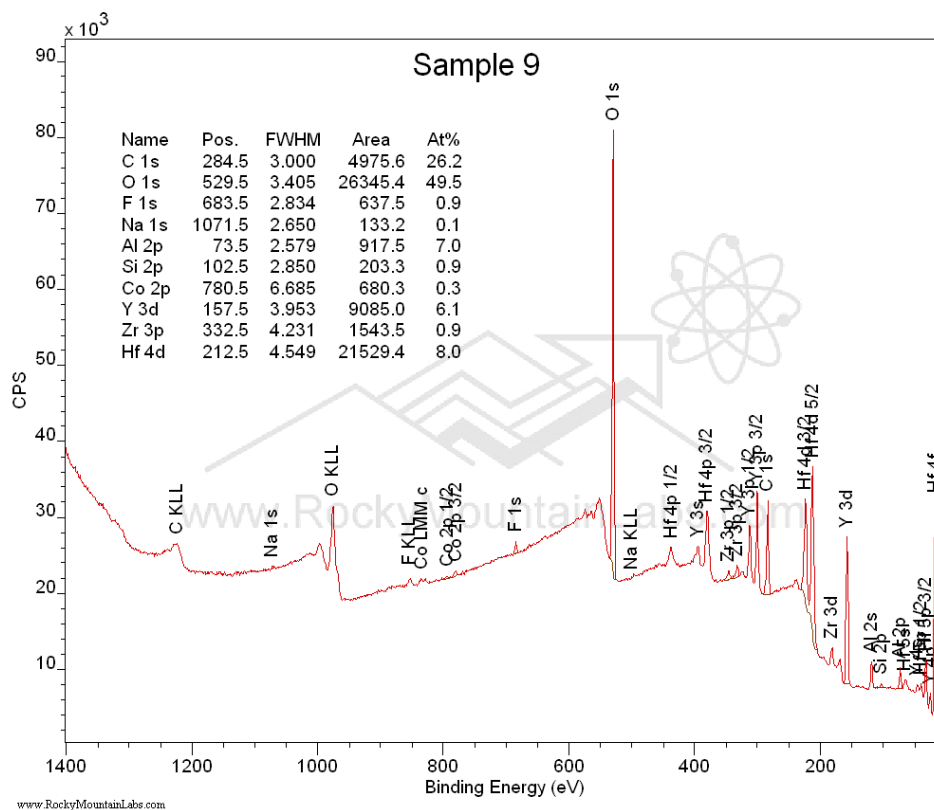


Figure 128. XPS surface survey of Sample 9

5.4. Discussion

Determining whether silicon (Si) is present in small quantities on the metal samples' surface areas analyzed with AES is extremely difficult in the presence of Hf, Ta, W, and Re due to spectral interference. The most reliable data is on the samples where a sub-surface survey was obtained after the depth profile (**Figure 111** and **Figure 124**).

The gold colored areas have a thin, 150-300 Å thick, oxide coating on the alloy surface. The grey colored area on Sample 4 (**Figure 119**) has a much thicker, >1300 Å, aluminum oxide layer.

The shiny spots on the castings and the ceramic shells are enriched in Ta, W, and Re.

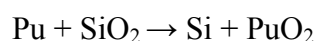
The sub-surface survey of the shiny spot on Sample 1 (**Figure 111**) has a carbidic carbon signal. This suggests that the Ta, W, and Re are segregating into carbide

particles. The heat treated section, Sample 5, does not appear to exhibit these shiny spots [96], suggesting that the heat treatment re-solutionizes these carbides.

The micro-calorimeter EDS detector (μ -EDS) minimizes peak-overlap problems for the myriad of K, L, M and N X-ray lines in the low voltage regime (0-4 keV). Conventional Si-EDS can not resolve the peaks of Ta, Si, W, and Re, whereas the μ -EDS resolves many of the peaks. Full spectra show that Ni, Al and Ta are enriched in γ' phase (Re low), whereas the Co, W and Re are enriched in γ phase. Using this technique, the Ta, Mb, and W, Ma peaks can be separated and elemental mapping is possible (**Figure 129**). As a result of the high peak-to-background ratio, and high spectral resolution of the μ -EDS, trace elements (<1 wt %) can be detected and quantified. In the case of a standard NIST test specimen, the presence of 0.8 wt% Ta and 0.13 wt% Si are easily detected (**Figure 130**). With a conventional Si-Li EDS, these two elements would not be resolved (Data supplied by D.E. Newbury, NIST.) [103].

5.4.1. Silicon contamination caused by quartz thermocouple tube in a metal casting

As early as August 1958 K.W.R. Johnson and J.W. Anderson reported that quartz tubes can be attacked by molten plutonium according to the follow reaction:



The reaction rate is a function of the temperature, and is relatively slow at

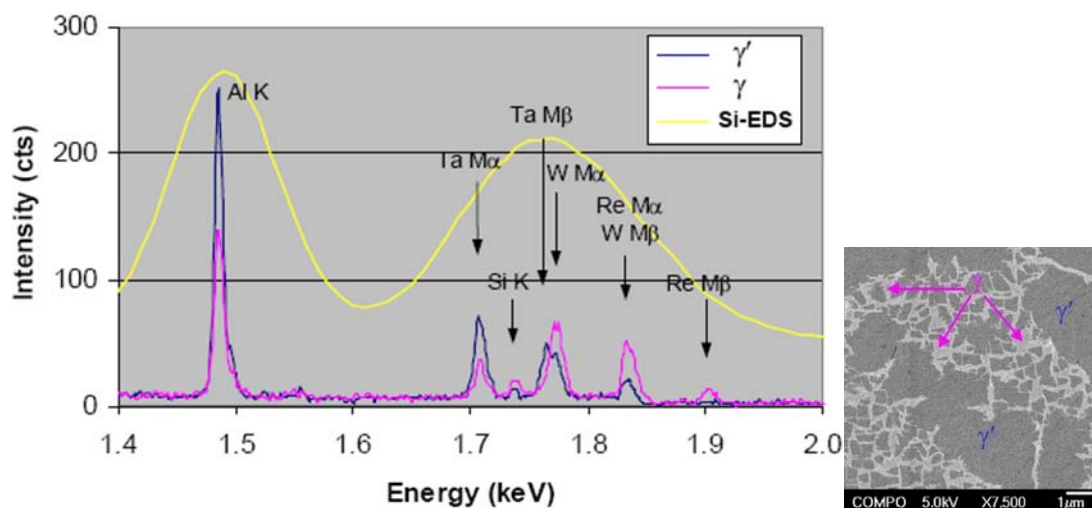


Figure 129. Microanalysis of phases in CMSX4 superalloy – μ -EDS vs Si-EDS spectra

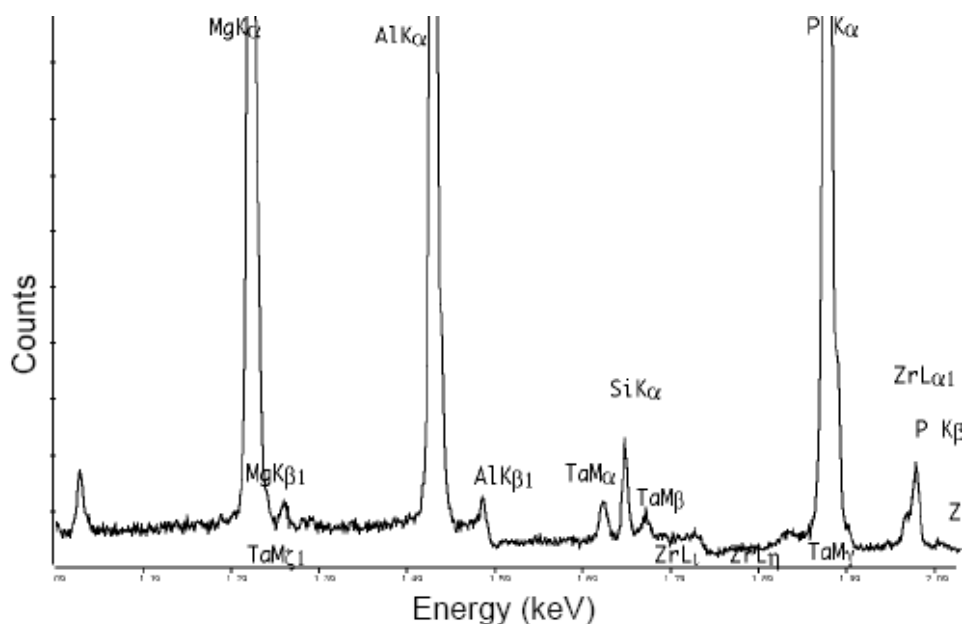


Figure 130. Microanalysis of Trace Elements by μ -EDS

temperatures below 1000 °C. Our experimental results in **Table 13** show a high level of silicon contamination (630 ppm) at the metal skin next the quartz tube even at relatively low casting temperatures (750 °C) [104]. CMSX-4 castings require the silicon content to be less than 400 ppm. This observed reaction causes us to predict that the thermocouple protection quartz tube will provide a source of Si to react with

the reactive elements (Hf, Al, Ti, C) in the molten CMSX-4 alloy during the melting operation.


<u>Sample</u>	<u>Silicon Concentration, ppm</u>
Feed	190
Rod (skin next to quartz) 	630
(0.005 in. below skin)	225
(0.010 in. below skin)	180
(0.015 in. below skin)	190
Center of rod	185

Table 13. Silicon contamination in a plutonium rod cast in a quartz tube 0.5 In. in a diameter and X 2 In. long. Melt temperature was 750 ° C and mold temperature before pour was 275 ° C.

5.4.2. Diffusion distances of some relevant alloying elements in pure Ni

From **Table 14** [105], we learn that the diffusion distance of Hf in pure Ni is much larger than Al, Ti, Cr, and Co. This may explain why the results of EDS, AES and XPS showed some high-Hf content features at the metal-mold interface. Nominally, CMSX-4 contains only 0.1 wt. % Hf.

Element	Diffusion distances (μm)			
	15min/1190°C	6000h/800°C	6000h/900°C	6000h/1000°C
Co	90	20	80	240
Cr	90	20	85	250
Al	130	40	150	430
Ti	140	50	160	450
Hf	270	100	320	880
C	1900	3500	6900	12300

Table 14. Diffusion distances of some relevant alloying elements in pure Ni

5.4.3. Nature of the metal-mold reaction layers of CMSX-4

castings

Metal-mold reaction layers of CMSX-4 castings showed oxidation features (**Table 10** and **Table 11**) and carbidic oxidation features (**Figure 110**). This shows the agreement with the metal-mold reaction definition given by GEAE [51, 64, 66, 67, 68].

Silicon also was found in some samples (**Table 10, Table 11, Table 12, Figure 81, Figure 82, Figure 85, Figure 108, Figure 112, Figure 115, Figure 118, Figure 126, and Figure 128**), but these results need further verification using other techniques such as the micro-calorimeter EDS detector (μ -EDS) or Glow Discharge Mass Spectrometry (GDMS) [106, 107, 108].

The gold-colored or light areas of reaction layer contain aluminum oxide, titanium oxide and tantalum oxide, and are relatively thinner than the dark areas which contain much more aluminum oxide combined with lower titanium oxide, or yttria, or zirconia and much lower tantalum oxide.

The shiny spots are Ta, W, and Re-rich compounds, which show the carbidic feature.

The shiny spots on the casting surface seem to diffuse back into the bulk after solution heat treatment, but the shiny spots attached on the shell mold (rich in some of these alloying constituents) will be permanently lost from the cast part. I.e., the serious metal-mold reaction of CMSX-4 may cause alloy depletion of W, Ta and Re elements—particularly in the near-surface region.

The nature of the metal-mold reaction layers of CMSX-4 castings will depend on the actual casting conditions.

5.4.4. Formation mechanism of metal-mold reactions of CMSX-4

castings

- ✧ Surface paint on the ingots can be a source of carbon and oxygen.
- ✧ Ingot with pipe defects and high levels of opened porosity may contain more air. This may cause oxygen and nitrogen contamination in melt.
- ✧ The molten metal may pick-up oxygen and silicon from the thermocouple protection tube, melting crucible, and shell mold/core through the reaction between aluminum, titanium and hafnium in the molten metal and silica in the thermocouple protection tube (100% silica, **Figure 131**), melting crucible (about 4% silica, **Figure 132**), pouring rate control bushing (about 80% silica) and shell mold (about 4% silica in slurry binder, and unknown percentage induced by wax pattern ash)/core (about 80% silica in flour, and unknown percentage induced by mold release, wax binder ash, dipping silica binder).
- ✧ Metal-ceramic reaction may cause inclusion problems [**Figure 47 b**], and further induce gas defects and grain defects (**Figure 133**) [109].
- ✧ The degree of metal-mold reaction also highly depends on the casting parameters such as pouring temperature, mold temperature, and withdrawal rate [62, 69, 110].
- ✧ The higher pouring temperature, mold temperature, and lower withdrawal rate; the higher metal-mold reaction tendency.
- ✧ The higher the silica level in the casting system, the higher the tendency to see metal-mold reactions.



Figure 131. Using quartz tubes as immersion thermocouple protection tubes, and alumina crucibles, CMSX-4 melt slag showed oxidation features.



Figure 132. Alumina crucibles were wetted by CMSX-4 melt

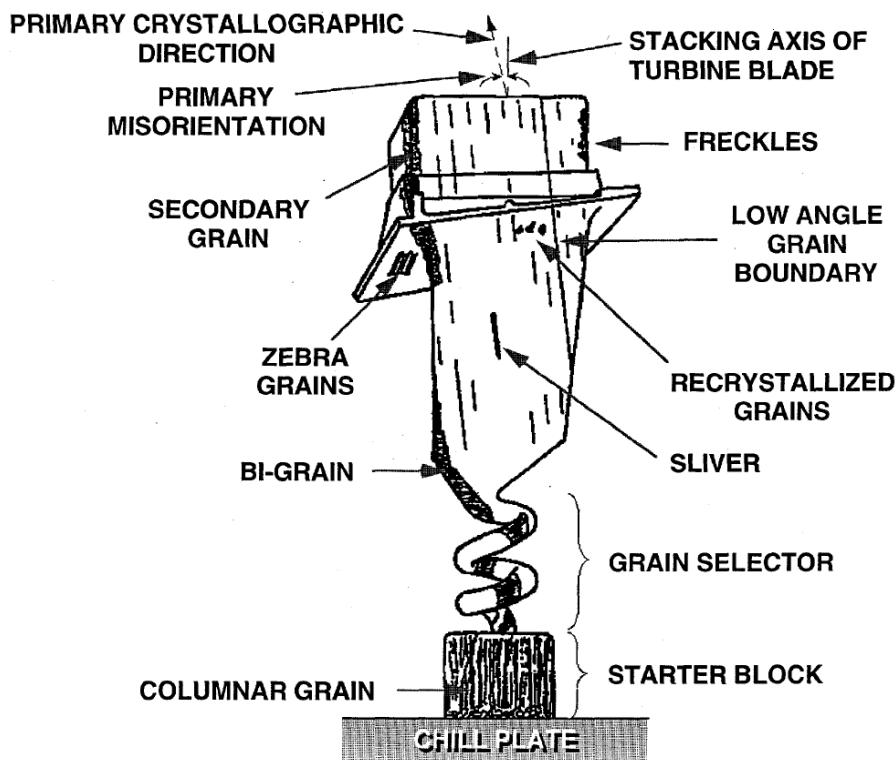


Figure 133. Grain defects in single crystal turbine blades

5.4.5. Possible mechanism of metal-mold reaction layer hardening after solution heat treatment

- ✧ The shiny spots on the metal-mold reaction surfaces are refractory elements (W, Ta and Re) rich, and they may form the oxide surface layer by diffusion during solution heat treatment, and induce the hard surface layers on the solution heat treated CMSX-4 castings.
- ✧ The high silicon content in the CMSX-4 casting induced by metal-mold reaction might promote the surface eutectic phase formation or form the eutectic phase with alumina or nickel oxide, and cause a hard surface layer on the solution heat treated CMSX-4 castings.

5.4.6. Recommended solutions for metal-mold reactions of

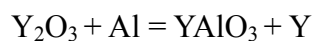
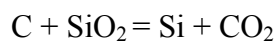
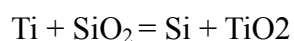
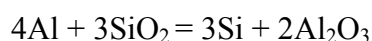
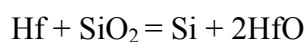
CMSX-4 castings

- ✧ Use silica free immersion thermocouple protection tubes (e.g. zirconia or alumina tubes) or change the test position for immersion temperature test (e.g. instead of locating sensors in the liquid metal, set temperature sensors above the liquid metal with a certain distance).
- ✧ Try to use non-contact temperature measurement technology such as the FAR Expert System SpectroPyrometer to accurately measure solid and liquid metal temperatures in CMSX-4 castings [111].
- ✧ Use zirconia crucibles, e.g. Zircoa 3001 or Remet Products.
- ✧ Use zirconia pouring rate control bushing.
- ✧ Use low-ash (less than 0.003%) pattern wax and Remet non-silicon mold release.
- ✧ Try Remet Tiwax® for reducing metal-mold reactions.
- ✧ Try Remet Ticoat®-N binder system with zirconia flour for face coat to reduce metal-mold reactions.
- ✧ Try less-reactive wash coat (yttria & zirconia) for reducing metal mold reactions.
- ✧ Improve shell mold surface quality to prevent undesirable porosity formation.
- ✧ Review and optimize the silica binder level of existing facecoat.
- ✧ Use non-silicon mold release for ceramic core injection molding.
- ✧ Use non-silica binder dipping cores.
- ✧ Use pipe-free charges only, chamfer the bottom sharp end of charges before production.
- ✧ Perform furnace temperature survey regularly.

- ✧ Perform oxygen and nitrogen analysis using LECO TC-500 on CMSX-4 castings daily to comply with the relative requirement in CNV 553 J specification.
- ✧ Optimize the existing casting parameters such as pouring temperature, mold temperature, withdrawal rate.
- ✧ Consider use of vacuum with argon partial pressure casting process instead of existing argon atmosphere protection casting process.

6. Conclusions

- MMR is a kind of surface defect, The MMR occur between the active elements (e.g. Hf, Al, Ti, C) in the alloy and reactive elements (e.g. O) or compound (e.g. SiO₂) in the casting system;
- The following reactions may occur in MMR of CMSX-4, so Si and Hf analysis is key to identifying the MMR:



- Yttria spray (alone) slightly reduces the amount of MMR of CMSX-4;
- Yttria spray coating, combined with the yttria binder wash, further reduces the MMR of CMSX-4.
- MMR layers of CMSX-4 showed oxidation, Si and Hf rich features.

- Hardening of MMR layers of CMSX-4 after heat treatment may be caused by the surfaces rich in refractory elements (e.g. W, Ta, Re), surface eutectic phases and surface oxide layers.
- Si and Hf analysis of CMSX-4 casting need using μ -EDS and GDMS for good resolution and sensitivity.
- All possible sources of silica, oxygen and carbon in the CMSX-4 casting system must be minimized to avoid MMR.

7. Future Works

- Perform an analysis of silicon and hafnium content in CMSX-4 castings with MMR and other casting defects by GDMS and μ -EDS, to determine if the Si and Hf content is out of the CMSX-4 specification because of MMR.
- Perform further characterization of shiny spots to find out its formation mechanism. This may help avoid surface hardening after heat treatment and alloy depletion induced by MMR.
- Perform casting trials using zirconia crucibles and immersion thermocouple protection tubes, paint and pipe-free ingots to reduce MMR. This will help confirm the effects of crucible and thermocouple silica, carbon in paint and oxygen in defective ingots on the MMR of CMSX-4 casting.
- Perform casting trials using Remet Ticoat®-N binder system with zirconia flour for face coat to learn the effects of silica binder on MMR.
- Perform further casting trials using non-reactive wash coats (yttria and

zirconia) to optimize the already-observed reduction of MMRs. For example, examine the roles of layer thicknesses and binder wash characteristics.

- Optimize the existing casting parameters such as pouring temperature, mold temperature, withdrawal rate.
- Perform casting trials using vacuum with argon partial pressure casting process instead of existing argon atmosphere protection casting process.
- Perform further analysis of the relationships of MMR layer and surface eutectic phases.
- Perform an analysis of oxygen in CMSX-4 castings with MMR and other casting defects using LECO TC 500.

References

- [1] http://www.c-mgroup.com/spec_sheets/CMSX_4.htm October 22, 2008
- [2] *The Gas Turbine Handbook* [*Buckets and Nozzles*](#) Stephen J. Balsone
GE Gas Turbines LLC Greenville, SC 29602
<http://www.netl.doe.gov/technologies/coalpower/turbines/refshelf/handbook/4.4.1.pdf>
October 22, 2008
- [3] Cyril L. Massar III, Alejandra Bolivar, Chromalloy Nevada
Metallurgical Laboratory Report 07AL-046
- [4] Cyril L. Massar III, Alejandra Bolivar, Chromalloy Nevada
Metallurgical Laboratory Report 07AL-073
- [5] Cyril L. Massar III, Alejandra Bolivar, Chromalloy Nevada
Metallurgical Laboratory Report 07AL-074
- [6] Cyril L. Massar III, Alejandra Bolivar, Chromalloy Nevada
Metallurgical Laboratory Report 07AL-078
- [7] Cyril L. Massar III, Alejandra Bolivar, Chromalloy Nevada
Metallurgical Laboratory Report 07AL-079
- [8] Cyril L. Massar III, Deborah Bentley, Chromalloy Nevada
Metallurgical Laboratory Report 07AL-544a
- [9] Cyril L. Massar III, Deborah Bentley, Chromalloy Nevada
Metallurgical Laboratory Report 07AL-556a
- [10] Cyril L. Massar III, Alejandra Bolivar, Chromalloy Nevada
Metallurgical Laboratory Report 07AL-574
- [11] Cyril L. Massar III, Piyush Kar, Chromalloy Nevada
Metallurgical Laboratory Report 08AL-226
- [12] Cyril L. Massar III, Alejandra Bolivar, Chromalloy Nevada
Metallurgical Laboratory Report 08AL-242
- [13] Roger C. Reed, *The Superalloys: Fundamentals and Applications*
Cambridge University Press, 2006, P.139
- [14] D. C. Cox, B. Roebuck, C. M. F. Rae and R.C. Reed
Recrystallisation of single crystal superalloy CMSX-4

Material science and Technology April 2003 Vol. 19

[15] C. Zambaldi ¹⁾, F. Roters ¹⁾, [D. Raabe](#)* ¹⁾, U. Glatzel ²⁾

1) Max-Planck-Institut für Eisenforschung Max-Planck-Str. 1, 40237 Düsseldorf, Germany

2) Metallische Werkstoffe, Universität Bayreuth, Ludwig-Thoma-Str. 36b, 95440 Bayreuth, Germany

Modeling and experiments on the indentation deformation and recrystallization of a single-crystal nickel-base superalloy

[16] M.C. THOMAS, R.C. HELMINK, D.J. FRASIER, J.R. WHETSTONE

Allison Engine Company Indianapolis, Indiana, USA

K. HARRIS, G.L. ERICKSON, S.L. SIKKENGA, J.M. ERIDON

Cannon-Muskegon Corporation [SPS Technologies] Muskegon, Michigan, USA

ALLISON MANUFACTURING, PROPERTY AND TURBINE ENGINE PERFORMANCE OF CMSX-4® SINGLE CRYSTAL AIRFOILS

Presented at the COST 501 Conference "Materials For Advanced Power Engineering 1994", Liege, October 3-6, 1994.

[17] S. D. BOND, J. W. MARTIN, University of Oxford, UK

Surface recrystallization in a single crystal nickel-based superalloy

JOURNAL OF MATERIALS SCIENCE 19 (1984) 3867-3872

[18] <http://www.pccsmp.com/InvestmentCasting.htm> October 25, 2008

[19] Keith P.L. Fullagar, Robert W. Broomfield, Mark Hulands

Rolls-Royce plc Bristol & Derby, UK

Ken Harris, Gary L. Erickson, Steven L. Sikkenga, Cannon-Muskegon Corporation [SPS Technologies] Muskegon, Michigan, USA

AERO ENGINE TEST EXPERIENCE WITH CMSX-4® ALLOY SINGLE CRYSTAL TURBINE BLADES

<http://www.c-mgroup.com/abstracts/aero.htm> October 22, 2008

[20] Gary L. Erickson, Cannon-Muskegon Corporation [SPS Technologies] Muskegon, Michigan USA

SUPERALLOY VIM AND EBCHR PROCESSES

http://www.c-mgroup.com/abstracts/superalloy_vim.htm October 22, 2008

[21] Septimus van der Linden, Chairman, ASME-IGTI (International Gas Turbine Institute) Electric Power Committee

Development Trends & the Role of Gas Turbines in the Future 30 Years

16th International Conference on Efficiency, Costs, Optimization, Simulation and Environmental Impact of Energy Systems Copenhagen, Denmark

June 30 - July 2, 2003

www.ecos2003.dtu.dk/keynotes/ECOS2003-BrulinAssocPresentation.pdf

- [22] http://www.c-mgroup.com/vacuum_melt_index/nickel_base_sx.htm
- [23] <http://www.investmentcastingwax.com/> October 25, 2008
- [24] Richard Hirst, EICF Best Practice Workshop Düsseldorf, March 26th 2004
Wax Chemistry, Properties and Selection
- [25] Phil Hancock, Blayson Olefines Ltd
Understanding how the Properties and Use of Wax can Affect Foundry Performance
Bilbao May 2006
- [26] Richard Hirst, EICF Best Practice Workshop Düsseldorf, March 26th 2004
Best Wax Injection & Assembly Practice
- [27] David Bond, Technical Manager -Blaysons Olefines Ltd
Koji Nishikawa, General Manager -Blayson Japan Co. Ltd
Investment Casting Wax Technology
<http://www.investmentcastingwax.com/downloads/tl5.pdf> October 25, 2008
<http://www.investmentcastingwax.com/structure.php> October 25, 2008
- [28] <http://www.investmentcastingwax.com/categories.php> October 25, 2008
- [29] Richard Hirst, FIMMM Blayson Olefines Ltd
Composition, Control and Use of Investment Casting Wax
<http://www.investmentcastingwax.com/downloads/tl14.pdf> October 25, 2008
- [30] Michael HENDRICKS, Mark BIJVOET, RANSOM & RANDOLPH
Ceramic Shell Basic Technology
EICF-BICTA Workshop, Duesseldorf 26 March 2004
- [31] Bob Brown, Remet
Refractory selection
Duesseldorf, March, 2004
- [32] ASM Handbook: Volume 15 *Casting*
By ASM international Handbook committee, D. M. Stefanescu
Published by ASM International, 1998, P.554
- [33] Peter Beeley, *Foundry Technology Second edition*, Butterworth-Heinemann
published, 2001, p. 574-575
- [34] Peter PINKE – Maroš MARTINKOVIČ, Slovak University of Technology
DIRECTIONAL SOLIDIFICATION OF CMSX-3 NICKEL BASED SUPERALLOY
http://www.kfki.hu/~anyag/Pinke_1.pdf

- [35] M.D. Asta, S.H. Davis*, D.N. Seidman, P.W. Voorhees, C.F. Woodward
Northwestern University, Evanston IL
T. M. Pollock, University of Michigan, Ann Arbor MI
J.E. Spowart, Air Force Research Laboratories, Dayton, OH
Defects Associated with Solidification of Melt Processed Superalloys for the Aerospace Industry
June 23, 2008
- [36] DAVID PARKER, LEEDS & BRADFORD BOILER
Best Practice Dewaxing
EICF-BICTA Workshop, Duesseldorf, 26 March 2004
- [37] <http://www.pccsmp.com/> October 25, 2008
- [38] (a) and (b) B. H.Kear, *Scientific American*, October 1986;
(c) *Advanced Materials and Processes*, October 1990, p. 29, ASM International
- [39] Peter Beeley, *Foundry Technology Second edition*, Butterworth-Heinemann
published, 2001, p. 587
- [40] B.C. Wilson, J.A. Hickman, and G.E. Fuchs
The Effect of Solution Heat Treatment on a Single-Crystal Ni-Based Superalloy,
JOM March 2003
- [41] Al Nakayama Chromalloy Nevada
Process specification CNV 548A April 15, 1996
Acceptability limits for metallographic inspection of investment cast turbine blades and vanes
- [42] Richard A Harding University of Birmingham
Some recent developments in the melting and casting of titanium alloys
IRC in materials processing
EICF conference, Bilbao, May2006
- [43] KIM Myoung-Gyun, SUNG Si-Young, KIM Young-Jig
Microstructure, metal-mold reaction and fluidity of investment cast-TiAl alloys
Materials transactions-JIM ISSN 016-1821, 2004 Vol. 45 No. 2 PP. 536-541
- [44] A. Alagarsamy Citation Corporation, Birmingham, Alabama
Casting defects analysis procedure and a case history
2003 Keith Mills Symposium on Ductile Cast Iron
- [45] Technical data sheet, No. WFP-37, 07/09/2002 Remet Corporation
Product name: TIWAX 288P28

- [46] Peter Beeley, *Foundry Technology* Second edition, Butterworth-Heinemann published, 2001, P.260
- [47] H. Frye, Techform, M. Yasrebi, D. H. Sturgis, PCC Structural, Inc.
Basic Ceramic Considerations for Lost Wax Processing of High Melting Alloys
© Platinum Guild International USA 2001 P.2
- [48] ASM Handbook: Volume 15 *Casting*
By ASM international Handbook committee, D. M. Stefanescu
Published by ASM International, 1998, PP.1188, 1194-1195
- [49] R.L.Saha Defence Metallurgical research laboratory, Hyderabad, India
K.T. Jacob Indian Institute of Science, Bangalore, India
Casting of Titanium and its alloys
Def Sci J, Vol 36, No 2, April 1986, PP. 121-141
- [50] Yoshisada UEDA, Koji TANI
Reactions at the interface of high chromium steel and austenitic stainless steel with olivine or silica sand mold
Imono (The journal of the Japan foundrymen' society), 57 (1985), 90
English version Nov. 1986, ©1987 ISIJ
- [51] GE Aircraft Engine specification No.P29TF34 Issue No: S5, September 9, 1992
Acceptability limits for metallographic inspection of investment cast turbine blades and vanes
- [52] Chromalloy Nevada process specification CNV 553 J
Premium quality cast single crystal CMSX-4 (ULS)
- [53] Celal Cingi
MOLD-METAL REACTIONS IN MAGNESIUM INVESTMENT CASTINGS
Dissertation for the degree of Doctor of Technology
Helsinki University of Technology (Espoo, Finland) November 2006
- [54] R.L.Naro, ASI International, Inc.
Porosity Defects in Iron Castings From Mold-Metal Interface Reactions
Silver Anniversary Paper, Div. 5 AFS Transactions, 99-206, PP. 839-851
- [55] *Superalloys: A Technical Guide*
By Matthew J. Donachie
Published by ASM International, 2002, P. 81
- [56] Mohd Hasbullah Idris, Ali Ourdjini, Esah Hamzah, Allen Clegg
Suppression of mold-metal reactions during investment casting

Magnesium Alloys and their Application Editor: B.L. Mordike, K.U.Kainer
April 8, 1999

[57] ASM Handbook: Volume 15 *Casting*
By ASM international Handbook committee, D. M. Stefanescu
Published by ASM International, 1998, P.195

[58] Ceramic test guidebook Revised 2005
8.11 Metal/Ceramic Reaction Investment Casting Institute, P.114

[59] *Superalloys: A Technical Guide*
By Matthew J. Donachie
Published by ASM International, 2002, P.204

[60] Aerospace Material Specification AMS 5391 E,
Issued JUN 1960, Revised JUN 1996
NICKEL ALLOY, CORROSION AND HEAT RESISTANT, INVESTMENT CASTINGS
73Ni-13Cr-45Mo-2.3Cb-0.75Ti-.6.0Al—0.010B-0.10Zr, Vacuum Cast, As Cast

[61] A.S. Khanna
Introduction to high temperature oxidation and corrosion
Second printing, December 2004 Copyright © 2002 by ASM international®

[62] R. Viswanathan and S.T. Scheirer
Materials Technology for Advanced Land Based Gas Turbines, .
EPRI technical paper (No. 01-201, Proc. of CREEP, JSME, Tsukuba, June 3-8, 2001)

[63] Timothy L. Donohue and Dr. Helmut F. Frye
TechForm - Advanced Casting Technology, L.L.C. 1999
Characterization and Correction of Casting Defects
<http://www.ganoksin.com/borisat/nenam/casting-defects.htm>

[64] Chromalloy Nevada process specification CNV 548 A 09/13/2001
Acceptability limits for metallographic inspection of investment cast turbine blades and vanes

[65] GE Aircraft Engine specification No.C50TF91 Issue No S3, June 7, 1990
Investment cast and HIPPED René 220 castings

[66] GE Aircraft Engine specification No.C50TF82 Issue No S7, May 2, 1990
Oxidation resistant René N-4 vacuum cast and directionally solidified turbine blades and vanes

[67] GE Aircraft Engine specification No.C50TF87 Issue No S3, July 21, 1990

Premium quality René N-5 vacuum cast and directionally solidified turbine blades and vanes

[68] Chromalloy Nevada process specification CNV 525 A 08/06/1998
Premium quality vacuum cast and directionally solidified turbine blades and vanes

[69] David Ford, DAF Associates
Definition of metal mold reaction of CMSX-4 casting
Technical consultant email reply, September 25, 2008

[70] G. BREWSTER, H.B. DONG, N.R. GREEN, and N. D'SOUZA
Surface Segregation during Directional Solidification of Ni-Base Superalloys
METALLURGICAL AND MATERIALS TRANSACTIONS B VOLUME 39B,
FEBRUARY 2008—87 © The Minerals, Metals & Materials Society and ASM
International 2008

[71] Peter Beeley, *Foundry Technology* Second edition, Butterworth-Heinemann
published, 2001, P.254

[72] K. Harris, G.L. Erickson and R.E. Schwer Cannon-Muskegon Corporation
*MAR M 247 DERIVATIONS - CM 247 LC DS ALLOY CMSX SINGLE CRYSTAL
ALLOYS PROPERTIES & PERFORMANCE*
TMS Superalloys 2001 Paper 01-1023-221

[73] Peter Beeley, *Foundry Technology* Second edition, Butterworth-Heinemann
published, 2001, P.280

[74] Kenneth Harris, Spring Lake; Gary L Erickson, Muskegon, both of Mich.
Low carbon directional solidification alloy
U S. Patent 5069873 Dec. 3, 1991

[75] Robert V. Miner, Jr.
*Effect of Silicon on the oxidation, hot-corrosion, and mechanical behavior of two cast
nickel-base superalloys*
Metallurgical transactions A Volume 8A, December 1977-1949

[76] Madeleine Durand-Charre
The microstructure of superalloys
Gordon and breach science publishers Copyright © 1997 OPA

[77] *ASM Handbook*, Volume 13, *Corrosion*, 1997 Copyright © 1987 by ASM
International P.142

[78] D.A. Jones
Principles and Prevention of Corrosion Prentice-Hall, Englewood-Cliffs (1996)

[79] Holt, R. T. NATIONAL AERONAUTICAL ESTABLISHMENT OTTAWA (ONTARIO)

Trace Elements and Residual Elements in Superalloys

Defense Technical Information Center Accession Number: ADP004228

[80] O P SINHA*, M CHATTERJEE, V V R S SARMA and S N JHA

Mishra Dhatu Nigam Limited, P.O. Kanchanbagh, Hyderabad 500 058, India

Effect of residual elements on high performance nickel base superalloys for gas turbines and strategies for manufacture

Bull. Mater. Sci., Vol. 28, No. 4, July 2005, pp. 379–382. © Indian Academy of Sciences

[81] D. A. Ford Rolls-Royce Ltd, Bristol

Importance of trace element control on mechanical and foundry properties of cast superalloys.

Material Technology October 1984 Vol. 11, ©1984 The Metals Society

[82] Cannon-Muskegon Corporation

CMSX-4 [SLS] [LA+Y] Alloy

Technical Bulletin February 2003

[83] Cyril L. Massar III, Piyush Kar, Chromalloy Nevada

Metallurgical Laboratory Report 08AL-227

[84] Erickson, Gary L. (Muskegon, MI)

Single crystal nickel-based superalloy

United States Patent 5540790 Publication Date: 07/30/1996 Filing Date: 12/29/1994

[85] Cannon-Muskegon Corporation

Certification of chemical analysis of CMSX-4 vacuum induction refined ingot

May 21, 2007

[86] D. A. Ford and R. P. Arthey

Rolls-Royce Limited Metallurgical Research Laboratories, England

DEVELOPMENT OF SINGLE CRYSTAL ALLOYS FOR SPECIFIC ENGINE APPLICATIONS

TMS Superalloys 2001, Paper 01-1023-115.

[87] Yizhou, Andreas Volek, and Robert F. Singer

Effect of grain boundary characteristics on hot tearing in directional solidification of superalloys

J. Mater. Res. Vol. 21, No. 9, Sep 2006, © 2006 Materials Research Society

[88] D.L. Sponseller, ERIM Transportation & Energy Materials Laboratory

DIFFERENTIAL THERMAL ANALYSIS OF NICKEL-BASE SUPERALLOY

TMS Superalloy 2001, Paper 01-352X-259

- [89] W.S. Walston, K.S. O'Hara, E.W. Ross, T.M. Pollock* and W.H. Murphy
René N6: THIRD GENERATION SINGLE CRYSTAL SUPERALLOY
GE Aircraft Engines, Cincinnati, Carnegie Mellon University, Pittsburgh
TMS Superalloys 2001 Paper 01-352X-27
- [90] Charles H. Matzek, REMET CORPORATION
Casting of Reactive Alloys: An Update of Current Technology
Presented at the Canon-Muskegon Technology Conference
In Conjunction With The Paris Air Show June 19, 1997
- [91] NYACOL Nano Technologies, Inc.
NYACOL® colloidal zirconias for investment casting
Zirconias For Investment Casting Technical Report
- [92] Robert A. Horton, PCC Airfoils, Inc.
Method of casting a reactive metal against a surface formed from an improved slurry containing yttria
U.S. Patent 4947927, Date of Patent: Aug. 14, 1990
- [93] NYACOL Nano Technologies, Inc.
NYACOL® colloidal yttria for investment casting
Yttria For Investment Casting Technical Report
- [94] David Alan Ford, Rolls-Royce (1971) Limited, Great Britain
Crucible for melting superalloys
U.S. Patent 4006891, Feb.8, 1977
- [95] Manuel Guerra, Technical Director, Remet Corporation
Yttria binder for reactive metal casting application
Technical consultant email reply, September 30, 2008
- [96] Colin W. Davis and Tom Massopust, Rocky Mountain Laboratory
Analysis of CMSX-4 Alloy Casting Sections and Ceramic Shell Sections
Report No. 9841, October 18, 2008
- [97] <http://www.zypcoatings.com/Datasheets/Arf/Arf.htm>
- [98] http://www.rockymountainlabs.com/tech_frame.html
- [99] <http://wings.buffalo.edu/faculty/research/scic/sem-eds.html>
- [100] ASM Handbook, Volume 10: *Materials Characterization*
Fifth printing, March 1998, Copyright © 1986 ASM International

- [101] Philippe Marcus Florian Mansfeld
Analytical Methods in CORROSION SCIENCE AND ENGINEERING
Published in 2006 by CRC Press Taylor & Francis Group
- [102] Evans Analytical Group, LLC
Auger electron spectroscopy (AES)
Technical Note, TN 101, October 14, 2008
- [103] E.A. Kenik (1), H. Demers (1,2), I.M. Anderson (1), and D.C. Joy (1,3)
High Spectral and Spatial Resolution X-ray Microanalysis of Materials with a Microcalorimeter EDS Detector
Oak Ridge National Laboratory (1), McGill University (2) and University of Tennessee (3)
- [104] K.W.R. Johnson and J.W. Anderson, Los Alamos Sci. Lab. of the University of California
The use of quartz tubes for sampling and casting plutonium
Report for contract W-7405-ENG. 36 with the U. S. Atomic Energy Commission
Report written: August 1958, publicly releasable 1-16-1996
- [105] M.J. Starink* and R.C. Thomson, Loughborough University, UK
THE EFFECT OF HIGH TEMPERATURE EXPOSURE ON DENDRITIC SEGREGATION IN A CONVENTIONALLY CAST NI BASED SUPERALLOY
J. Mater. Sci., 2001, vol. 36, 5603-5608
- [106] Evans Analytical Group LLC
News and information, April 2007, Specialists in Materials Characterization
© Copyright 2007 Evans Analytical Group LLC
<http://www.eaglabs.com/publications/newsletters/gdms/April2007.pdf>
- [107] Evans Analytical Group LLC
TN 102 Glow Discharge Mass Spectrometry (GDMS)
Technique note, October 13, 2008 (Version 1.0)
<http://www.cea.com/files/techniquenote/TN102.pdf>
- [108] James L. Smialek, NASA Glenn Research Center, Cleveland, OH 44135
The Effect of Hydrogen Annealing on the Impurity Content of Alumina-Forming Alloys
http://ntrs.nasa.gov/archive/nasa/casi.ntrs.nasa.gov/20000057042_2000074989.pdf
- [109] Boyd A. Mueller, Robert A. Spicer
Land-Based Turbine Casting Initiative
Conference: Advanced Turbine Systems Annual Program Review, October 17-19, 1995
<http://www.osti.gov/bridge/servlets/purl/218688-Pymv19/webviewable/218688.pdf>
- [110] Craig Hayes, Peter O' Neill, PCC Airfoils, Inc.
Turbine Airfoil Manufacturing Technology

DOE Contract Number: DE-AC05-84OR21400, 1997

[111] Derek M. Olinger, Jimmie V. Gray, ESCO Turbine Technologies

Ralph A. Felice, FAR Associates

Successful Pyrometry in Investment Casting

Presented at the Investment Casting Institute 55th Technical Conference and Expo, Oct.
14 – 17, 2007, Cleveland, Ohio

Appendix 1. Structures and thermal properties of selected oxides

Source: ASM Handbook, Volume 13, *Corrosion*, 1997 Copyright © 1987 by ASM PP. 130-133

Oxide	Structure	Melting point		Boiling or decomposition, d.		Molar volume ^(a)		Volume ratio
		°C	°F	°C	°F	cm ³	in. ³	
α -Al ₂ O ₃	D5 ₁ (corundum)	2015	3659	2980	5396	25.7	1.568	1.28
γ -Al ₂ O ₃	(defect-spinel)	$\gamma \rightarrow \alpha$	26.1	1.593	1.31
CaO	B1 (NaCl)	2580	4676	2850	5162	16.6	1.013	0.64
CaO ₂	C11 (CaC ₂)	d.275	d.527	24.7	1.507	0.95
CoO	B1 (NaCl)	1935	3515	11.6	0.708	1.74
Co ₂ O ₃	Hexagonal	d.895	d.1643	32.0	1.953	2.40
Co ₃ O ₄	H1 ₁ (spinel)	\rightarrow CoO	39.7	2.423	1.98
Cr ₂ O ₃	D5 ₁ (α Al ₂ O ₃)	2435	4415	4000	7232	29.2	1.782	2.02
FeO	B1 (NaCl)	1420	2588	12.6	0.769	1.78 on α -iron
α -Fe ₂ O ₃	D5 ₁ (hematite)	1565	2849	30.5	1.861	2.15 on α -iron
	1.02 on Fe ₃ O ₄
γ -Fe ₂ O ₃	D5 ₇ cubic	1457	2655	31.5	1.922	2.22 on α -iron
Fe ₃ O ₄	H1 ₁ (spinel)	d.1538	d.2800	44.7	2.728	2.10 on α -iron
	~1.2 on FeO

- Molar volume at 25 °C (77 °F) or at transition temperature for structures not stable at 25 °C (77 °F).
- Oxide/metal volume ratio (Pilling-Bedworth ratio)

Appendix 1 (cont.). Structures and thermal properties of selected oxides

Source: ASM Handbook, Volume 13, *Corrosion*, 1997 Copyright © 1987 by ASM PP. 130-133

HfO ₂	Cubic	2812	5094	~5400	~9752	21.7	1.324	1.62
La ₂ O ₃	D5 ₂ hexagonal	2315	4199	4200	7592	50.0	3.051	1.10
MgO	B1 (NaCl)	2800	5072	3600	6512	11.3	0.690	0.80
MoO ₃	Orthorhombic	795	1463	30.7	1.873	3.27
Nb ₂ O ₅	Monoclinic	1460	2660	59.5	3.631	2.74
NiO	B1 (NaCl)	1990	3614	11.2	0.683	1.70
ReO ₂	Monoclinic	d.1000	d.1832	19.1	1.166	2.16
SiO	Cubic	~1700	~3092	1880	3416	20.7	1.263	1.72
SiO ₂	β cristobalite C9	1713	3115	2230	4046	25.9	1.581	2.15
Ta ₂ O ₅	Triclinic	1800	3272	53.9	3.289	2.47

- Molar volume at 25 °C (77 °F) or at transition temperature for structures not stable at 25 °C (77 °F).
- Oxide/metal volume ratio (Pilling-Bedworth ratio)

Appendix 1 (cont.). Structures and thermal properties of selected oxides

Source: ASM Handbook, Volume 13, *Corrosion*, 1997 Copyright © 1987 by ASM PP. 130-133

Oxide	Structure	Melting point		Boiling or decomposition, d.		Molar volume ^(a)		Volume ratio
		°C	°F	°C	°F	cm ³	in. ³	
α -Al ₂ O ₃	D5 ₁ (corundum)	2015	3659	2980	5396	25.7	1.568	1.28
γ -Al ₂ O ₃	(defect-spinel)	$\gamma \rightarrow \alpha$	26.1	1.593	1.31
TiO	B1 (NaCl)	1750	3182	~3000	~5432	13.0	0.793	1.22
TiO ₂	C4 (rutile)	1830	3326	~2700	~4892	18.8	1.147	1.76
Ti ₂ O ₃	D5 ₁ (α -Al ₂ O ₃)	d.2130	d.3866	31.3	1.910	1.47
VO ₂	C4 (TiO ₂)	1967	3573	19.1	1.166	2.29
V ₂ O ₃	D5 ₁ (α -Al ₂ O ₃)	1970	3578	30.8	1.879	1.85
V ₂ O ₅	D8 ₇ orthorhombic	690	1274	d.1750	d.3182	54.2	3.307	3.25
WO ₂	C4 (TiO ₂)	~1550	~2822	~1430	~2606	17.8	1.086	1.87
β -WO ₃	Orthorhombic	1473		32.4	1.977	3.39
W ₂ O ₅	Triclinic	Sublimation, ~850	~1562	~1530	~2786	29.8	1.819	3.12
Y ₂ O ₃	D5 ₃ (Sc ₂ O ₃)	2410	4370	45.1	2.752	1.13
ZnO	B4 (wurtzite)	1975	3587	14.5	0.885	1.58
ZrO ₂	C43 monoclinic	2715	4919	22.0	1.343	1.57

- Molar volume at 25 °C (77 °F) or at transition temperature for structures not stable at 25 °C (77 °F).
- Oxide/metal volume ratio (Pilling-Bedworth ratio)

Appendix 2. Instrument specifications and capabilities notes



Rocky Mountain Laboratories, Inc.

602 Park Point Drive, Suite 101
 Golden, Colorado 80401
 Phone: (303) 526-9449 Fax: (303) 526-0877
 (800) PRO-LABS [776-5227]
 www.RockyMountainLabs.com

Instrument Specifications

Capabilities Note

Capability	XPS/ESCA	Auger	EDS/EDX	SIMS
Principle Input Output	X-rays Electrons	Electrons Electrons	Electrons X-rays	Ions Ions
Model	Kratos Axis HSi	PHI 610	iXRF Model 510D	PHI SIMS II
Information	Elemental Chemical Depth profile	Elemental Chemical Depth profile	Elemental Best mapping Line scanning	Elemental (DSIMS) Chemical (SSIMS) Isotopic Depth profile
Smallest area	30 μm diameter	1 μm diameter	1-5 μm diameter	200 μm diameter
Largest area	2 mm x 0.8 mm	1 mm diameter	50 x 70 :m	1 x 1 cm
Smallest feature	~ 25 μm	0.5 μm	1 μm	400 μm
Smallest sample	10 μm (fiber)	10 μm (fiber)	1 mm	10 μm (fiber)
Largest Sample	1/4" x 4" 8 mm thick	2.5 cm diameter 5 mm thick	2.5-5 cm or 10 cm	2.5 cm diameter 5 mm thick
Analysis depth	1-10 nm with tilt 3-30 monolayers	5-10 nm 10-15 monolayers	1-5 μm @ 20 keV	<3 nm (SSIMS) surface monolayers any depth (DSIMS)
Spatial resolution	10 μm lateral 1 \AA depth	0.2 μm lateral <5 nm depth	10 nm	1 mm (SSIMS) 200 μm dyn. Image 5 nm depth
Spectral resolution	0.48 eV; Ag 3d _{5/2}	dE/E = 0.3%	145 eV @ Mn	1 amu
Sensitivity	0.005-1 atom%	0.1-2 atom%	0.05-2%	<<1 atom%(DSIMS)
Accuracy	±20%	±20%	±5% with standards	±100%
Precision	±0.5%	±5%	±2%	±1%
Best samples	All nonvolatile	Conductors Thin films	Conductive	SSIMS: well ordered polymers DSIMS: oxides
Worst samples	Outgassing Nonhomogeneous	Outgassing Thick insulators	Outgassing	Outgassing
Best elements	Heavy elements	S, Cl, Ar, K, Pd, Ag, Cd, In, Sn	High Z	Halogen (-ions) Noble metal (+ions) 511 amu max.
Worst elements	No H or He Interferences: B/P, Ba/Co, Mn/Ni	No H or He Interferences: S/Mo, N/Ti, Cr/O	Low Z (no Z<B)	Nobel gases High amu
Matrix effects	Little	Moderate	Moderate	Large
Quantification	Excellent	Good	Good	Good with close standard
Analysis time	20 min – 2 hr	15 min – 2 hr	10 min – 1 hr	15 min – 2 hr
Sputter rate	>10 nm/min SiO ₂ @ 2 kV with Ar ⁺	>10 nm/min SiO ₂ @ 2 kV with Ar ⁺	N/A	>10 nm/min SiO ₂ @ 2 kV with Ar ⁺
Destructive	No	No	No	Yes
Unknown survey	Good	Good	Good	Poor
Magnification		5,000X		



Rocky Mountain Laboratories, Inc.

602 Park Point Drive, Suite 101
 Golden, Colorado 80401
 Phone: (303) 526-9449 Fax: (303) 526-0877
 (800) PRO-LABS [776-5227]
 www.RockyMountainLabs.com

Instrument Specifications

Capabilities Note

Capability	FTIR	Raman	SEM	FESEM	SPM
Principle Input Output	Absorption IR IR	Light Light	Electrons Electrons	Electrons Electrons	AFM & SPM Piezoelectric Feedback
Model	Mattson Polaris	Renishaw RM1000	JEOL 6400	JEOL 6320F	Veeco DI Dimension 3100 Nanoscope™ IV
Information	Chemical	Chemical	Topographical Atomic # (Z) with backscatter	Topographical	Topographical Magnetic field intensity
Smallest area	20 μm diameter	1 μm	1.5 μm diameter	100 nm	No limit
Largest area	5 mm diameter	5 μm	7.5 mm diameter	100 μm	125 x 125 μm
Smallest feature	15 μm	0.5 μm	10 nm	1 nm	5 nm
Smallest sample	10 μm	0.5 μm	1 mm	1 mm	5 μm
Largest Sample	10-13 cm	2" tall 3" x 3"	2.5-5 cm or 10 cm	2.5-5 cm	1.5 cm diameter x 1 cm high or 15 cm long (Dim 3000)
Analysis depth	50 nm - mms	2 μm	2-5 nm	2-5 nm	5 μm max. relief
Spatial resolution		1 μm	10 nm @ 100,000X	1.2 nm @ 300,000X	<1 nm lateral <1 Å vertical
Spectral resolution	0.5 cm ⁻¹	4 cm ⁻¹			
Sensitivity	1 ppm	1 pp thousand			1 Å vertical
Accuracy			±2%	±2%	±1% or 5 nm
Precision			±1%	±1%	±2%
Best samples	Organics Liquids & solids KBr pellets	Organics (double bonds) Solids	Conductive	Conductive Better on insulators than SEM	Smooth
Worst samples	Opaque in IR Transparent in IR Multicomponent	Fluorescing Materials Mixtures	Outgassing	Outgassing	Macroscopically rough Mobile surface features
Best elements	Requires molecular bonds	Requires molecular bonds	Highest)Z for backscatter	N/A	
Worst elements	Weak IR absorber Metal compounds Salts	Metals, Minerals		N/A	
Matrix effects	Water	Mixtures a problem			
Quantification	Poor	Poor	Good	Excellent	Excellent
Analysis time	10-30 min	30-60 min	10-30 min	10-30 min	30-60 min
Destructive	No	Laser may melt samples	No	No	No
Unknown survey					
Magnification			15-300,000X	1,000-650,000X	200,000X